Reducing Computational Effort in Structural Topology Optimization Using Reanalysis With a Stiff Reference Matrix

Research Thesis

Submitted In Partial Fulfillment of The
Requirements for the Degree of
Master of Science in
Civil Engineering - Structural Engineering

by

Matthew Spicer

Submitted to the Senate of
the Technion - Israel Institute of Technology

Adar bet 5779, Haifa
March 2019

Acknowledgments

This research thesis was done under the supervision of Assistant Prof. Oded Amir from the faculty of Civil and Environmental Engineering.

I wish to express my gratitude to Assistant Prof. Oded Amir for the guidance, advice and permanent help throughout the work on this research.

The generous financial help of the Technion - Israel Institute of Technology is gratefully acknowledged.

Finally, I wish to thank my parents and my wife Meirav for their patience, encouragement and support along the way.

Contents

List of Figures

List of Tables

Abstract

Topological optimization for continuum structures is a computational method that strives to obtain the optimal material distribution in a given design space, usually discretized using the finite element method. The method is based on the distribution of material so that high stress areas will receive more material, while reducing material in low stress areas, aiming eventually to obtain a final structure that will be more efficient. As a result of significantly increasing progress in computational and 3D printing capabilities that enable the construction of complex structures, the method has become a central part of the design process in the automotive and aviation industries. One of the main challenges of topology optimization is managing to provide results in a reasonable time for nonlinear cases and large scale problems. The computational effort in structural optimization is influenced by 3 main factors: the complexity of the model, the type of analysis and the optimization formulation. In the nested formulation of topology optimization where the state variables are "nested" in the design variables, the analysis of the structure will cost the most computational effort. In complex structures where the model is discretized into a large scale finite element model, the analysis is the most influential factor in the computational effort and can consume over 95% of the CPU time. Reanalysis methods were developed for this exact reason. The Combined Approximation (CA) reanalysis method developed by Kirsch was found to be applicable for topology optimization methods and significant computer effort can be reduced.

The primary goal of this research is to reduce the computational effort involved in solving topology optimization problems by reducing the number of matrix factorizations required. The focus of this research is on solving a variety of problems and exploring the advantage of stiff preconditioning formulation. First, we integrated CA in topology optimization of truss structures and compared two formulations of the problem. Afterwards we referred to continuum structures considering geometrical large deformations. Reanalysis was integrated in the solution of the problem and advantage was recognized for the

stiff preconditend matrix formulation. Last, CA was blended into topology optimization with buckling eigenvalue problems. To the best of our knowledge, the integration of CA in topology optimization for truss structures and for buckling eigenvalue problems has not been accomplished yet. This work adds more insights on the subject of reanalysis in topology optimization and brings additional tools to reduce the computational effort. Original Matlab codes were used throughout the research work, including the Finite Element Analysis, nonlinear solutions, and reanalysis methods.

Nomenclature

List of symbols

a	Area
$\mathbf{B}$	Compatibility matrix
C	Constitutive tensor
C^*	Compliance constraint
E	Young modulus
e_{ij}	Strain tensor
$\mathbf{f}_{ext}$	External force vector
$\mathbf{f}_{int}$	Internal force vector
$\mathbf{f}_B$	Reduced basis force vector
$\mathbf{K}_L$	Linear stiffness matrix
$\mathbf{K}_{NL}$	Nonlinear stiffness matrix
$\mathbf{K}_B$	Reduced basis stiffness matrix
L	Length
p	Penalization parameters
$\mathbf{q}$	Member force vector
$\mathbf{S}$	Second Piola-Kirchhoff stress tensor
$\mathbf{R}_B$	Basis vectors
r_{min}	Filter radius
$\mathbf{u}$	Displacement vector
u_p	Prescribed displacement value
$\mathbf{V}_B$	Orthogonalized basis vectors
V^*	Volume fraction constraint
v	Volume
w	Weighting function

y	Vector of coeffivients in reanalysis
β	Heaviside sharpness control
$\tilde{\beta}$	Buckling load factor
ϵ_{ij}	Green-Lagrange strain tensor
η_e	Eroded Heaviside threshold
η_d	Dilated Heaviside threshold
η_i	Intermediate Heaviside threshold
θ	Displacement control load factor
Λ^*	Critical load constraint
Λ	Lagrange multiplier
$\boldsymbol{\lambda}$	Adjoint vector
ν	Poisson's ratio
ρ	Element density
$\tilde{\rho}$	Filtered element density
$\bar{\rho}$	Projected element density
τ_{ij}	Cauchy stress tensor
$\boldsymbol{\Phi}$	Eigenvector

Abbreviations

2D	Two-Dimentional
3D	Three-Dimentional
BESO	**B**i-direction **E**volutionary **S**tructure **O**ptimization
CA	**C**ombined **A**ppriximation
CPU	**C**entral **P**rocessing **U**nit
DOF	**D**egrees **O**f **F**reedom
ESO	**E**volutonary **S**tructure **O**ptimization
FEA	**F**inite **E**lement **A**nalysis
FNR	**F**ull **N**ewton-**R**aphson
GNL	**G**eometric **N**on **L**inearity
KKT	**K**arush-**K**uhn-**T**ucker conditions
MMA	**M**ethod of **M**oving **A**symptotes
MNR	**M**odified **N**ewton-**R**aphson
N	number of nodes
Nbar	Number of bars
Ndof	Number of degrees of freedom
Nel	Number of elements
nelx	Number of elements in x direction
nely	Number of elements in y direction
OC	**O**ptimality **C**riteria
PCG	**P**re-condtioned **C**ojugate **G**radient
RAMP	**R**ational **A**ppoximation of **M**aterial **P**roperties
RIA	**R**esidual **I**ncrement **A**pproximation
RUK	Re-using the tangent stiffness matrix scheme
RUS	Re-using the solved displacements scheme
SIMP	**S**olid **I**sotropic **M**aterial with **P**enalization
SLP	**S**equential **L**iner **P**rogramming
SQP	**S**equential **Q**uadratic **P**rogramming

Chapter 1

Introduction

This thesis is focused on the integration of reanalysis methods in various topology optimization problems. The main method implemented follows the Combined Approximations (CA) approach. Ultimately, the goal is to find the most efficient way to integrate the methods in the various formulations and reduce the computational effort of the entire process.

1.1 Motivation

Modern structures that are investigated these days are becoming increasingly complex. The demand for more accurate structural analysis solutions with high resolution of the model in 2D and 3D, leads to a large number of elements in the structural model and creates a significant difficulty in the topology optimization process in terms of computational effort. This gives an incentive to find methods for reducing the cost of optimization without compromising the exact solution.

Although computer processing has been continuously developed in the last few decades, engineers are still struggling with long computer runs of the analysis. Hence reanalysis methods are investigated to improve the computational effort. It has been noted that in structural optimization problems with a large number of design variables and a small number of constraints, the structural analysis is the most dominant procedure and consumes the most CPU time. Reducing computational effort for the repetitive analyses is the main goal of reanalysis methods. The main concept of solving the problem with

reanalysis methods is not to solve the new system of governing equations modified by the changes of the structure, but to evaluate the response by reusing the decomposed stiffness matrix. When nonlinear assumptions are considered, the analysis solution is performed in a costly iterative process. As a result, the problem mentioned above aggravates and obtaining optimal structures becomes a very difficult task. Previous publications show that the CA method is efficient and appropriate for topology optimization problems of linear structures.

In this thesis CA is utilized as a reanalysis method for the investigation of topology optimization problems with truss structures considering static linear analysis. Further, the CA method is integrated in the solution of topology optimization problems with geometrical nonlinearity considering large deformations and buckling eigenvalue problems. The investigation focuses on the influence of a stiff reference matrix on the application of the CA method and its effect on reducing computational effort. To the best of our knowledge, the integration of CA in truss structures and in buckling eigenvalue problems has not been accomplished yet. This work adds more insights on the subject of reanalysis in topology optimization and brings additional tools to reduce the computational effort.

1.2 Scope

This research work goal is to investigate efficient implementation of reanalysis methods in topology optimization problems considering linear and nonlinear structural behavior. This is achieved by several numerical experiments for different problem formulations. The research is carried out in two main stages:

- Topology optimization formulations for a given structure and assimilation of reanalysis methods in the solution process. Three types of structural problems are investigated: Linear truss structures; Continuum structure considering geometrical nonlinearity and last a model assuming linearized buckling effect.
- A comparison of the results for each structural model in terms of computational cost. The center of the comparison is the number of matrix factorizations needed for achieving the optimized result.

This thesis consists of 8 chapters and is organized as follows. Chapter 2 gives some background and literature review of the development of topology optimization, reanalysis by CA and the point both of them meet. Chapter 3 presents the development of the structural modeling approach and the appropriate solution for: 1) The linear truss bars and the truss assembly; 2) The finite element analysis for continuum structures assuming large deformations. In Chapter 4 the full formulation of renalysis by CA is developed for static linear equations and for eigenvalue problem solution. In Chapter 5 the integration of reanalysis in the linear truss optimization is shown, presenting also the mathematical formulations and the sensitivity analysis of the problem. Chapter 6 presents topology optimization examples with geometrical nonlinearity. The full formulation of the optimization problems and the corresponding sensitivity analysis are developed. Reanalysis schemes are presented and demonstrated. In Chapter 7 topology optimization with linearized buckling is considered. Again similar to the other chapters, the optimization formulations are presented followed by the sensitivity analysis development. Finally in Chapter 8 the thesis is summarized and future work is proposed.

Chapter 2

Literature review

In this chapter a literature review of structural optimization and reanalysis methods are presented. First the development of mathematical design optimization is presented followed by the three common structural optimization approaches: size, shape and topology optimization. Further, different numerical considerations and optimization solution schemes are presented. Finally, the development of reanalysis of structures and its implementations in topology optimization is reviewed.

2.1 Structural optimization

Optimization, in its general definition is a mathematical process which finds the best solution for a given problem, on the basis of predetermined constraints. The goal of structural optimization is to obtain an improved design of a given structure. Historically the subject started back in the days of Galileo Galilei when he was seeking for the optimal shape of an element subjected to external loads. Designers seek to derive the optimal structure in terms of strength, stability, cost, weight or even aesthetics. Obviously, achieving all of these parameters is an impossible task. Nevertheless, structural engineers strive to achieve the maximum desired results for the designed structure. Traditionally, the optimization has been assimilated in the design process in an iterative way. After composing the initial plan, the structure is analyzed by engineering measures and improved to suit the structure's requirements. This trial and error process is based mainly on designers and engineering intuition. In addition, design time may be relatively long

and usually will not be followed by new conceptual designs. Therefore, the traditional techniques do not always provide satisfying results. Mathematical optimization of structures was developed to overcome this difficulty.

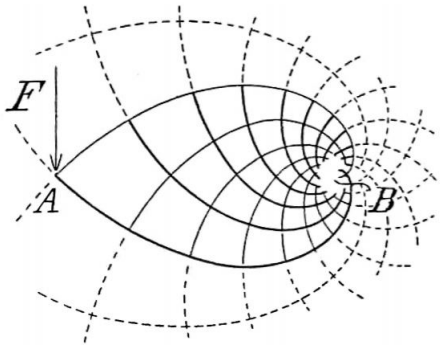

FIGURE 2.1: An analytical solution by Michell for a cantilever truss with a single end load (Michell, 1904).

2.2 Mathematical design optimization

The well known contribution of Michell is considered to be the first analytical optimization work (Michell, 1904) providing a basic theory for the optimal layout of a two-dimensional truss under a single load and subject to stress constraints. A typical Michell structure is shown in Figure 2.1. Despite this remarkable work, truss optimization methods began its mass development only half a century later with the progress in computers technology (Dorn et al., 1964). In the 60's Lucien Schmit was working as a stress analyst for an aircraft corporation and later on as a structure research engineer in M.I.T. He describes in (Schmit, 1981) how the analysis of aircraft structures was changing from physical testings to digital computer platforms followed by computer programs which became more and more commercially available. On the other hand he was learning to solve mathematical optimization problems participating in M.I.T courses. Finally in (Schmit, 1960) he first offered a general new approach to structural optimization which he called "*structural synthesis*". In this work he introduced the idea of coupling structural analysis and nonlinear mathematical programming, establishing the automated optimum design. This innovative work opened an age of a new philosophical approach to structural optimization and initiated the process we see nowadays of mathematical structure optimization. The mathematical design optimization method, seeks to formulate the structure's requirement as a mathematical optimization problem and the restrictions as constraints. Clearly

not all factors can be formulated in mathematical ways. Displacements and stress, for example, can be measured in mathematical means, however aesthetic and architectural properties will be quite difficult to formulate. The formulation of a structural optimization problem starts with determining the objective function. This function which will be usually minimized indicates if the design has improved or not. The optimization problem's variables are the design and state variables. Design variables will be a function or vector that represents the design, such as the area of bars. The state variables will usually be a function of the design variables and represent the structure's response, such as the displacement. Commonly structural optimization is divided into three main categories, i.e. size, shape and topology optimization (Christensen and Klarbring, 2009) as illustrated in Figure 2.2 .

1. **Size** optimization is the case where design variables are the size of each element in the structure. The goal is to reach the optimal design by changing these variables. A possible sizing problem could be a truss structure where the bar's cross-section areas are the design variables. The structure's contour in this case does not change and the joints stay in their initial coordinates.

2. **Shape** optimization is the case where design variables are parameters that represent the initial boundary of the structure. An example for this case is finding the boundary of a continuum structure or determining the location of the nodes for achieving an optimal truss structure. In this case the number of elements, their sizes and connectivity stay in their initial state.

3. **Topology** optimization is the most general method of structural optimization and can be preformed as part of the conceptual design (Bendsøe and Sigmund, 2003). For discrete structures e.g. trusses and frames, the bars cross-section are the design variables. For a given initial domain, the optimal design will evolve by removing bars, namely giving variables the value of zero. Topology optimization of continuum structures seeks to find the optimal distribution of material in a given design domain. When discretized by the finite element method, the design variables are the physical existence of every element in the domain.

As mentioned above' the most general type of structural optimization is the topology optimization method, due to the fact that less details are required for the initial stages of structural design. Consequently, it is the most popular optimization method.

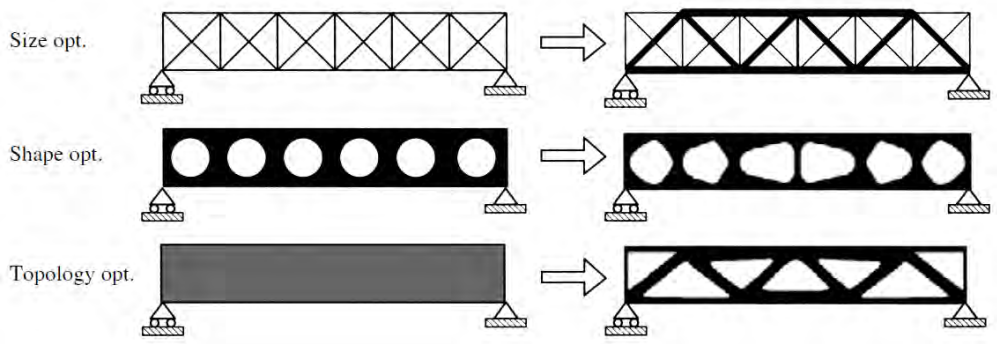

FIGURE 2.2: Typical distinction between optimization categories: size, shape and topology (Bendsøe and Sigmund, 2003).

2.3 Topology optimization

The topology optimization method is the most general one, where for a given domain, loads and boundary conditions the goal is to distribute the material in a way that will improve its performance. The optimization model is divided in general into two main types: 1) Discrete models (frames, trusses etc.) and 2) Continuum models. In this thesis topology optimization will be implemented in two dimensional plane truss structures in Chapter 5 where the design space is based on the ground structure concept. Later on in Chapters 6 and 7 the continuum models will be considered. In the continuum model the design space is discretized by the popular finite element method.

2.3.1 Topology optimization of truss structures

Truss optimization began a century ago with the innovative work of Michell (Michell, 1904), where he defined analytically the optimal truss structure for a given set of loads and boundary conditions. Later in (Rozvany, 1972) Rozvany extended Michell's approach to beam grid-type structures. Linear programming was used successfully in many types of standard truss structural optimization problems (Dorn et al., 1964; Pedersen, 1970). Pedersen in (Pedersen, 1970) used hierarchical methods for integrating geometry and topology truss optimization. Optimal design of truss structures can be found also in (Kirsch, 1989). This thesis uses the popular ground structure formulation proposed by (Dorn et al., 1964). Examples of truss optimizations can be found in (Bendsøe et al., 1994; Ben-Tal and Bendsøe, 1993).

A plane truss is a discrete structure assembled by a set of one dimensional bars interconnected with hinged joints. The Loads are assumed to apply only at the nodes. Results of the truss analysis will only provide axial forces of tension or compression in the bars. Each bar needs only a cross sectional area to define its geometry and the length is determined by the location of its nodes. The formulation of truss optimization is commonly based on the ground structure concept proposed by (Dorn et al., 1964) who solved the classical truss problem and is widely used in topology optimization of trusses. In this approach the structure's layout is composed with a relatively large number of bars and nodes. The most general ground structure is when the connections are assumed to be set for all possible options. In practice the connections are restricted by a connectivity number as shown in Figure 2.3. This can inflict on different optimized structures for the same conditions. In the topology optimization process, bars that have zero cross sectional area are eliminated from the ground structure in order to reach the best substructure that satisfies the load and support conditions. However removing bars with small or zero area may violate the stress constraint, also known as the stress singularity (Kirsch, 1989; Rozvany, 2001). One acceptable way to overcome this phenomena is not to allow the bars to actually get a value of zero but a value close enough to zero. Meaning that the optimization can be also referred as a standard sizing method.

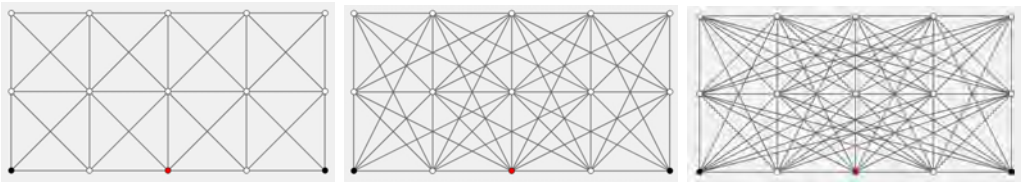

FIGURE 2.3: Three types of ground structures
with different number of bar connectivity

For trusses under a single load and neglecting self-weight, the problem can be formulated in different ways as presented in (Bendsoe and Sigmund, 2013). A popular mathematical formulation of the optimization problem is the plastic design as shown in Equation 2.1, minimizing the weight of the truss structure under stress constraints while

satisfying the static equilibrium equations.

$$\begin{aligned} \min_{\mathbf{a},\mathbf{u}} \quad & \sum_{i=1}^{nbar} (a_i l_i) \\ \text{S.T} \quad & \mathbf{Bq} = \mathbf{f} \\ & a_i \sigma^{\min} \leq q_i \leq a_i \sigma^{\max} \\ & a_i > 0 \quad i = 1, ..., nbar \end{aligned} \tag{2.1}$$

Here a_i is the cross-sectional area and l_i is the length of bar i; $\mathbf{B}$ is the compatibility matrix ; $\mathbf{f}$ is the external force vector; $\mathbf{q}$ is the vector of member forces; and σ^{min} and σ^{max} are the stresses constraints for both tension and compression.

Another classical way to achieve an optimized truss is the elastic design formulation known as "the stiffest truss" as shown in Equation 2.2. Here for a given volume V^*, load vector $\mathbf{f}$ and displacement vector $\mathbf{u}$ the bars are eliminated to minimize the objective compliance function $\mathbf{f}^T\mathbf{u}$. Finding the minimum compliance truss for a given volume of material is formulated as follows:

$$\begin{aligned} \min_{\mathbf{a},\mathbf{u}} \quad & \mathbf{f}^T\mathbf{u} \\ \text{S.T} \quad & \sum_{i=1}^{nbar} \left(\frac{E_i a_i}{l_i} K_i \right) \mathbf{u} = \mathbf{f} \\ & \sum_{i=1}^{nbar} (a_i l_i) \leq V^* \\ & a_i > 0 \quad i = 1, ..., nbar \end{aligned} \tag{2.2}$$

K_i is the stiffness matrix of bar i; E_i is the elastic modulus; and $\mathbf{u}$ is the unknown displacement vector. Note that the plastic design formulation is linear and the elastic formulation is non-linear. Hence the first can solved using linear programing methods. It can be shown (Bendsoe and Sigmund, 2013) that these are equivalent formulations. Meaning that in the same time solving the plastic design and achieving a fully stressed truss we also obtain the stiffest truss with minimum volume.

While truss optimization was the first step towards analytical optimal structures, its practical applications in industry are not significant. Since the 80s, with the advancement of topological optimization based on modeling of continuum structures, the subject has

been assimilated much more widely and has been developing since then. The development of topology optimization for continuum structures is presented in the following section.

2.3.2 Topology optimization of continuum structures

Topological optimization for continuum structures is a computational method that strives to obtain the optimal material distribution in a given design space, usually discretized using the finite element method. The method is based on the distribution of material so that high stress areas will receive more material and reduce material in low stress areas, aiming eventually to obtain a final structure that will be more efficient. As a result of significantly increasing progress in computational and 3D printing capabilities that enable the construction of complex structures, the method has become a central part of the design process of the automotive and aviation industries.

The development of topology optimization for continuum structures started with the optimal design of a Variable Thickness Sheet (VTS) proposed by (Rossow and Taylor, 1973). Its mass growth was after Bendsøe & Kikuchi presented their landmark paper on generating optimal topologies in structural design using a homogenization method (Bendsøe and Kikuchi, 1988). Based of the finite element method the homogenization approach was introduced and based the artificial material distribution with composite micro-structures. Each element composed from a perforated micro-structure, where the variables are the hole sizes in the micro-structure as shown in Figure 2.4, reducing the complex topology problem to a more simple sizing optimization problem.

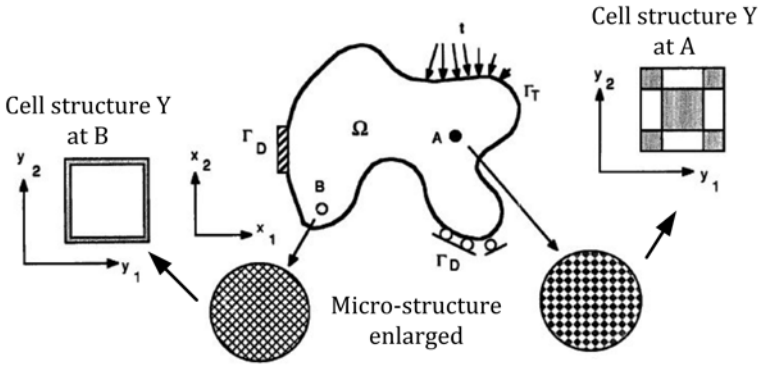

FIGURE 2.4: A structure with composite micro-structure. The holes dimensions of each micro-structure are the problem's variables (Bendsøe and Kikuchi, 1988).

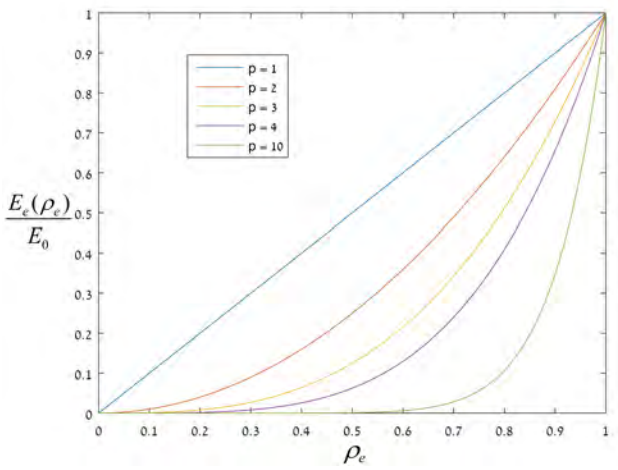

FIGURE 2.5: SIMP function, E_0 is the original element elastic module, ρ_e is the elements density and E_e is the final elastic module.

A year later,Bendsøe presented the common approach of the Solid Isotropic Material with Penalization, known as SIMP (Bendsøe, 1989) and later on by (Zhou and Rozvany, 1991). In this approach isotropic material properties are assumed and the elastic module of each element is set as a function of its density:

$$E_e(\rho) = \rho^P E_e. \tag{2.3}$$

Where E_e is the Young's modulus of the solid material; ρ_e is the element density and P is the penalization parameter larger than one. The function drives elements with intermediate densities between 0 and 1 to preform as full material or void with no intermediate values as shown in Figure 2.5. In (Bendsøe and Sigmund, 1999) the value of $p = 3$ was confirmed as a good value for achieving convergence, as well as satisfying the Hashin–Shtrikman bound. In (Sigmund and Torquato, 1997) the modified SIMP was suggested, where $E_{\min}$ is the stiffness of "void" materials and is non-zero in order to avoid singularity of the stiffness matrix,

$$E_e(\rho_e) = E_{\min} + \rho_e^P(E_0 - E_{\min}). \tag{2.4}$$

.

Similar to SIMP interpolation is the Rational Appoximation of Material Properties (RAMP) provided by (Stolpe and Svanberg, 2001), The main advantage of RAMP over

SIMP is that the derivatives of $E(\rho)$ at $\rho = 0$ are non-zero,

$$E_e(\rho_e) = E_{\min} + \frac{\rho_e}{1 + q(1 - \rho_e)}(E_0 - E_{\min}). \tag{2.5}$$

where q is the penalization parameter.

Further in (Xie and Steven, 1993) the ESO - Evolutionary Structural Optimization approach was suggested. In this case the elements with the lowest stresses are removed. The main problem with this method is that the elements can not return and a local minimum may be difficult to avoid. For that reason an improved method was presented in (Querin et al., 2000), the Bi-directional Evolutionary Structural Optimization (BESO) adding the option for removed elements to return. These density-based methods are most common today in the framework of topological optimization. A different approach is the boundary variation method, based on shape optimization. The design variables are the structure's internal and external boundaries and additionally to regular shape optimization new holes can develop. Level-Set (Wang et al., 2003; Allaire et al., 2004) and Phase-Field (Burger and Stainko, 2006; Wallin et al., 2012) are examples for boundary variation methods. An overview on different topology optimization methods can be found in (Sigmund and Maute, 2013).

Several solution methods for mathematical structural optimization problems are in use, such as: SLP (Sequential Linear Programming), SQP (Sequential Quadratic Programming), OC (Optimality Criteria) and MMA (Method of Moving Asymptotes). Clearly the choice of solution method depends on the optimization problem and its complexity. An overview of these methods can be found in (Christensen and Klarbring, 2009). The numerical solution of the optimization problem can result in poor numerical and physical solutions. Some techniques to overcome these problems will be discussed in the next section.

2.3.3 Numerical considerations

In order for topological optimization methods to be used as a design tool in *real life*, the final layout must be physical and constructible. Three main problems arise from the numerical solution of density based formulation:

(A) (B)

FIGURE 2.6: Examples for (A) The checkerboard problem;
(B) The density filter effect on the solution.

1. **checkerboard** refers to the problem where the regions formation is shaped by alternating solid and void elements ordered in a checkerboard like pattern. These patterns that occur in density-based approaches are illustrated in Figure 2.6. The phenomenon is attributed to the structural modeling of the finite element. A corner connection between elements creates an artificial stiffness and a structure that can-not be manufactured. A variety of approaches have been proposed to address this problem, including the use of smoothing with image processing, higher order finite elements (Diaz and Sigmund, 1995; Jog and Haber, 1996) and filtering the sensitivities.

2. **Mesh dependence** problem is illustrated in Figure 2.7. Allegedly, refinement of the finite element mesh should result in a better modeling of the same optimal structure. Instead a more detailed and qualitatively different structure is obtained. The mesh-dependence problem is divided into two: (1) Obtaining finer and finer structures with mesh refinement; (2) Non-uniqueness of the problem. An extension of the checkerboard filter mentioned earlier (Sigmund, 1994; Sigmund and Torquato, 1997) is commonly used to solve this issue.

3. **Local minimum** occurs due to the non-convex formulation of the topology optimization problem of continuum structures. Depending on the optimization approach and small variations in initial parameters such as penalty value, move limits, geometry of the design domains, number of elements or filter parameter, etc. The optimized result can change significantly and obtain different solutions for a certain problem.

A survey dealing with numerical instabilities as checker-board, mesh dependencies, local minimum and techniques for obtaining manufacturable designs can be found in (Sigmund and Petersson, 1998)

(A) A mesh of 100X50 with $r_{min} = 0.05$

(B) A mesh of 400X200 with $r_{min} = 0.0125$

(C) A mesh of 400X200 with $r_{min} = 0.05$

FIGURE 2.7: Density filter effect r_{min} on the mesh-dependence problem, the structure is a 2 by 1 half MBB beam with a single load.

2.3.4 Filtering

Preventing check-board patterns and mesh-dependence problem is a crucial task in order to obtain final constructible results, as presented above in Section 2.3.3. In this thesis, classical density filtering is implemented in continuum topology optimization and the scheme is presented shortly in this section. To avoid the numerical instability filtering was first proposed by Sigmund in (Sigmund, 1994) using sensitivity filtering for and later in (Sigmund, 2007) it was suggested to filter the densities directly . The filtered element density is given by,

$$\widetilde{\rho}_e = \frac{\sum\limits_{i \in N_e} w(\mathbf{x}_i) v_i \rho_i}{\sum\limits_{i \in N_e} w(\mathbf{x}_i) v_i} \tag{2.6}$$

where N_e is the element's neighborhood, v_i denotes the volume of element i, $\mathbf{x}_i$ is the center location of element i and $w(\mathbf{x}_i)$ is a weighting function depending on the distance between element e and its neighboring element i. The main idea behind density filtering is to modify each element's density according to the element densities in its surrounding neighborhood. In this work, a constant and linear (cone-shape) weighting functions were used, given by

$$w(\mathbf{x}_i) = R - \|\mathbf{x}_i - \mathbf{x}_e\| . \tag{2.7}$$

Here R is the specified filter radius and $\mathbf{x}_i$ and $\mathbf{x}_j$ contain the central coordinates of the design cells i and j respectively. Applying the density filter means that the original densities have no physical meaning and are only used as mathematical variables in the

optimization solution. The material interpolation, structural analysis and sensitivity analysis are all performed with the filtered densities $\widetilde{\rho}_i$.

The sensitivity of a function f with respect to a change in design variable ρ_e is found by the use of the chain rule

$$\frac{\partial f}{\partial \rho_e} = \sum_{i \in N_e} \frac{\partial f}{\partial \widetilde{\rho}_i} \frac{\partial \widetilde{\rho}_i}{\partial \rho_e} \tag{2.8}$$

where the sensitivity of the filtered density $\widetilde{\rho}_i$ with respect to a change in design variable ρ_e is found as

$$\frac{\partial \widetilde{\rho}_i}{\partial \rho_e} = \frac{w(\mathbf{x}_j) v_e}{\sum\limits_{j \in N_i} w(\mathbf{x}_j) v_j}. \tag{2.9}$$

As can be concluded, a filter radius ia essential for both checker-board and mesh dependence problems. Note, the filter radius size can be a control parameter on the minimum length scale of the optimal design achieved in the optimization process. However, picking a filter radius too high can result in a non-optimal solution or even non-convergence.

2.3.5 Heaviside projection

Density based methods such as SIMP presented above, strive to spread the material in form of solid and void only. However, there are areas, especially in the transition between phases, that the element's densities are not sharp 0/1 but have some intermediate values. Heaviside projections of the filtered design were found applicable to make the interface between void and material sharper, as first proposed by (Guest et al., 2004). Due to the discontinuous property of the step function an approximated function is used for the projection of the filtered densities $\widetilde{\rho}$

$$\overline{\widetilde{\rho}} = \frac{\tanh(\beta\,\eta) + \tanh(\beta\,(\widetilde{\rho} - \eta))}{\tanh(\beta\,\eta) + \tanh(\beta\,(1 - \eta))}. \tag{2.10}$$

With a sharpness control of β and threshold point of η, the Heaviside function is illustrated is Figure 2.10. The sensitivity of a function f with respect to a change in design variable ρ_i is found by the use of the chain rule as shown in Equation (2.8) for the filtered densities. The projected densities are defined as $\overline{\widetilde{\rho}}$ and with the added sensitivity term we obtain

$$\frac{\partial f}{\partial \rho_i} = \sum_{i \in N_e} \frac{\partial f}{\partial \overline{\widetilde{\rho}}_i} \frac{\partial \overline{\widetilde{\rho}}_i}{\partial \widetilde{\rho}_i} \frac{\partial \widetilde{\rho}_i}{\partial \rho_i} \tag{2.11}$$

where $\frac{\partial\bar{\widetilde{\rho}}_i}{\partial\widetilde{\rho}_i}$ is calculated explicitly by the derivation of Equation (2.8)

$$\frac{\partial\bar{\widetilde{\rho}}_i}{\partial\widetilde{\rho}_i} = \frac{\beta\left(1-\left(\tanh\left(\beta\ \left(\widetilde{\rho}-\eta\right)\right)\right)^2\right)}{\tanh\left(\beta\,\eta\right)+\tanh\left(\beta\ \left(1-\eta\right)\right)}. \tag{2.12}$$

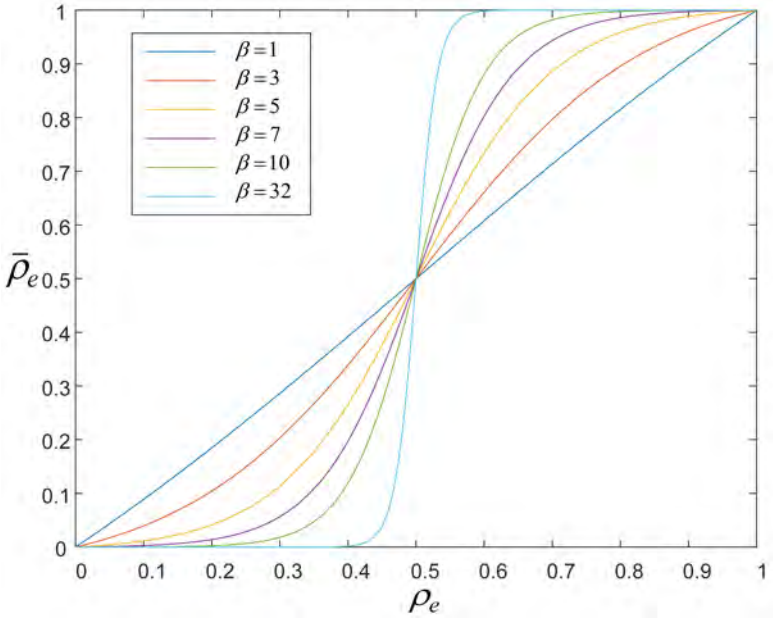

FIGURE 2.8: The Heaviside projection function graphs for different values of β

It has been found that convergence for $\eta = 0.5$ is smooth and almost discrete designs are obtained. However, the projection does not enforce length scale on the 0/1 design even though length scale is introduced in the filtered design space by the density filter. Therefore, a new projection method called robust Heaviside was suggested in (Wang et al., 2011) to execute three different projections each one with different threshold values.

$$\eta_e \ < \ \eta_i \ < \ \eta_d \tag{2.13}$$

The first threshold is called the intermediate threshold where like before $\eta_i = 0.5$ and the projected values denoted with the i index are ρ_i. The two additional threshold values are the eroded and dilated projections, η_e and η_d respectively. The eroded threshold is a value higher than the intermediate one and provides a thinner projected layout compared to the original one. For the dilated layout a value below of the threshold is determined and the projected layout has thicker densities than the intermediate projected design Equation (2.13). After implantation of the three projections the eroded design is used

for the calculations of stiffness and the dilated design is used for the volume calculation. As mentioned the robust Heaviside projections helps to keep the length scale control of the final design. Additionally, the three threshold projections provide a final design that is robust with respect to manufacturing errors.

2.4 Optimization solution schemes

Every optimization cycle the updated design is obtained by solving the mathematical optimization problem. This field of subject is filled with various methods to achieve this goal. In this research work the Optimality Criteria (OC) method and the Method of Moving Asymptotes (MMA) are utilized.

2.4.1 Optimality criteria method

Optimality Criteria (OC) is a well-known method which is often used for this purpose. The method is based on redistributing the material by a constant strain energy density derived from the KKT conditions (Karush, 1939; Kuhn and Tucker, 1951). By using a simple bi-section scheme, the Lagrange multiplier corresponding to the constraint is found. Then, by an iterative procedure the density distribution is updated followed by the update of the Lagrange multiplier. In Chapter 5 the method is utilized for solving the linear truss optimization problem.

2.4.2 Method of Moving Asymptotes

A more general algorithm solution for a non-convex optimization problem is the method of moving asymptotes (MMA) proposed by Svanberg (Svanberg, 1987) and is nowadays quite popular due to the large range of problems that it can deal with. This optimization algorithm builds a convex asymptotic approximation of the problem and efficiently solves this convex subproblem in every iteration. Moving asymptotes are used to control the convergence of the process. MMA is generally used in topology optimization because of its fast convergence and ability to deal with a large number of design variables efficiently. The method of moving asymptotes is a gradient-based algorithm. The convex sub-problems are generated using information on both the function values of the real problem at a

certain design and the derivatives of those functions. Hence, the sensitivity information of the structure is required. In Chapters 6 and 7 the method is utilized for solving the mathematical optimization problems.

2.5 Geometrical nonlinearity in topology optimization

For a given load, a structure may deform in a way that the initial shape configuration is different from the deformed one. These structures are said to be under geometric nonlinearity. Optimum structures with geometric nonlinearity is an important subject that has only in the last two decades begun to receive research attention. Compared to countless publications on structures with small deformations in the linear regime, a limited number of articles were published on the subject of geometric nonlinearity. Neves in (Neves et al., 1995) offered the maximization of the minimum buckling load for a continuum structure subjected to a volume constraint. Buhl in (Buhl et al., 2000) defined different objective functions for compliance minimization. In the same year, (Pedersen, 2000) considered using the SIMP approach to maximize the minimum eigenvalue of a structure. Both (Neves et al., 1995; Pedersen, 2000) observed spurious localized modes. Also in (Neves et al., 2002) considered the problem of minimizing a linear combination of the homogenized elastic properties of the structure subject to volume and buckling constraints applied to periodic micro-structures. They do not use the SIMP method to penalize intermediate densities but instead add a penalty term to the objective function considered. They noted that "the appearance of low-density regions may result in non-physical localized modes in the low-density regions, which are an artifact of the inclusion of these low-density regions that represent void in the analysis". Their strategy of eradicating these spurious buckling modes was setting the stress in low density regions to an insignificant value. For the compliant mechanism (Pedersen et al., 2001) considered large deformations and (Bruns and Tortorelli, 2001) additionally added material and geometric nonlinearity. A SIMP approach to buckling optimization on a continuum structure was used by (Rahmatalla and Swan, 2003) in 2003. Instability consideration was introduced by (Kemmler et al., 2005). Problems of mechanisms that exhibit snap-through behaviors were investigated by (Bruns et al., 2002) and (Bruns and Sigmund, 2004). Low density elements with low stiffness generate numerical problems in the nonlinear topology optimization. Several ways to overcome this phenomena have been suggested.

The obvious way is simply removing zero elements from the structure. However, allowing element restoration is essential in topology optimization. The scheme proposed by (Buhl et al., 2000) seems to be the most efficient and is implemented in this work. Basically the idea is to ignore non-convergence of the Newton-Raphson stopping criteria for elements that have zero density or surrounded by them.

2.5.1 Numerical considerations

Optimizing structures with geometric nonlinearity considered in the model leads to numerical problems that linear models do not suffer from. As implied above, a problem in topology optimization with buckling constraints is local buckling of the void areas. Because the void elements have a non-zero density they contribute to the geometric stiffness matrix. The first buckling modes will then arise in the void elements, having no physical meaning. The occurrence of such modes is also a problem for dynamic topology optimization problems with eigen-frequency analysis. There are three main solution methods for the void buckling problem. The first method is to artificially set all stresses in the elements with densities below a certain threshold value to zero. This method is proposed by (Neves et al., 2002). While this method suppresses the void buckling modes, it is not very suitable for the gradient based optimization methods used in topology optimization. The geometric stiffness matrix is in this formulation a discontinuous, non differentiable function of the element densities. A more refined method is to use a different penalization on the physical stiffness matrix and the geometric stiffness matrix as presented in Equation (2.14). This has the same effect: low density elements do not contribute to the geometric stiffness matrix. This method was proposed by (Bendsøe and Sigmund, 2003). The main advantage of this method over the previous method is the fact that the geometric stiffness matrix is now a continuous, differentiable function of the element densities. This makes this method better suited for gradient based optimization methods and is used in this research work.

$$\begin{aligned} &\text{For the linear matrix :} && E = E_{\min} + \rho_e^p (E_0 - E_{\min}) \\ &\text{For the geometric matrix :} && E_g = \rho^p E_0 \end{aligned} \tag{2.14}$$

A last approach to avoid buckling in void area is to completely remove the void elements (Pedersen, 2000). This gives the best resemblance with the physical situation. To avoid local minimum the removed elements should be able to return. Therefore, not all void

elements are removed, but a border of elements surrounding the structure are kept. Another problem that arises is the switching of modes. This issue was first investigated by (Ma et al., 1995) in the context of vibration. Switching of modes occurs if during the optimization there is a switch of the lowest critical value. The resulting objective value is then a non-smooth function of the design variables. A solution for this problem is to include multiple buckling loads in the objective.

Models using geometrically nonlinear finite element analysis are crucial for the stability of soft structures, mechanisms and slender structures. Using the small deformation assumption in the optimization for those type of structures does not provide a sufficient result. Therefore the field of nonlinear geometrical structures is necessary for the increasing development of topology optimization as a design tool. In Chapter 6 large deformation assumptions are considered and in Chapter 7 buckling effects are taken in account.

2.6 Reanalysis of structures

Structural analysis is essential to determine the response (e.g displacement, stresses) of a structure under specific loads and is preformed numerous times during the design process, e.g. optimization, loading conditions, structural damage analysis and so on. Modern structures that are investigated these days are becoming increasingly complex. Moreover, the demand for more accurate structural analysis with high resolution in 2D and 3D creates a significant difficulty in the optimization process in terms of computational considerations. Even though computer processing has been continuously developed in the last few decades, engineers are still struggling with long computer runs of the analysis as reviewed in (Venkataraman and Haftka, 2004). Hence reanalysis methods are investigated to improve the computational effort. In topology optimization it has been noted that for a high number of design variables and low a number of constraints the structural analysis consumes at least 95% of the CPU time (Aage et al., 2015). Reducing computational effort for the repetitive analyses is the main goal of reanalysis methods. The main concept of solving the problem with reanalysis methods is not to solve the new system of governing equations modified by the changes of the structure but to evaluate the response by reusing the decomposed stiffness matrix (Kirsch, 2008).

2.6.1 Reanalysis methods

Structural reanalysis is general divided into two categories (Kirsch, 2008): Direct methods and approximated methods. Roughly the direct method is suitable for low rank changes in the structure and the approximate method for larger rank of changes.

Direct methods originated with Sherman-Morrison formula (Sherman and Morrison, 1950) for structures with changes in only one element. The inverse of the modified stiffness matrix is calculated indirectly. For two elements and extra changes in the structure, the Woodbury formula was presented (Woodbury, 1950). More elements with changes will bring more computational effort and in some stage the method will not be efficient enough.

Approximated methods are useful when changes occur in a large number of elements of the structure. Naturally, these methods are suitable for reducing the computational effort of the optimization process. Three main approximate reanalysis techniques are classified - Local, Global and Combined approximations:

1. Local approximation (single point approximation) is an effective method for a structure under small changes in the design variables. The approximation is commonly based on the Taylor series or the binomial expansion of a single point of the design. The problem in this method is that large changes of the design variables can provide inaccurate results. Several techniques were proposed to improve the accuracy of the results, such as second order approximation, convex approximations, reciprocal and hybrid variables (Fleury, 1989; Fuchs, 1980; Schmit and Farshi, 1974; Starnes Jr and Haftka, 1979; Svanberg, 1987). Naturally, improved results will cost higher computational effort and may not be worthwhile.

2. Global approximation (multi-point approximation) is suitable for large changes in the structure and is more accurate. However, for a large number of design parameters the global method could be computationally expensive. The method is mainly based on polynomial fitting, response surface or reduced basis methods. Polynomial fitting and response surface use the response of a number of design points (e.g displacement) and construct a polynomial function to approximate the response at other design points. The main idea of reduced basis methods is to

calculate the response of a large system by a linear combination of preselected basis vectors.

3. Combined approximation (CA), introduced by Kirsch (Kirsch, 1991) is a local united with a global approximation approach and an effective reanalysis method that produces results with high accuracy. The method includes series expansion, reduced basis and Gram-Schmidt orthogonalization. The combination of efficient calculation of local approximation (series expansion) utilized as basis vectors for the accurate global approximation (reduced basis) yields a high quality method.

The CA method has been proven to be efficient and suitable for a various structural analysis and optimization scenario, such as static linear and nonlinear, vibration and dynamic cases (Kirsch, 2008).

2.6.2 Combined Approximation method

Research on the CA method started almost 30 years ago when Kirsch (Kirsch, 1991) presented the Combined Approximation (CA) method for the static linear case. High-quality approximations were achieved with small computational effort and for large changes in the stiffness matrix. After obtaining a single precise solution, the CA method approximates the next solution by expanding a binomial series used as basis vectors. Later on, (Kirsch and Liu, 1995) showed that first order reduced basis approximations for truss structures provide exact stresses and displacements. In (Kirsch, 1999) the Gram-Schmidt orthogonalization procedure was utilized to generate a new set of basis vectors. In this scheme, well-conditioned basis vector terms are obtained and additional vectors can be calculated without re-calculating all the terms. Later on, (Kirsch and Papalambros, 2001) CA reanalysis was used to calculate the response of a truss under significant changes of its topology. The reanalysis procedure with CA was also implemented in the numerical solution of dynamic eigenvalue problems (Kirsch and Bogomolni, 2004) where in the dynamic problem the solution is obtained by solving repeatedly the eigenvalue problem. Further in (Kirsch et al., 2006) the method was used to reduce the computational effort for calculating the derivatives of a nonlinear dynamic response and in (Kirsch and Bogomolni, 2007) the eigenvalue problem was reduced with CA to a less heavy computational problem. In non-linear problems it was found that CA also provides an

efficient solution (Amir et al., 2008). In large nonlinear problems, reanalysis is even more important due to the set of linear equations that are solved repeatedly during the solution of the non-linear problem. An extended method based on CA was published by (Chen and Yang, 2000) . The reduced basis vectors are assembled with the use of second order eigenvector terms, therefore the large eigenvalue problem is reduced to a 3-by-3 problem, saving sufficient time and maintaining accuracy.

Further implementations of the CA method can be found in the literature: structures under dynamic and nonlinear analysis (Kirsch et al., 2007), (Kirsch and Bogomolni, 2007), (Bogomolni et al., 2006); potential damage scenarios (Kirsch and Moses, 1999); and approximation for plane truss (Kirsch, 1993). In 2002 (Kirsch et al., 2002) proved that CA is a particular case of the Preconditioned Conjugate Gradient (PCG) method, providing identical results that are practically equivalent, where the pre-conditioner is the Cholesky factorization of the reference stiffness decomposed matrix. Every PCG iteration is equivalent to one basis vector term. As shown in Figure 2.9, PCG is numerically more stable than the CA method.

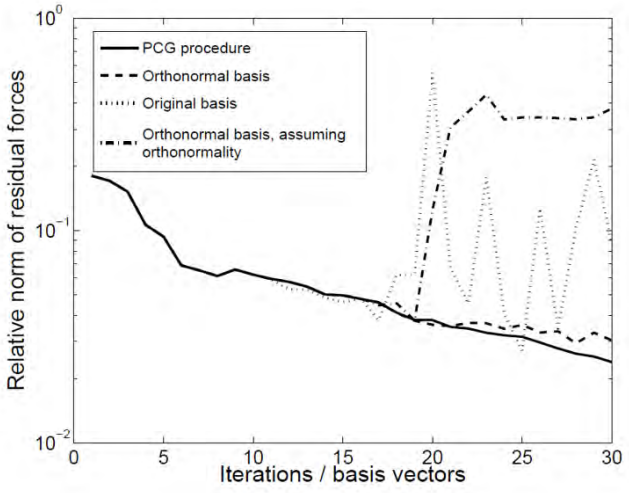

FIGURE 2.9: A relative norm of the residual forces for every basis vector in CA and iterations for the PCG procedure (Amir et al., 2012)

2.6.3 CA in topology optimization

One of the main challenges of topology optimization is managing to provide results in a reasonable time for nonlinear cases and large scale problems. The computational effort in structural optimization is influenced by 3 main factors: the complexity of the model,

type of analysis and the optimization formulation. In the nested formulation of topology optimization where the state variables are "nested" in the design variables, the analysis of the structure will cost the most computational effort. In complex structures where the model is discretized into a large scale finite element model, the analysis is the most influential factor in the computational effort and can consume over 95% of the CPU time (Aage et al., 2015; Amir and Sigmund, 2011). Starting with changes in the topology and the number of degrees of freedom in a truss structure, (Kirsch and Papalambros, 2001) found that the CA method can be utilized in the reanalysis. In (Amir et al., 2009) CA was integrated into a standard topology optimization. From a previous optimization step, CA utilized the stiffness matrix as a reference for the next solution. Sensitivity analysis was calculated consistently and even rough approximations of the structural response yield optimized design that are practically identical to those obtained using standard procedures. Later on in (Amir et al., 2012) it was found that even without calculating the exact derivatives and using approximated sensitivity analysis, good results can be obtained and in some cases even more precise. Neglecting the need to calculate the consistent sensitivity analysis reduces the computational cost by not needing to calculate the adjoint term of the CA procedure. Bogomolny in (Bogomolny, 2010) showed the implementation of CA in free vibration topology optimization. Reference stiffness matrix, eigenvalue and eigenvector from previews optimal design were utilized for reducing the eigenvalue problem with CA. Significant reduction of computational effort was noted for 3D problems. Testing on 3D examples in (Amir and Sigmund, 2011), it was found that it is possible to reduce computational effort in topology optimization by an order of magnitude. A different approach for nonlinear reanalysis in topology optimization was proposed by (Materna and Kalpakides, 2016). The approach is based on residual increment approximation (RIA). The approximation is based on local approximation with a rational approximation method, evaluating only the residual vectors. In (Gogu, 2015) a different approach for constructing the reduced basis vectors in the context of topology optimization was proposed. The approach uses previously calculated solutions of the equilibrium equitations to construct the reduced basis. Fast iterative solvers for large three dimensional topology optimization problems was addressed by (Wang et al., 2007) significantly reduced the number of iterations and the runtime of the linear solver by recycling selected search spaces from previous linear system. (Amir, 2015) presented an effective recycling of pre-conditioners in continuum structural topology optimization. The results pointed out the advantage of stiff preconditioning. It was shown that for

reanalysis the minimum volume formulation leads to a more efficient procedure than the minimum compliance approach. When $K_{ref} \succ K$ ("stiffer"), the convergence of PCG is guaranteed and faster than the opposite situation where the convergence is still possible but expected to be slower.

This chapter provided a literature review of the popular topology optimization method. Reanalysis methods for reducing the computational effort in structural analysis were reviewed. Although significant progress has been made in research and implementation of topology optimization over the last three decades, the application for structures with nonlinear properties still requires a high computational cost. Therefore, as shown above, attempts are being made to improve computational efficiency in order to achieve optimal designs even for complex and large problems. The CA method was found to be applicable for topology optimization methods and significant computer effort was reduced. This work aims to add more insights on the subject and to bring additional tools to reduce the computational effort. The research focuses mainly on the attempt of reducing the number of matrix factorizations required for the solution and the advantage of stiff preconditioning formulation. Essentially, the research refers to nonlinear cases, such as geometrical nonlinearity and buckling eigenvalue problems.01/.

Chapter 3

Essential background on structural analysis

The design of a structure is planned to fulfill its service purpose and be able to sustain the defined loads. Therefore some responses need to be calculated e.g. displacement, stress and strain. This is where structural analysis takes place. Our goal is to make a mathematical model of the structure that will be on the one hand as close as possible to the real structure behavior and on the other hand as simple as possible so computational effort will remain reasonable.

The first step of the structural analysis is defining the type of model . Two main categories of mathematical models are usually considered - discrete models and continuum models (Bathe, 2006). In the discrete mathematical model, the actual system response is directly described by the solution of a finite number of state variables. For the continuum mathematical model, the formulation of the governing equations are achieved also by a discrete model, but instead of a set of algebraic equations for the unknown state variables, differential equations govern the response. Solving the differential equations is performed by numerical procedures. These procedures reduce the continuous mathematical model to a discrete idealization that can be solved in the same manner as the discrete model. The most popular numerical method used for idealization of structural analysis of continuum models is the finite element method (FEM). Using FEM, two-dimensional and three-dimensional continuum structures such as plates, shells and solids, as well as trusses and frames, can be modeled and analyzed. The main feature of FEM is the assumption of

the displacement field within a small element as a combination of a few simple functions, known as shape functions. The actual structure is replaced by a discrete model, divided into small elements, also known as finite elements, which are connected together at their boundaries. According to the shape functions used, the stiffness matrix of each element in the model is calculated and then the stiffness matrix of the whole structure can be assembled. Equilibrium at every node of the discrete structure is satisfied by solving a set of simultaneous algebraic equations and obtaining the nodal displacements. The results are then post-processed to determine the stresses and internal forces at each element. Three types of structural analysis are usually addressed: linear static analysis, nonlinear static analysis and dynamic analysis. In linear static analysis, we assume linear relations between the applied loads and the displacements of the structure. This assumption is based on linear material laws and linear kinematics (small displacements, rotations and strains). In nonlinear analysis, one or more of these assumptions may not be suitable: the material law could be nonlinear; the kinematics could be nonlinear such as large displacements and rotations; or the boundary conditions might change like in contact problems. In order to perform a nonlinear finite element analysis, a set of nonlinear algebraic equations should be solved.
In this research work two types of models are utilized in the investigation. First, a truss structure assuming linearity in all parameters in Chapter 5. Second, a continuum model with geometric non-linearity in Chapters 6 and 7 .

3.1 Linear analysis

Linear static analysis represents the most basic type of structural analysis. Practically nothing is really linear, and a number of assumptions must be taken into account when solving structures in a linear way: small deformations and small strains compared to the model's size; constant material properties; loading direction and magnitude do not change and the structure returns to its original form after removing the loads. For obtaining the unknown displacement vector the linear equilibrium equations to be solved are

$$\mathbf{Ku} = \mathbf{f} \tag{3.1}$$

where $\mathbf{K}$ is the stiffness matrix; $\mathbf{f}$ is the load vector and $\mathbf{u}$ is the unknown displacement vector. The stiffness matrix and force vector assembly is carried out according to the model that is analyzed. Determining the displacements $\mathbf{u}$ is by inverting the stiffness matrix and multiplying it by the force vector. Practically, the process of inverting a matrix is too long and involves too much computational effort. Therefore, typically a process based on the Gauss elimination method is used. The stiffness matrix which is symmetric and positive definite is usually given in its Cholesky decomposed formulation

$$\mathbf{K} = \mathbf{U^T U} \tag{3.2}$$

where $\mathbf{U}$ is an upper triangular matrix and the solution is calculated simply by forward and backward substitutions,

$$\mathbf{U^T y} = \mathbf{F} \tag{3.3}$$

and

$$\mathbf{U u} = \mathbf{y}. \tag{3.4}$$

When the finite element model is large, it is not practical to discompose the stiffness matrix due to memory limitations. Thus, iterative methods are used to solve the set of linear equilibrium equations.

3.2 Truss structure model

A linear truss structure is built from elastic straight bars that are connected by pin joints where the bars can turn freely. The internal axial forces are only along the bar and they are one-dimensional. Suppose the truss has M number of bars with N number of nodes. Each node has two displacements components horizontal $\mathbf{u}^h$ and vertical $\mathbf{u}^v$ as shown if Figure 3.1 The vector $\mathbf{u}$ has $n = 2N - FN$ where FN is the number of fixed known displacements. In the same way the known force vector has $n = 2N - FN$ components where each node has two forces horizontal and vertical.

To compose the stiffness matrix of the structure the strain calculation will be presented. For a bar with the original length of L_0 and its angle is θ, then the extension horizontally is $u^h = L_0 cos\theta$ and vertically $u^v = L_0 sin\theta$ as shown in Figure 3.2. Then the new length is $L = L_0 + \Delta L$ and extension is calculated assuming small deformations and

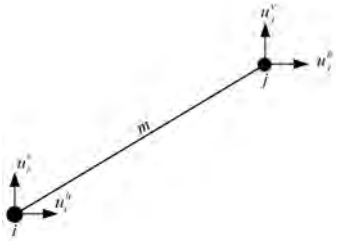

FIGURE 3.1: Bar number m with 4 displacement components

small strains:

$$L^2 = (L_0 \cos\theta + u_j^h - u_i^h)^2 + (L_0 \sin\theta + u_j^v - u_i^v)^2 \tag{3.5}$$

$$L \approx L_0 + (u_j^h \cos\theta + u_j^v \sin\theta - u_i^h \cos\theta - u_i^v \sin\theta) \ = L_0 + \Delta L \tag{3.6}$$

Then finally the compatibility matrix $\mathbf{B}$ is composed where a column of $\mathbf{B}$ for the bar m that connects node i to node j is:

$$\begin{aligned} \mathbf{b}_m = &[0 \quad 0 \ldots \cos\theta \quad \sin\theta \ldots -\cos\theta \quad -\sin\theta \ldots 0 \quad 0]^T \\ &u_1^h \ u_1^v \quad u_j^h \quad u_j^v \qquad u_i^h \qquad u_i^v \qquad u_n^h \ u_n^v \end{aligned} \tag{3.7}$$

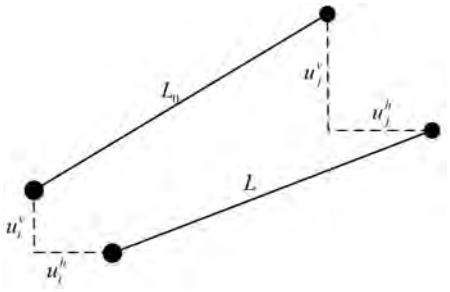

FIGURE 3.2: Illustration of a bar deformation

The force equilibrium equation takes place between the matrix $\mathbf{B}$, the member force $\mathbf{q}$ and $\mathbf{f}$ the nodal force vector

$$\mathbf{Bq} = \mathbf{f}. \tag{3.8}$$

From Hooke's constitutive law with the modulus of elasticity E the member forces can be calculated as

$$q_m = \sigma_m a_m = E \frac{\mathbf{b}_m}{l_m} a_m u_m. \tag{3.9}$$

Now the stiffness matrix is established, where in the local coordinates of bar m, $\mathbf{b}_m$ is the i'th column of $\mathbf{B}$; a_m is the cross-section of the bar and the local bar stiffness matrix

is

$$k_m = \frac{Ea_m}{l_m}\mathbf{b}_m\mathbf{b}_m^T. \tag{3.10}$$

The global stiffness matrix of the truss is assembled by adding all local stiffness matrices

$$\mathbf{K} = \sum_{m=1}^{M} \frac{Ea_m}{l_m}\mathbf{b}_m\mathbf{b}_m^T. \tag{3.11}$$

Finally the global set of linear equilibrium equations to be solved are

$$\mathbf{Ku} = \mathbf{f}. \tag{3.12}$$

3.3 Nonlinear structural mechanics

In the previews section we assumed for linear analysis that the deformations and strains of the structure are infinitesimally small, the material law is linear and the load is constant and independent. In the linear case the stiffness matrix $\mathbf{K}$ was considered to be constant and independent of the displacements. Further, the relation between the load and displacement was linear leading to the equilibrium equation in Equation (3.1). This situation does not always reflect the real physical case and may not provide accurate enough results. Nonlinear analysis deals with these type of situations. The nonlinear analysis usually deals separately with material nonlinearity and kinematic nonlinearity. Material nonlinearity assumes infinitesimal displacements and strains and involves nonlinear behavior in the stress-strain relation. The kinematic nonlinearity refers to large displacements and large rotations, the strain may be large or small. In this thesis the relation between stress and strain is assumed to be linear and kinematic nonlinearity is taken into account with small strains as illustrated in Figure 3.3 .

When including nonlinear geometric conditions, the equilibrium relations need to be solved in an iterative solution. Newton-Raphson is the most popular incremental-iterative scheme for solving nonlinear equations. The general basic problem is to find the state equilibrium of a body corresponding to the applied loads (Bathe, 2006),

$$\mathbf{R}(\mathbf{u}) = \mathbf{f}_{int} - \mathbf{f}_{ext} \tag{3.13}$$

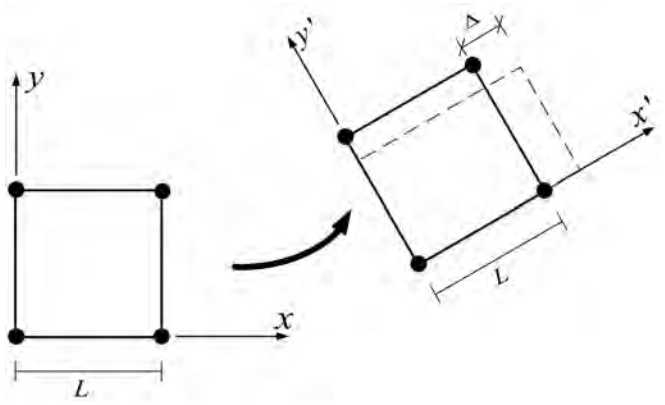

FIGURE 3.3: An illustration of large displacements and rotations with small strains in a single element

where $\mathbf{f}_{int}$ is a vector of the internal forces at the nodal points, $\mathbf{f}_{ext}$ is the vector of corresponding external loads and $\mathbf{R}(\mathbf{u})$ is the residual vector. Due to the unknown body configuration the well known Cauchy stress tensor is not applicable any more. Solving the set of nonlinear equations requires the utilization of a step by step solution. The concept of pseudo-time can be employed to apply the external load in a number of time steps (or increments). Assume that a solution is given in time t and the requirement is to find the next step solution at time $t + \Delta t$. Lagrangian description is the most suitable way of describing the statics and kinematics of a structure subject to large displacements (other then the Eulerian way). The equilibrium of the body at time $t + \Delta t$ with the principle of virtual work requires that

$$\int_{{}^{t+\Delta t}V} {}^{t+\Delta t}\tau_{ij}\delta_{t+\Delta t}e_{ij}d^{t+\Delta t}V = {}^{t+\Delta t}\mathbb{R} \tag{3.14}$$

where ${}^{t+\Delta t}\tau_{ij}$ are the cartesian components of the Cauchy stress tensor, $\delta_{t+\Delta t}e_{ij}$ is the strain tensor corresponding to virtual displacements and ${}^{t+\Delta t}V$ is the volume at time $t + \Delta t$. The fundamental difficulty in the general application of Equation (3.14) is that the configuration of the body at time $t + \Delta t$ is unknown. This is an important difference compared with linear analysis in which it is assumed that the displacements are infinitesimally small and the original configuration is used.

Introducing the Green-Lagrange strain tensor,

$${}^{t}_{0}\varepsilon_{ij} = \frac{1}{2}({}^{t}_{0}u_{i,j} + {}^{t}_{0}u_{j,i} + {}^{t}_{0}u_{k,i}{}^{t}_{0}u_{k,j}) \tag{3.15}$$

where u is the displacement field, i, j and k represent the Cartesian axes, $u_{i,j} = \dfrac{\partial u_i}{\partial u_j}$ and the ${}^t_0$ notation means evaluation at time t in the initial coordinate system corresponding to time 0. We should note that in the definition of the Green-Lagrange strain tensor, all derivatives are with respect to the initial coordinates. Therefore, the strain tensor is defined with respect to the initial coordinates of the body. The appropriate stress tensor to use with the Green-Lagrange strain tensor is the second Piola-Kirchhoff stress tensor ${}^t_0\mathbf{S}$ which is work-conjugated with the Green-Lagrange strain tensor,

$$ {}^t_0S_{ij} = \frac{{}^0\rho}{{}^t\rho} {}^0_t x_{i,m} \, {}^t\tau_{mn} \, {}^0_t x_{j,n}. \tag{3.16} $$

For computing the Green- Lagrange strain tensor it is convenient to use the deformation gradient

$$ {}^t_0\mathbf{X} = \begin{bmatrix} \frac{\partial^t x_1}{\partial^0 x_1} & \frac{\partial^t x_1}{\partial^0 x_2} & \frac{\partial^t x_1}{\partial^0 x_3} \\ \frac{\partial^t x_2}{\partial^0 x_1} & \frac{\partial^t x_2}{\partial^0 x_2} & \frac{\partial^t x_2}{\partial^0 x_3} \\ \frac{\partial^t x_3}{\partial^0 x_1} & \frac{\partial^t x_3}{\partial^0 x_2} & \frac{\partial^t x_3}{\partial^0 x_3} \end{bmatrix}. \tag{3.17} $$

Note that the second Piola-Kirchhoff stress hase little physical meaning and Cauchy stress must be calculated as-well. Applying the principal of virtual work with respect to an unknown deformed configuration at time t results in the basic equation in the Total-Lagrange formulation

$$ \int_{{}^0V} {}^{t+\Delta t}_0 S_{ij} \delta \, {}^{t+\Delta t}_0 \varepsilon_{ij} \, d^0V = {}^{t+\Delta t}\mathbb{R} \tag{3.18} $$

All stresses and strains, including the increments, are referred to the original configuration, therefore the stresses and strains are incrementally decomposed,

$$ \begin{aligned} {}^{t+\Delta t}_0 S_{ij} &= {}^t_0 S_{ij} + {}_0 S_{ij} \\ {}^{t+\Delta t}_0 \varepsilon_{ij} &= {}^t_0 \varepsilon_{ij} + {}_0 \varepsilon_{ij}. \end{aligned} \tag{3.19} $$

Additionally the linear and nonlinear terms of the incremental strains are decomposed, where ${}_0e_{ij}$ is the linear term and ${}_0\eta_{ij}$ is the nonlinear strain term

$$ \begin{aligned} {}_0\varepsilon_{ij} &= {}_0e_{ij} + {}_0\eta_{ij} \\ {}_0e_{ij} &= \frac{1}{2}({}_0u_{i,j} + {}_0u_{j,i} + {}^t_0u_{k,i} \, {}_0u_{k,j} + {}_0u_i \, {}^t_0u_{k,j}) \\ {}_0\eta_{ij} &= \frac{1}{2} {}_0u_{k,i} \, {}_0u_{k,j} \end{aligned} \tag{3.20} $$

With Equation (3.18) and the decomposed incremental strains we obtain the equation

$$\int_{{}_0V} {}_0S_{ij}\delta_0\varepsilon_{ij}d^0V + \int_{{}_0V} {}^t_oS_{ij}\delta_0\eta_{ij}d^0V = {}^{t+\Delta t}\mathbb{R} - \int_{{}_0V} {}^t_oS_{ij}\delta_0 e_{ij}d^0V \tag{3.21}$$

Linearization of the equation, using the approximation ${}_0S_{ij}={}_0\mathrm{C}_{ijrs}{}_0e_{rs}$ and $\delta_0\varepsilon_{ij} = \delta_0 e_{ij}$ we obtain

$$\int_{{}_0V} {}_0\mathrm{C}_{ijrs}{}_0e_{rs}\delta_0 e_{ij}d^0V + \int_{{}_0V} {}^t_oS_{ij}\delta_0\eta_{ij}d^0V = {}^{t+\Delta t}\mathbb{R} - \int_{{}_0V} {}^t_oS_{ij}\delta_0 e_{ij}d^0V \tag{3.22}$$

where ${}_0\mathrm{C}_{ijrs}$ is the constitutive tensor in the original configuration. The previous relationships in Equation (3.20) lead to the formulation of the corresponding strain-displacement matrices, ${}^t_0\mathbf{B}_L$ and ${}^t_0\mathbf{B}_{NL}$. The first is the strain-displacement transformation matrix, corresponding to linear terms of incremental strains. The second matrix corresponds to the nonlinear terms of incremental strains. At any iteration within time step t, the tangent stiffness matrix and the internal forces are computed as follows

$$\begin{aligned}
{}^t_0\mathbf{K}_L &= \int_{{}_0V} {}^t_0\mathbf{B}_L^T \cdot {}_0\mathbf{C} \cdot {}^t_0\mathbf{B}_L d^0V \\
{}^t_0\mathbf{K}_{NL} &= \int_{{}_0V} {}^t_0\mathbf{B}_{NL}^T \cdot {}^t_0\mathbf{S} \cdot {}^t_0\mathbf{B}_{NL} d^0V \\
{}^t_0\mathbf{f}_{int} &= \int_{{}_0V} {}^t_0\mathbf{B}_L^T \cdot {}^t_0\hat{\mathbf{S}} d^0V
\end{aligned} \tag{3.23}$$

where ${}^t_0\mathbf{K}_L$ and ${}^t_0\mathbf{K}_{NL}$ are the linear and nonlinear parts of the stiffness matrix, based on the known configuration at time t. ${}^t_0\mathbf{S}$ represents the second Piola-Kirchoff stresses in matrix format; ${}^t_0\hat{\mathbf{S}}$ represents the same stresses in vector format. The linearized algebraic equation system that is solved every time step can be written as

$$\left({}^t_0\mathbf{K}_L + {}^t_0\mathbf{K}_{NL}\right)\Delta\mathbf{u} = {}^{t+\Delta t}_0\mathbf{f}_{ext} - {}^t_0\mathbf{f}_{int} \tag{3.24}$$

${}^{t+\Delta t}_0\mathbf{f}_{ext}$ is the external load vector at time step $t+\Delta t$. This is a typical iterative equation system establishing the starting point for an iterative solution, where the stiffness and internal forces from step t are used as initial approximations for the solution at step $t+1$. These are then corrected iteratively until the external and internal forces are balanced.

3.4 Nonlinear analysis

In the last section, equations of the finite element problem were derived. Since geometrically nonlinear problems are path-independent, it would in principle be possible to impose the entire external load in a single step. For very large loading steps it is usually difficult to obtain a properly converged solution. Furthermore, one is often interested in the full equilibrium path. Therefore, an incremental-iterative solution procedure is best suited for these nonlinear problems. In an incremental-iterative procedure, each load step consists of an increment of the external load. The most commonly used technique is the Newton-Raphson method, which involves repeated linearization of the nonlinear equations. This technique is very suitable because of its quadratic convergence and because the factorized tangent stiffness matrices can be used later in the sensitivity analysis of the optimization problem. The Newton-Raphson incremental-iterative solution procedure is graphically displayed in Figure 3.4.

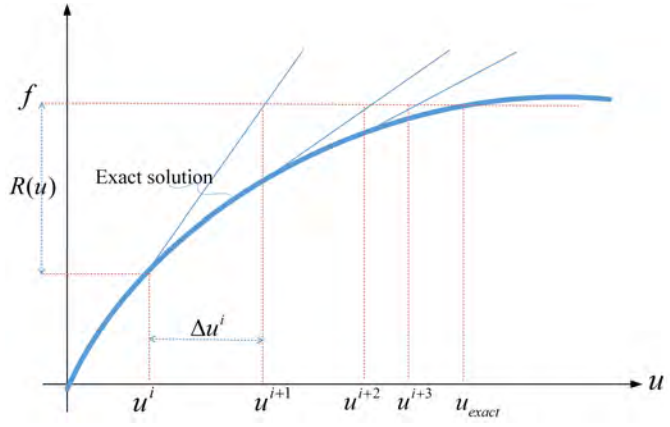

FIGURE 3.4: Illustration of the Newton-Raphson iterative procedure for a single DOF system

3.4.1 Newton-Raphson scheme

The basic Newton-Raphson scheme is by the control over the force vector. The residual force is defined as the difference between the external and internal forces,

$$\mathbf{R}(\mathbf{u}) = {}^{t+\Delta t}\mathbf{f}_{ext} - {}^{t+\Delta t}\mathbf{f}_{int} \tag{3.25}$$

where $\mathbf{f}_{ext}$ and $\mathbf{f}_{int}$ are the vectors of external and internal nodal forces respectively. It is assumed that the external loads do not depend on the displacements and are constant.

The system is in equilibrium if the residual force is equal to zero, so the goal of this procedure is to solve the residual equations

$$\mathbf{R}(\mathbf{u}) = \mathbf{0}. \tag{3.26}$$

Assume that in the iterative solution we have evaluated ${}^{t+\Delta t}\mathbf{u}^{(i-1)}$. Expanding a Taylor series expansion and neglecting high terms we obtain

$$\mathbf{R}(\mathbf{u}) = \mathbf{R}({}^{t+\Delta t}\mathbf{u}^{(i-1)}) + \left.\frac{\partial \mathbf{R}(\mathbf{u})}{\partial \mathbf{u}}\right|_{{}^{t+\Delta t}\mathbf{u}^{(i-1)}} (\mathbf{u} - {}^{t+\Delta t}\mathbf{u}^{(i-1)}) \tag{3.27}$$

Substituting Equation (3.25) into Equation (3.27) with the assumption that external forces are constant and independent of the displacements we obtain

$$\left.\frac{\partial \mathbf{f}_{int}}{\partial \mathbf{u}}\right|_{{}^{t+\Delta t}\mathbf{u}^{(i-1)}} (\mathbf{u} - {}^{t+\Delta t}\mathbf{u}^{(i-1)}) = {}^{t+\Delta t}\mathbf{f}_{ext} - {}^{t+\Delta t}\mathbf{f}_{int} \tag{3.28}$$

Defining the displacement and increment correction $\Delta\mathbf{u}^{(i)}$ and recognizing the tangent stiffness matrix ${}^{t+\Delta t}\mathbf{K}^{(i-1)}$ we obtain

$${}^{t+\Delta t}\mathbf{K}^{(i-1)}\Delta\mathbf{u}^{(i)} = {}^{t+\Delta t}\mathbf{f}_{ext} - {}^{t+\Delta t}\mathbf{f}_{int}^{(i-1)}. \tag{3.29}$$

From the equation's solution, the next displacement approximation in calculated by adding the iterative correction

$${}^{t+\Delta t}\mathbf{u}^{(i)} = {}^{t+\Delta t}\mathbf{u}^{(i-1)} + \Delta\mathbf{u}^{(i)} \tag{3.30}$$

The internal forces and tangent stiffness are evaluated for the next iteration step. The iterations are continued until appropriate convergence is satisfied. Throughout this thesis, the value of the iterative unbalanced forces is measured relatively to the external forces added in the current increment:

$$\frac{\left\| {}^{t+\Delta t}\mathbf{f}_{ext} - {}^{t+\Delta t}\mathbf{f}_{int}^{(i-1)} \right\|_2}{\left\| {}^{t+\Delta t}\mathbf{f}_{ext} - {}^{t}\mathbf{f}_{ext} \right\|_2} \leq \varepsilon. \tag{3.31}$$

When this relative norm of the residual forces is smaller than ε, it is said that the incremental solution converged. A reasonable magnitude of ε for structural analysis is 10^{-6} or smaller.

Full Newton-Raphson (FNR) method refers to the case where the tangent stiffness matrix is factorized every iteration. Then the computational effort is dominated by the calculation and factorization of the tangent stiffness matrix. For large order systems the computational effort can be excessively high.

Modified Newton-Raphson method For reducing the total computational cost it is possible to re-use available factorizations. For instance, factorizing the tangent stiffness matrix at the beginning of increment t and then using this factorized tangent stiffness matrix for all iterations within this increment. This is known as the Modified Newton-Raphson method (MNR). Convergence will slow down but fewer factorizations will be needed for the solution. It is difficult to know in advance which of the two procedures will lead to a lower computational cost, but the convergence rate of FNR is promised to be higher. In Chapter 6 the FNR and MNR are utilized for the solution of nonlinear structures in the topology optimization process.

Displacement control In some cases it is preferable to increment a prescribed displacement instead of a prescribed load. An external normalized force vector is set and a single displacement is prescribed. The total number of unknowns remains unchanged except for the prescribed displacement which is replaced with an unknown load factor that multiplies the normalized external load. Equation (3.29) is rewritten according to the prescribed displacement,

$$^{t+\Delta t}\mathbf{K}^{(i-1)}\Delta\mathbf{u}^{(i)} = {}^{t+\Delta t}\theta\hat{\mathbf{f}}_{ext} - {}^{t+\Delta t}\mathbf{f}_{int}^{(i-1)}. \tag{3.32}$$

Here θ is the unknown load factor and $^{t+\Delta t}\theta\hat{\mathbf{f}}_{ext}$ is the external normalized load vector. For topology optimization the prescribed displacement procedure is very useful and can improve the numerical stability. In Chapter 6 this method is used.

3.4.2 Linearized buckling analysis

Estimating the maximum load a structure can sustain before buckling is an essential goal of nonlinear analysis. Incremental analysis with the nonlinear formulation presented above is one way to calculate the load magnitude. An advantage of this full nonlinear analysis is that the complete structural behavior can be evaluated with little assumptions

made about the structure. Moreover, the procedure works for any structure with any imperfections. However, the full nonlinear analysis is computationally expensive. An alternative is to analyze the structure using linear buckling analysis. The main assumption that needs to be taken in account is that the pre-buckling behavior of the structure is linear and structural deformations are relevantly small. For achieving the structural behavior according to this assumption, we define the parameter $\tilde{\beta}$ as shown in Figure 3.6. The smaller the magnitude of $\tilde{\beta}$ is, the more likely that the linearized buckling assumptions will be reliable.

Linear buckling analysis is based on solving an eigenvalue problem and finding the smallest positive eigenvalue, namely the buckling load. This can be a reasonable estimate of the actual collapse load when the pre-buckling displacements are relatively small.

FIGURE 3.5: A demonstration of a possible instable structure

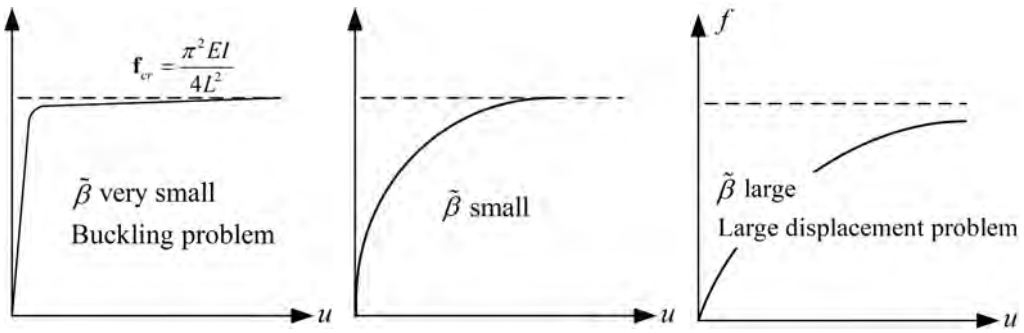

(A) (B) (C)

FIGURE 3.6: Depending on the size of the perturbation β three types of structural response are illustrated (Bathe, 2006)

Linearized buckling eigenvalue analysis takes place as follows: A prescribed external load $\mathbf{f}_{ext}$ is applied to the structure with its magnitude necessarily smaller than required to cause geometric instability in the structure. Once the resulting linear displacement solution $\mathbf{u}$ is obtained by solving ${}^0\mathbf{K}_L\mathbf{u} = \mathbf{f}_{ext}$, where ${}^0\mathbf{K}_L$ is the initial linear stiffness matrix. For calculating the tangent stiffness matrix at the collapse time τ, we perform a linearized buckling analysis. We assume that at any time

$$^{\tau}\mathbf{K} = {}^{t-\Delta t}\mathbf{K} + \tilde{\beta}({}^{t}\mathbf{K} - {}^{t-\Delta t}\mathbf{K}). \tag{3.33}$$

$$^{\tau}\mathbf{f}_{ext} = {}^{t-\Delta t}\mathbf{f}_{ext} + \tilde{\beta}({}^{t}\mathbf{f}_{ext} - {}^{t-\Delta t}\mathbf{f}_{ext}). \tag{3.34}$$

When the initial step is preformed at time $\Delta t = t$, and small pre-buckling displacements are considered. The initial stiffness matrix contains only the linear part from Equation 3.23. The equations above can be rewritten

$$^{\tau}\mathbf{K} = {}^{0}\mathbf{K_L} + \tilde{\beta}({}^{t}\mathbf{K} - {}^{0}\mathbf{K_L}). \tag{3.35}$$

$$^{\tau}\mathbf{f}_{ext} = \tilde{\beta}^{t}\mathbf{f}_{ext}. \tag{3.36}$$

For simplicity, the time subscript notation is omitted and the nonlinear stiffness matrix is subscript by $\mathbf{K}_G$. Due to the small deformations assumption this nonlinear stiffness matrix is equivalent to the nonlinear part from Equation (3.23).

$$^{\tau}\mathbf{K} = \mathbf{K}_L + \tilde{\beta}\mathbf{K}_G. \tag{3.37}$$

$\mathbf{K}_G$ is the nonlinear stiffness matrix equivalent to the nonlinear part from Equation (3.23). The linear stiffness matrix is the same as in linear problems, because the assumption of small deformations for pre-buckling loads. It is also assumed that the nonlinear stiffness matrix is zero in the undeformed configuration and that it is scaled linearly with $\tilde{\beta}$ during the force loading. The structure loses its stability when the tangent stiffness matrix becomes singular. The physical phenomena of buckling is represented by the mathematical criterion

$$\left|\mathbf{K}_L + \tilde{\beta}\mathbf{K}_G\right| = 0 \tag{3.38}$$

or

$$(\mathbf{K}_L + \tilde{\beta}\mathbf{K}_G)\mathbf{\Phi} = 0 \tag{3.39}$$

where $\mathbf{\Phi}$ is the eigenvector corresponding to the appropriate eigenvalue. After obtaining the buckling load factor $\tilde{\beta}$, the buckling load is calculated by

$$\mathbf{f}_{buckling} = \tilde{\beta}_1 \mathbf{f}_{ext} \tag{3.40}$$

where $\tilde{\beta}_1$ is the smallest eigenvalue and $\mathbf{f}_{ext}$ is the load vector for the first load step. As $\mathbf{K}_L$ is positive definite and as $\mathbf{K}_G$ may not be so, it is convenient to work with $\tilde{\lambda} = 1/\tilde{\beta}$ as the eigenvalue (Bendsøe and Sigmund, 2003). Thus, Equation (3.39) is modified to

$$(\mathbf{K}_G + \tilde{\lambda}\mathbf{K}_L)\mathbf{\Phi} = 0. \tag{3.41}$$

Linearized buckling eigenvalue analysis for topology optimization is an efficient way to obtain structures with high stability that are less sensitive to imperfections. In Chapter 4 efficient buckling reanalysis is developed, based on the combined approximation approach. In Chapter 7 the eigenvalue problem is assimilated in the optimization formulation for several examples.

Chapter 4

Reanalysis of structures

During the design process, structural analysis is preformed many times to determine the structural response under a set of loads and boundary conditions. Nowadays, engineers are dealing with complex models with a demand for high accuracy of the results and high resolution of the structural model. As a result, significant difficulties occur in terms of computational effort. Even with the continuously developed of computer processing the CPU running time is still extremely high.

Reanalysis methods where developed for this exact reason as mentioned above in Chapter 2. The Combined approximation (CA) method proposed by Kirsch (Kirsch, 2008) is utilized as a reanalysis tool in this work and is presented in this chapter.

4.1 Static reanalysis

Linear static reanalysis is useful for a wide range of applications in structural design problems. For the static linear case the solution is obtained by solving the equilibrium equations for a given initial structure

$$\mathbf{K}_0\mathbf{u}_0 = \mathbf{f}_0 \tag{4.1}$$

where $\mathbf{K}_0$ is the stiffness matrix; $\mathbf{f}$ is the load vector and $\mathbf{u}_0$ is the displacement vector solution of the equations. In an optimization process, $\mathbf{K}_0$ is a stiffness matrix from a

previous optimization iteration usually given in its Cholesky decomposed form

$$\mathbf{K}_0 = \mathbf{U}_0^T \mathbf{U}_0 \tag{4.2}$$

where $\mathbf{U}_0$ is an upper triangular matrix.
Consider a new structure to be analyzed.

$$\mathbf{K}\mathbf{u} = \mathbf{f} \tag{4.3}$$

with the corresponding stiffness matrix $\mathbf{K}$ and displacement vector $\mathbf{u}$ and $\mathbf{f}$ is the same load vector which is assumed to be constant and design independent in this work. The main idea of the CA approach is to obtain the solution of the new structure in an approximated manner, consequently saving computational effort. The modified stiffness matrix can be composed

$$\mathbf{K} = \mathbf{K}_0 + \Delta\mathbf{K} \tag{4.4}$$

where $\Delta\mathbf{K}$ are the changes in the stiffness matrix. For calculating the updated displacement vector $\mathbf{u}$ the reanalysis equations takes place as follows,

$$(\mathbf{K}_0 + \Delta\mathbf{K})\mathbf{u} = \mathbf{f}_0. \tag{4.5}$$

4.1.1 Reduced basis method

Structural optimization includes solving repeatedly a large system of simultaneous equations in order to obtain the response of the structure every iteration. As mentioned, this process is computationally expensive, especially for nonlinear analysis. The main feature of the reduced basis approach is transforming a problem with a large number of DOF into a much smaller one with fewer DOF. The structural response if found by an approximation using a linear combination of pre-selected basis vectors. The new problem is then set in terms of a small number of unknown coefficients of the basis vectors. The computational efficiency is thanks to the fact that for evaluating the response only the corresponding small system of equations must be solved. For the linear static reanalysis by CA we assume that the displacement vector $\mathbf{u}$ can be approximated by a linear

combination of pre-selected s linerly independet basis vectors

$$\tilde{\mathbf{u}} = y_1\mathbf{u}_1 + y_2\mathbf{u}_2 + y_3\mathbf{u}_3 + ... + y_s\mathbf{u}_s = \mathbf{R}_B\mathbf{y} \tag{4.6}$$

where y is the vector of unknown coefficients; s is a relatively small number compared to the number of DOF; $\mathbf{R}_B$ is the $n \times s$ matrix of the basis vectors

$$\begin{aligned} \mathbf{R}_B &= [\mathbf{u}_1, \mathbf{u}_2, ..., \mathbf{u}_s] \\ \mathbf{y}^T &= [y_1, y_2, ..., y_s]. \end{aligned} \tag{4.7}$$

Substituting Equation (4.6) into Equation (4.3) and pre multiplying the equation by $\mathbf{R}_B^T$ provides

$$\mathbf{R}_B^T\mathbf{K}\mathbf{R}_B\mathbf{y} = \mathbf{R}_B^T\mathbf{f}. \tag{4.8}$$

The reduced basis subspace is a much smaller set of equilibrium equations approximated by a smaller system of equations for the unknowns y. Introducing the notation of the reduced stiffness matrix and load vector

$$\mathbf{K}_B = \mathbf{R}_B^T\mathbf{K}\mathbf{R}_B \qquad \mathbf{f}_B = \mathbf{R}_B^T\mathbf{f} \tag{4.9}$$

finally the system to be solved is

$$\mathbf{K}_B y = \mathbf{f}_B. \tag{4.10}$$

The matrix $\mathbf{K}_B$ is full, symmetric and a much smaller matrix than the original $\mathbf{K}$ stiffness matrix. Meaning that computing the $s \times s$ system is more efficient than solving the exact $n \times n$ original system.

4.1.2 Determination of the basis vectors

The first terms of the binomial series expantion are used as basis vectors in the CA approach. Pre-multiplying both side of Equation (4.5) by $\mathbf{K}_0^{-1}$ gives

$$\mathbf{K}_0^{-1}(\mathbf{K}_0 + \Delta\mathbf{K})\mathbf{u} = \mathbf{K}_0^{-1}\mathbf{f}_0. \tag{4.11}$$

Rearranging the multiplied equation and using the known previous solution of Equation (4.1), where $\mathbf{I}$ is an identity matrix and defining the matrix $\mathbf{B}$ we obtain

$$(\mathbf{I} + \mathbf{K}_0^{-1}\Delta\mathbf{K})\mathbf{u} = \mathbf{u}_0 \tag{4.12}$$

$$\mathbf{B} = \mathbf{K}_0^{-1}\Delta(\mathbf{K}) \tag{4.13}$$

leading to the calculation of the new displacement vector of the modified structure

$$\mathbf{u} = (\mathbf{I} + \mathbf{B})^{-1}\mathbf{u}_0. \tag{4.14}$$

By expanding $(\mathbf{I} + \mathbf{B})^{-1}$ by the binomial series expansion

$$(\mathbf{I} + \mathbf{B})^{-1} = \mathbf{I} - \mathbf{B} + \mathbf{B}^2 - \mathbf{B}^3 + ... \tag{4.15}$$

and substituting Equation (4.15) in to Equation (4.14) we obtain the series

$$\mathbf{u} = (\mathbf{I} - \mathbf{B} + \mathbf{B}^2 - \mathbf{B}^3 + ...)\mathbf{u}_0. \tag{4.16}$$

The first term of the series is defined as $\mathbf{u}_0$. Additional terms can be easily calculated with the following recurrence relation

$$\mathbf{u}_0 = \mathbf{K}_0^{-1}\mathbf{f} \tag{4.17}$$

$$\mathbf{u}_i = -\mathbf{B}\mathbf{u}_{i-1} \tag{4.18}$$

Note that the first term is known from the previous optimization step. The other terms are easily computed by forward and backward substitutions based on the factorized matrix $\mathbf{K}_0 = \mathbf{U}_0^T\mathbf{U}_0$, given as-well from the previous optimization step.

4.1.3 Orthogonalization of the basis vectors

The Gram-Schmidt orthogonalization scheme is utilized for generating an improved set of basis vector. The new set of basis vectors are formed such that the set of reduced analysis equations are uncoupled with respect to $\mathbf{K}$. Identical results are achieved with the new set of equations or the original one. The advantage of using the orthogonalization procedure

is that all the expressions for evaluating the displacements become explicit functions of the design variables. Thus, more basis vectors can be added without modifying the calculations that were achieved for previous terms. Additionally, results obtained by the orthogonalized basis vectors are more well-conditioned. The goal is to transfer the reduced system of Equation (4.10) to an uncoupled set of equations with respect to $\mathbf{K}$. For this purpose a new set of vectors $\mathbf{v}_i$ are generated from the original vectors $\mathbf{u}_i$, such that

$$\mathbf{v}_i^T \mathbf{K} \mathbf{v}_j = \delta_{ij} \quad i, j = 1, 2, ..., s \tag{4.19}$$

where δ_{ij} is the kronecker delta ($\delta_{ij} = 0 \quad (i \neq j); \quad \delta_{ii} = 1$). If the conditions in Equation (4.19) are satisfied, $\mathbf{v}_i$ and $\mathbf{v}_j$ are orthogonal with respect to $\mathbf{K}$. The procedure for generating the new set of basis vectors is as follows. The first normalized vector is calculated

$$\mathbf{v}_1 = \frac{\mathbf{u}_1}{|\mathbf{u}_1^T \mathbf{K} \mathbf{u}_1|^{1/2}} \tag{4.20}$$

For generating the second normalized vector $\mathbf{v}_2$ a non-normalized vector $\overline{\mathbf{v}}_2$ is composed from a linear combination of $\mathbf{v}_1$ and $\mathbf{r}_2$

$$\overline{\mathbf{v}}_2 = \mathbf{r}_2 - \alpha \mathbf{v}_1 \tag{4.21}$$

where α is chosen to satisfy the orthogonality condition of Equation (4.19)

$$\overline{\mathbf{v}}_2 \mathbf{K} \mathbf{v}_1 = 0. \tag{4.22}$$

Substituting Equation (4.21) in to Equation (4.22) we obtain

$$\overline{\mathbf{v}}_2^T \mathbf{K} \mathbf{v}_1 = \mathbf{u}_2^T \mathbf{K} \mathbf{v}_1 - \alpha \mathbf{v}_1^T \mathbf{K} \mathbf{v}_1 = 0 \tag{4.23}$$

since $\mathbf{v}_1^T \mathbf{K} \mathbf{v}_1 = 1$ the equation above becomes

$$\alpha = \mathbf{u}_2^T \mathbf{K} \mathbf{v}_1. \tag{4.24}$$

Substituting Equation (4.24) into Equation (4.21) yields

$$\overline{\mathbf{v}}_2 = \mathbf{u}_2 - (\mathbf{u}_2^T \mathbf{K} \mathbf{v}_1) \mathbf{v}_1. \tag{4.25}$$

After normalizing $\overline{\mathbf{v}}_2$ we finally get the normalized second vector

$$\mathbf{v}_2 = \frac{\overline{\mathbf{v}}_2}{|\overline{\mathbf{v}}_2^T \mathbf{K} \overline{\mathbf{v}}_2|^{1/2}} \tag{4.26}$$

As mentioned above, additional vectors can be calculated without modifying previous terms. The general expression for all non-normalized vectors is

$$\overline{\mathbf{v}}_i = \mathbf{u}_i - \sum_{j=1}^{i-1} (\mathbf{u}_i^T \mathbf{K} \mathbf{v}_j) \mathbf{v}_j \tag{4.27}$$

and for the normalized vector

$$\mathbf{v}_i = \frac{\overline{\mathbf{v}}_i}{|\overline{\mathbf{v}}_i^T \mathbf{K} \overline{\mathbf{v}}_i|^{1/2}} \tag{4.28}$$

where $\overline{\mathbf{v}}_i$ and $\mathbf{v}_i$ are the i'th non-normalized and normalized vectors.

Further on, for evaluating the displacements the new orthogonal basis vectors are used as follows. From Equation (4.4) and Equation (4.19) it can be noticed that the diagonal elements of the new reduced stiffness matrix equals unity and all other elements are zero. Therfore, the new reduced stiffness matrix if the identity matrix $\mathbf{I}$ and we get

$$\mathbf{I}\mathbf{z} = \mathbf{z} = \mathbf{V}_B^T \mathbf{f} \tag{4.29}$$

where $\mathbf{V}_B$ is an $n \times s$ matrix containing the orthogonal basis vectors and z is a vector of s unknown coefficients.

$$\mathbf{V}_B = [\mathbf{v}_1, \mathbf{v}_2, ..., \mathbf{v}_s] \tag{4.30}$$

$$\mathbf{z}^T = z_1, z_2, ..., z_3 \tag{4.31}$$

The coefficients z can be directly determined by Equation (4.29). Since this system is uncoupled, the final displacements are calculated by an explicit expression

$$\tilde{\mathbf{u}} = \mathbf{V}_B \mathbf{z} = \mathbf{V}_B (\mathbf{V}_B^T \mathbf{f}) \tag{4.32}$$

Finally, an additively separable quadratic function of the basis vectors $\mathbf{v}_i$ can be developed to calculate the displacements

$$\tilde{\mathbf{u}} = \sum_{i=1}^{s} \mathbf{v}_i (\mathbf{v}_i^T \mathbf{f}) \tag{4.33}$$

4.2 Buckling reanalysis

Linearized buckling analysis is based on solving an eigenvalue problem and finding the smallest positive eigenvalue, namely the buckling load. When buckling analysis is assimilated in topology optimization, the main computational effort is spent on the solution of the eigenproblem. Topology optimization problems are normally defined by a large number of design variables and degrees of freedom. Exact solutions of these large problems may require extremely high computational cost. In this chapter effective procedures for buckling reanalysis, based on the CA approach, are presented.

4.2.1 Problem formulation

For a given initial reference structure, assuming linear buckling behavior, we have a linear stiffness matrix $\mathbf{K}_{L,0}$ and the corresponding geometric stiffness matrix $\mathbf{K}_{G,0}$. The 0 subscript notation is for the reference structure. The initial i'th buckling load factor $\tilde{\beta}_{0i}$ and the eigenvector $\mathbf{\Phi}_{0i}$ can be calculated from the solution of the initial eigenvalue problem from Equation (3.39). As mentioned above in Chapter 3 it is convenient to use $\tilde{\lambda}_{0i} = \dfrac{1}{\tilde{\beta}_{0i}}$. Substituting $\tilde{\lambda}_{0i}$ into Equation (3.39) we obtain

$$\mathbf{K}_{G,0}\mathbf{\Phi}_{0i} + \tilde{\lambda}_{0i}\mathbf{K}_{L,0}\mathbf{\Phi}_{0i} = \mathbf{0}. \tag{4.34}$$

Now for a new structure assume that the changes in the linear and geometrical stiffness matrices, $\Delta\mathbf{K}_{L,0}$ and $\Delta\mathbf{K}_{G,0}$ are given by

$$\Delta\mathbf{K}_{L,0} = \mathbf{K}_L - \mathbf{K}_{L,0} \qquad \Delta\mathbf{K}_{G,0} = \mathbf{K}_G - \mathbf{K}_{G,0}. \tag{4.35}$$

The modified analysis equations to be solved are

$$\mathbf{K}_G\mathbf{\Phi}_i + \tilde{\lambda}_i\mathbf{K}_L\mathbf{\Phi}_i = \mathbf{0}. \tag{4.36}$$

Substituting Equation (4.35) into Equation (4.36) and the reanalysis problem takes the form of

$$\mathbf{K}_G\mathbf{\Phi}_i + \tilde{\lambda}_i(\mathbf{K}_{L,0} + \Delta\mathbf{K}_{L,0})\mathbf{\Phi}_i = 0. \tag{4.37}$$

Solving Equation (4.37) in an approximated manner is the main intention of the reanalysis method. Namely, evaluating in an efficient way and with high accuracy the modified eigenpairs λ and $\mathbf{\Phi}$ due to changes in the design. We assume that the buckling mode shape of the new design can be approximated by a linear combination of s preselected, linearly independent basis vectors $\mathbf{r}_1, \mathbf{r}_2 ... \mathbf{r}_s$. Similar to Equation (4.6) in the static linear reanalysis case,

$$\mathbf{\Phi}_i = y_1\mathbf{r}_1 + y_2\mathbf{r}_2 + ... + y_s\mathbf{r}_s = \mathbf{R}_B\mathbf{y} \tag{4.38}$$

where s is the chosen number of preselected basis vectors and is much smaller than the number of degrees of freedom n; $\mathbf{R}_B$ is a $n \times s$ matrix containing the basis vectors and $\mathbf{y}$ is the vector of unknown coefficients, as presented above in Equation (4.7).

A reduced basis method as in Section 4.1.1 is used for modifying the equations and approximating the solution by a smaller system of equations. Substituting Equation (4.38) into Equation (4.36) and pre-multiplying the equation by $\mathbf{R}_B$ gives the $s \times s$ reduced basis system of equations

$$\mathbf{R}_B^T\mathbf{K}_G\mathbf{R}_B\mathbf{y} + \tilde{\lambda}\mathbf{R}_B^T\mathbf{K}_L\mathbf{R}_B\mathbf{y} = 0. \tag{4.39}$$

Presenting the notation of the reduced linear and geometrical stiffness matrices

$$\mathbf{K}_{L,R} = \mathbf{R}_B^T\mathbf{K}\mathbf{R}_B \qquad \mathbf{K}_{G,R} = \mathbf{R}_B^T\mathbf{K}_G\mathbf{R}_B. \tag{4.40}$$

Substituting Equation (4.40) into Equation (4.39), the reduced eigenvalue problem is obtained

$$\mathbf{K}_{G,R}\mathbf{y} + \tilde{\lambda}\mathbf{K}_{L,R}\mathbf{y} = 0. \tag{4.41}$$

This reduced eigenproblem is much more economical in computational terms due to the fact that the problem is significantly smaller. For the exact solution computing the original problem is a large $n \times n$ size of problem. The reduced one is $s \times s$ where $s \ll n$ and therefore is less costly.

For evaluating the eigenvector the solution of the reduced $s \times s$ eigenproblem for the first eigenvalue $\tilde{\lambda}_1$ and the corresponding eigenvector $\mathbf{y}_1$ takes place

$$\mathbf{K}_{G,R}\mathbf{y}_1 + \tilde{\lambda}_1\mathbf{K}_{L,R}\mathbf{y}_1 = 0. \tag{4.42}$$

The next step is to calculate the eigenvector $\mathbf{\Phi}$ as follows from Equation (4.38)

$$\mathbf{\Phi}_i = \mathbf{R}_B \mathbf{y}_1. \tag{4.43}$$

The eigenvalue is simply the result of solving Equation (4.42). The scheme for determining the basis vector is presented below.

4.2.2 Determination of the basis vectors

As shown above, the buckling mode shape of the new design is approximated by a linear combination of s preselected linearly independent basis vectors $\mathbf{r}_1, \mathbf{r}_2 ... \mathbf{r}_s$. Starting with pre-multiplying Equation (4.37) by $\mathbf{K}_{L,0}^{-1}$ we obtain

$$(\mathbf{I} + \mathbf{K}_{L,0}^{-1} \Delta \mathbf{K}_{L,0}) \mathbf{\Phi}_i + \tilde{\beta}_i \mathbf{K}_{L,0}^{-1} \mathbf{K}_G \mathbf{\Phi}_i = 0 \tag{4.44}$$

The matrix $\mathbf{B}$ and vector $\mathbf{r}_1$ are defined as

$$\mathbf{B} = \mathbf{K}_{L,0}^{-1} \Delta \mathbf{K}_{L,0} \tag{4.45}$$

$$\mathbf{r}_1 = \tilde{\beta}_i \mathbf{K}_{L,0}^{-1} \mathbf{K}_G \mathbf{\Phi}_i. \tag{4.46}$$

Substituting $\mathbf{B}$ and $\mathbf{r}_1$ in Equation (4.44) we obtain

$$(\mathbf{I} + \mathbf{B}) \mathbf{\Phi}_i = \mathbf{r}_1. \tag{4.47}$$

Pre-multiplying Equation (4.47) by $(\mathbf{I} + \mathbf{B})^{-1}$ and expanding

$$(\mathbf{I} + \mathbf{B})^{-1} = \mathbf{I} - \mathbf{B} + \mathbf{B}^2 - \mathbf{B}^3 + ... \tag{4.48}$$

we obtain the binomial series

$$\mathbf{\Phi}_i = (\mathbf{I} - \mathbf{B} + \mathbf{B}^2 - \mathbf{B}^3 + ...) \mathbf{r}_1. \tag{4.49}$$

The terms of Equation (4.49) are considered as basis vectors, with the first basis vector already defined in Equation (4.46). Since multiplying the modes by a scaler does not effect the results, $\tilde{\beta}$ can be omitted . Because $\mathbf{r}_1$ is unknown it is convenient to assume

the known expression

$$\mathbf{r}_1 = \mathbf{K}_{L,0}^{-1}\mathbf{K}_G\mathbf{\Phi}_{0i} \tag{4.50}$$

Similar to static reanalysis presented above, additional basis vectores are easily calculated by

$$\mathbf{r}_j = -\mathbf{B}_{j-1} \qquad (j = 2, .., s) \tag{4.51}$$

There are different ways to normalize the basis vectors, one possibility is as follows.

Consider again the non-normalized first basis vector

$$\mathbf{r}_1 = \mathbf{K}_{L,0}^{-1}\mathbf{K}_G\mathbf{\Phi}_{0i} \tag{4.52}$$

The first basis vector normalization is

$$\hat{\mathbf{r}}_1 = \frac{\mathbf{r}_1}{(\mathbf{r}_1^T\mathbf{K}_{G,0}\mathbf{r}_1)^{1/2}} \tag{4.53}$$

Additional non normalized vectors are calculated as in Equation (4.51) and the normalized basis vectors are calculated by

$$\hat{\mathbf{r}}_j = \frac{\mathbf{r}_j}{(\mathbf{r}_j^T\mathbf{K}_{G,0}\mathbf{r}_j)^{1/2}} \qquad (j = 2, .., s) \tag{4.54}$$

The improved basis vectors help to achieve with a small number of basis vectors, high accuracy of the first mode shapes. High modes may be less accurate. The Gram-Schmidt orthogonalization scheme can also be utilized in this case for generating an improved set of basis vector. The process is identical to the scheme presented above in Section 4.1.3. In Chapter 7 the CA method is used for reducing the effort instead of solving the eigenvalue equation of the buckling problem.

Error evaluation

To evaluate the errors from the CA procedure for buckling analysis, we define the error vector of the eigenvalue problem equations.

$$\mathbf{R} = \mathbf{K}_G\mathbf{\Phi}_i + \tilde{\lambda}_i\mathbf{K}_L\mathbf{\Phi}_i. \tag{4.55}$$

Where $\tilde{\lambda}_i$ and $\mathbf{\Phi}_i$ are the approximated eigenvalue and eigenvector. The following relative norm is used in this work as a measure for evaluating the error:

$$\varepsilon(\mathbf{R}) = \frac{||R||}{||\mathbf{K}_L \mathbf{\Phi}_i||} \tag{4.56}$$

Chapter 5

Reanalysis in truss optimization

In this chapter assimilation of reanalysis in truss topology optimization is presented. The main objectives of the investigation are: First to present the integration of CA in truss reanalysis; Second, to compare the numerical efficiency of two different optimization problems with reanalysis by CA. For both, we examine the influence of a stiff reference stiffness matrix.

In Section 5.1 two different formulations of the optimization problem are presented: Minimum volume under a compliance constraint and minimum compliance under a volume constraint. The sensitivity analysis equations are derived for solving both problems. In Section 5.2, two types of numerical examples are presented. First reanalysis of different truss structures with different reference stiffness matrices is presented. Later, the integration of reanalysis in truss optimization is examined in relation to the two types of problem formulations.

5.1 Truss topology optimization

In this chapter two classical optimization formulations are used. In this section the formulations are presented. The ground structure truss is modeled as presented in chapter 3.2 where the "densities" of the truss bars are used as continuous variables for defining the truss topology optimization problem. Furthermore, for the problem solution, derivatives of the objective and constraint functions are computed and used for the sensitivity analysis.

5.1.1 Problem formulations

The first problem is a single load minimum compliance problem with a volume constraint, as presented in Equation (5.1). V^* is a positive constant volume value larger than zero that is set in the initialization step of the process. The problem is also referred to as the "Maximum stiffens" problem,

$$\begin{aligned} \min_{\boldsymbol{\rho}} \quad & f_c = \mathbf{f}^T\mathbf{u} \\ \text{S.T} \quad & g_v = \sum_{e=1}^{nbar} (\rho_e a_e l_e) \leq V^* \\ & 0 < \rho_{min} \leq \rho_e, \quad e = 1...nbar \\ with : \; & \mathbf{Ku} = \mathbf{f} \end{aligned} \tag{5.1}$$

The optimization variables ρ_e are the densities of the bars and are bounded for numerical reasons by ρ_{min}; a_e is the bars cross-section area, which is set in the examples here to a value of 1 for all bars; l_e is the length of bar e; $\mathbf{f}$ is the load vector; $\mathbf{K}$ is the stiffness matrix and $\mathbf{u}$ is the unknown displacement vector that is found by solving the linear equilibrium equations. The second formulation is simply the vice versa version. The objective function is to minimize the volume of the structure under a given compliance constraint, presented in Equation (5.2):

$$\begin{aligned} \min_{\boldsymbol{\rho}} \quad & f_v = \sum_{e=1}^{nbar} (\rho_e a_e l_e) \\ \text{S.T} \quad & g_c = \mathbf{f}^T\mathbf{u} \leq C^* \\ & 0 < \rho_{min} \leq \rho_e, \quad e = 1...nbar \\ with : \; & \mathbf{Ku} = \mathbf{f} \end{aligned} \tag{5.2}$$

Here, C^* is a constant required value of the compliance constraint. Both of the problems are solved by the optimality criteria (OC) method that was mentioned above in Section 2.4.1.

5.1.2 Solution method

For the numerical examples in this chapter the solution is carried out by the classical optimality criteria (OC) update scheme. The Lagrangian $\mathcal{L}$ for a general nested problem

can be written as

$$\mathcal{L}(\rho, \Lambda) = f(\rho) + \Lambda g(\rho). \tag{5.3}$$

The KKT conditions are necessary and sufficient for the optimum solution, due to convexity of the problem. OC method aims to find that point where the KKT conditions are satisfied. From these conditions we observe that for a variable not governed by the box constraints

$$\begin{gathered} \frac{\partial \mathcal{L}}{\partial \rho_i} = \frac{\partial f(\boldsymbol{\rho})}{\partial \rho_i} + \Lambda \frac{\partial g(\boldsymbol{\rho})}{\partial \rho_i} = 0 \\ \boldsymbol{\rho}_{min} < \boldsymbol{\rho} < \boldsymbol{\rho}_{max} \end{gathered} \tag{5.4}$$

where Λ is the Lagrange multiplier. Rewriting Equation (5.4), we obtain

$$-\frac{\dfrac{\partial f(\rho)}{\partial \rho_i}}{\Lambda \dfrac{\partial g(\rho)}{\partial \rho_i}} = 1. \tag{5.5}$$

This relation can be referred to as the constant strain energy density. Within every design iteration, the material is distributed according to the relation above. The Lagrangian multiplier Λ corresponding to the constraint is found by a simple bi-section scheme. The density is redesigned until the constraint is satisfied up to a tolorance of 10^{-3} in our examples. The update scheme is:

$$\rho_e^{k+1} = \begin{cases} \max(\rho_e^k - \zeta, 10^{-6}) & \text{if } \rho_e^k B_e^k \leq \max(\rho_e^k - \zeta, 10^{-6}), \\ \min(\rho_e^k + \zeta, 1) & \text{if } \min(\rho_e^k + \zeta, 1) \leq \rho_e^k B_e^k, \\ \rho_e^k B_e^k & \text{otherwise.} \end{cases} \tag{5.6}$$

Here ζ is a move limit set to 0.2 for all examples in this chapter and with B_e^k given as

$$B_e^k = \left(-\frac{\dfrac{\partial f(\rho)}{\partial \rho_i}}{\Lambda \dfrac{\partial g(\rho)}{\partial \rho_i}} \right)^{0.8} \tag{5.7}$$

For the minimum compliance problem presented in Equation (5.1), the constraint functional is linear and the process presented above is quite simple. However, for the minimum volume formulation the constraint is a nonlinear compliance functional and a certain difficulty arises from this fact. The optimality criteria development in (Amir, 2015), with

approximations of the compliance constraint, is utilized in this case.

5.1.3 Sensitivity analysis

The OC method is gradient based and therefore the derivatives of the objective and constraint functions are necessary for the solution of the optimization problem. Design sensitivities of the volume functional are linear and therefore are computed in a simple way. On the other hand, for the compliance functional adjoint method is utilized in order to compute the design sensitivities. By adding a zero term to the compliance functional, we obtain the augmented function,

$$\tilde{f}_c(\boldsymbol{\rho}, \mathbf{u}) = \mathbf{f}^T\mathbf{u} - \boldsymbol{\lambda}^T\mathbf{R}(\boldsymbol{\rho}, \mathbf{u}) \tag{5.8}$$

where $\boldsymbol{\lambda}$ contains the adjoint unknown variables and $\mathbf{R}$ is the zero residual for the nested system of equations. The minus sign is arbitrary and is chosen for the convenience of the equations development. In this linear case, the relation leads to

$$\tilde{f}_c(\boldsymbol{\rho}, \mathbf{u}) = \mathbf{f}^T\mathbf{u} - \boldsymbol{\lambda}^T(\mathbf{f} - \mathbf{K}(\boldsymbol{\rho})\mathbf{u}). \tag{5.9}$$

With the assumption that the load is design independent, differentiation of the augmented function with respect to a certain element density is:

$$\frac{\partial f_c}{\partial \rho_e} = \mathbf{f}^T\frac{\partial \mathbf{u}}{\partial \rho_e} + \boldsymbol{\lambda}^T\frac{\partial \mathbf{K}}{\partial \rho_e}\mathbf{u} + \boldsymbol{\lambda}^T\mathbf{K}\frac{\partial \mathbf{u}}{\partial \rho_e}. \tag{5.10}$$

For avoiding the explicit computation of the displacement derivatives with respect to $\boldsymbol{\rho}$, all terms involving this derivative must sum to zero,

$$\mathbf{f}^T\frac{\partial \mathbf{u}}{\partial \rho_e} + \boldsymbol{\lambda}^T\mathbf{K}\frac{\partial \mathbf{u}}{\partial \rho_e}. \tag{5.11}$$

Since the stiffness matrix $\mathbf{K}$ is symmetric, the adjoint equation system is obtained,

$$\mathbf{K}\boldsymbol{\lambda} = -\mathbf{f}. \tag{5.12}$$

Resulting that the adjoint vector is $\boldsymbol{\lambda} = -\mathbf{u}$. Finally, the derivatives of the compliance functional is given by

$$\frac{\partial f_c}{\partial \rho_e} = \frac{\partial g_c}{\partial \rho_e} = -\mathbf{u}^T \frac{\partial \mathbf{K}}{\partial \rho_e} \mathbf{u} \tag{5.13}$$

where the stiffness matrix $\mathbf{K}$ is an explicit expression of the design variable ρ_e so the derivatives can be computed easily.

5.2 Numerical examples

The first numerical example is utilizing the CA and PCG methods as reanalysis tools for approximating the response of a linear truss structure submitted to a single load. Five different truss structures are considered and reanalysis by the CA and PCG method are applied between all the five to approximate the response. Second, a cantilever structure modeled with the ground structure approach was taken as an initial structure for a linear static topology optimization problem with two types of optimization formulations as presented above. Moreover, reanalysis by PCG was assimilated in the process of both formulations. In the last example, a so-called Michell structure was modeled and optimized in the same manner as in the previous example.

5.2.1 Reference design comparison

We start with the utilization of CA and PCG as reanalysis tools for approximating the response of linear truss structures from the topology optimization process. We follow the article presented above (Amir, 2015) where the results pointed out that stiff pre-conditioning is more effective for continuum structures. The idea is demonstrated by five different structures from five optimization steps, all with different compliance values. The problem is minimum compliance with volume constraint as presented in Equation (5.1) for a truss structure. Naturally, the formulation provides a "stiffer structure" every optimization cycle. The comparison takes place between all 20 options of matrix reanalysis and the results are compared in terms of PCG iterations. For instance structure number #1 is given in its decomposed form together with its displacement solution. Now for all the other structures the response is computed by reanalysis methods and reusing information from #1. Note, that the PCG method is equivalent to the CA method presented in Chapter 4 and each PCG iteration is equal to one basis vector. The

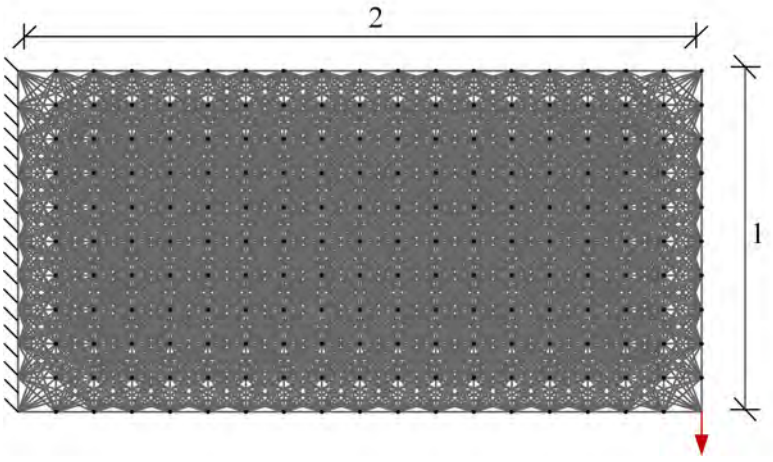

FIGURE 5.1: Initial cantilever ground structure subjected to a single load (arrow in red)

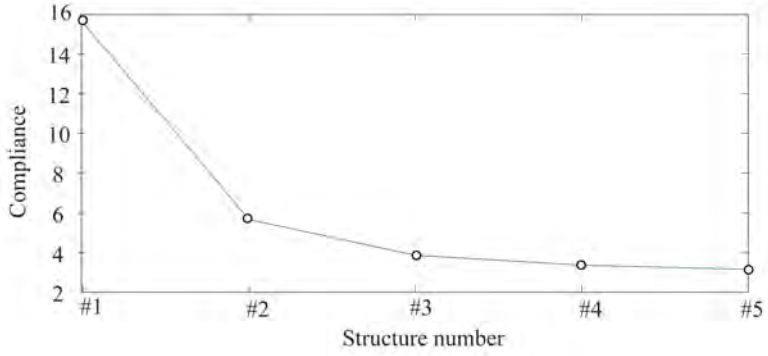

FIGURE 5.2: The value of compliance for each structure

efficiency of the procedure is compared in terms of PCG iterations or for the CA method by the number of basis vectors needed for convergence.

Consider the ground structure shown in Figure 5.1, with initial width in x direction of $L_x = 2$ and the height of $L_y = 1$. The domain is divided into 21 and 11 nodes in x and y directions respectively. The ground structure is assembled with 2878 bars and 462 degrees of freedom and the connectivity number is 3. The structure is subjected to a single load on one side and fixed on the other side as presented in the Figure 5.1. In this example, five different stiffness matrices were taken from five different optimization steps and the use of reanalysis for each of the matrices was examined.

For a demonstration of the CA and PCG equivalence, Figure 5.3 shows two reanalysis cases. Figure 5.3a presents the residual of the unbalanced force for the reanalysis of structure #5 by reusing the decomposed stiffness matrix and solution of structure #1. In Figure 5.3b the same is presented for the opposite case where structure #5 is the reference structure. For both of the cases reanalysis was performed by the standard CA,

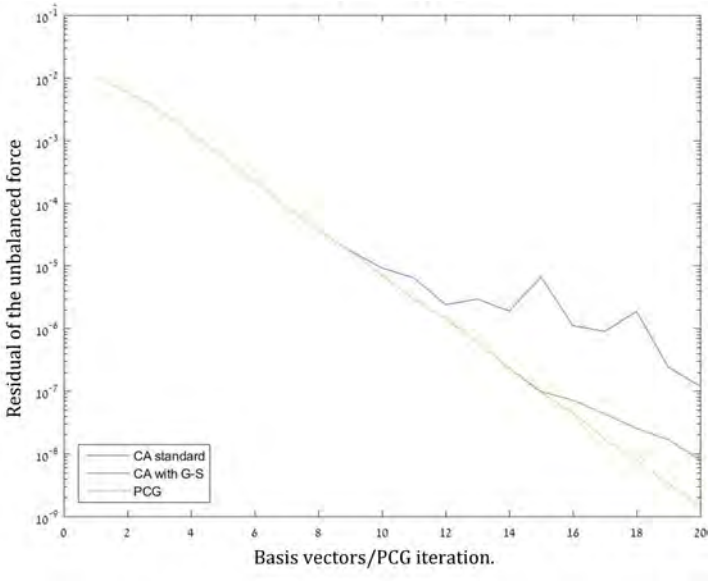

(A) Structure #5 reanalyzed with the reuse of structure #1

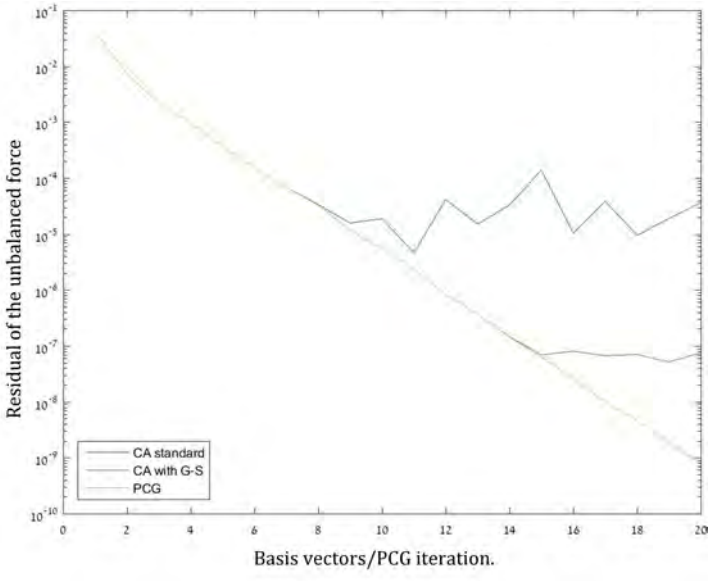

(B) Structure #1 reanalyzed with the reuse of structure #5

FIGURE 5.3: Residual of the unbalanced force for every additional basis vector or PCG iteration. For standard CA; Gram-Schmidt orthogonalization assimilated in CA; and PCG reanalysis.

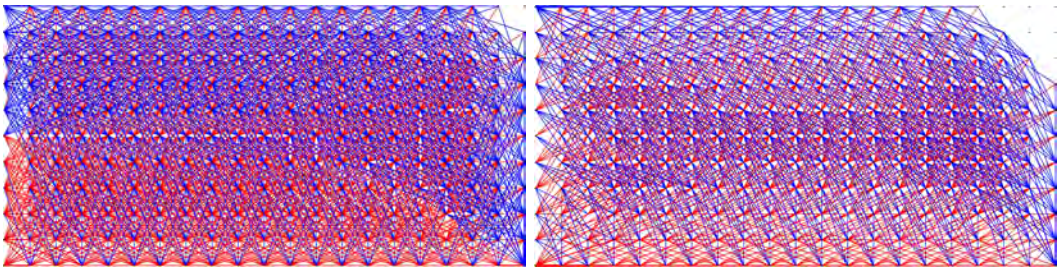

(A) Layout of structure #1 (B) Layout of structure #5

FIGURE 5.4: Layouts of structures with topology changes from the optimization process

CA with Gram-Shmidt orthogonalization and by the PCG method. As it can seen the stability of the orthogonalized CA and PCG is higher than the standard CA. As noted above the methods are practically equivalent and ons PCG iteration is equal to one basis vector.

We continue with the formulation of minimum compliance. As shown in Figure 5.2 the structure's stiffness at each step increases. Namely, the last stiffness matrix is the stiffest. PCG reanalysis is preformed between all five structures using a maximum of 1000 PCG iterations and a tolerance of $\varepsilon = 1e - 10$ for the unbalanced forces.

In Table 5.1 the number of PCG iteration required for convergence is presented where the maximum number of iteration allowed is 1000, if this number is reached the meaning is that the method did not converge. In Table 5.2, the condition numbers of the preconditioned system are presented as PCG's convergence is often associated to this value. The values on the lower side of Table 5.1 are the number of PCG iterations for reanalysis with a stiff pre-conditioner. As shown, most of the values are lower than the opposite value on the table. For instance from the table, when the response of structure #2 is reanalyzed by the reference structure number #4, the number of PCG iterations is 118. When structure #4 is reanalyzed by the reference structure number #2, the number of PCG iterations is 138. The conclusion for this case is that first reanalysis is more efficient for solving with the PCG method.

Table 5.2 presents the condition number of the pre-conditioned system and is associated with the efficiency of the convergence of PCG method. In this table, most of the lower valuer are smaller than the upper ones. Looking again at the reanalysis between structure #2 and #4. When the response of structure #2 is reanalyzed by the reference structure number #4, the condition number of the pre-conditioned system is $1.13e3$. When structure #4 is reanalyzed by the reference structure number #2, the condition

number is 1.35e3. In other words, the condition number of the stiff preconditioned system for reanalysis with PCG has a lower condition number than the vice versa reanalysis. From the results obtained above it is possible to identify a certain advantage of the stiff-preconditioning as the condition number of the pre-conditioned system is mostly lower.

TABLE 5.1: Number of PCG iterations for each reanalysis

	Reanalyesd design				
Reference design	1	2	3	4	5
1	-	371	422	843	981
2	352	-	88	138	198
3	407	78	-	50	69
4	1000	118	53	-	26
5	1000	189	63	26	-

TABLE 5.2: Condition number of the pre-conditioned system

	Reanalyesd design				
Reference design	#1	#2	#3	#4	#5
#1	-	1.66e5	1.04e6	1.54e7	1.24e7
#2	1.47e5	-	5.05e2	1.35e3	2.43e3
#3	3.69e5	7.11e2	-	1.34e2	2.57e2
#4	3.70e6	1.19e3	1.11e2	-	6.29e1
#5	3.21e6	3.31e3	1.82e2	5.90e1	-

5.2.2 Truss topology optimization with reanalysis

In this numerical example, reanalysis is assimilated in the truss topology optimization for both formulations presented in the previous section. First, topology optimization is performed for minimizing the compliance with a volume constraint and for minimizing the volume with a compliance constraint. In the next stage the PCG method was added to the optimization for solving the linear equilibrium equations in an approximated way. The reference stiffness matrices are given from earlier cycles of the optimization. The following controls were set for the reanalysis procedure:

1. The standard Cholesky decomposition is preformed in the 1st iteration and when the residual PCG solution exceeded 10^{-3}.

2. A maximum number of 3 PCG reanalysis iterations are allowed.

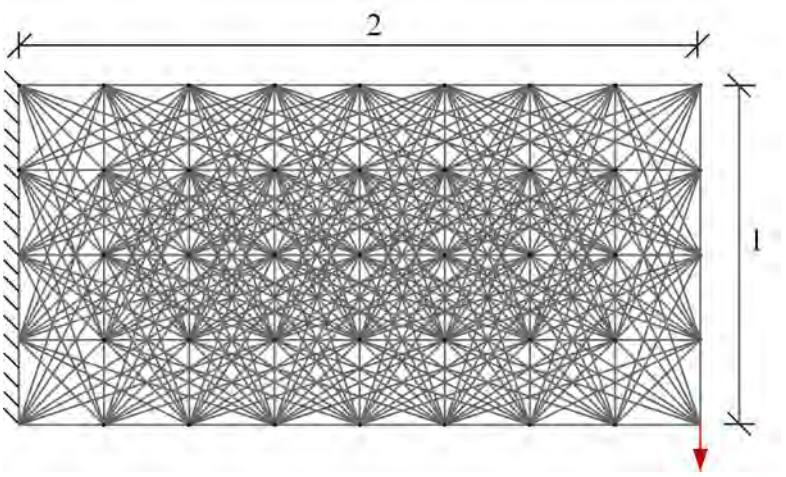

FIGURE 5.5: Initial layout of the ground structure for the topology optimization

The reanalysis is demonstrated by two types of structures: A cantilever and a so-called Michell type structure, both loaded with a single point load.

Cantilever

Consider the ground structure shown in Figure 5.5, modeled with linear elastic bars and analyzed as shown in Chapter 3.2. The bars density vector ρ are the design variables. The width in x direction is $L_x = 2$ and the height in y direction is $L_y = 1$. The domain is divided into 9 and 5 nodes in x and y directions respectively. The ground structure is assembled with 388 bars and 90 degrees of freedom and the connectivity number is 3. The structure is subjected to a single load on one side and fixed on the other side as presented in Figure 5.5. In this example, the optimization is implemented by two formulations, minimum compliance under a volume constraint and the vice versa formulation of minimum volume under a compliance constraint. The stopping criteria on the maximum change in the bars densities was set to 10^{-6}. A maximum number of 200 optimization cycles was set for both formulations.

For the minimum compliance problem the structure starts with equal bar densities that satisfy the volume constraint and every design cycle the bars are updated using the optimality criteria (OC) procedure. The volume constraint is set to $V^* = 7$ and the final value of the objective function obtained after 200 design cycles is $f_C = 7.947$. The minimum volume formulation is solved also by the OC method. The compliance constraint is set to $C^* = 7.947$ and the result is the exact same structure with a volume

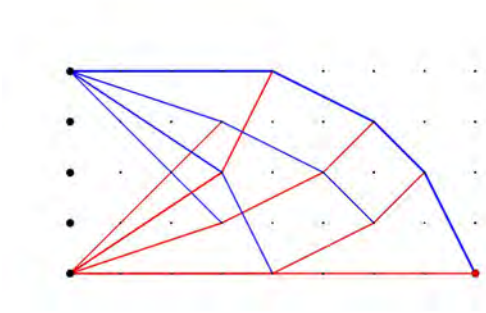

(A) Final layout for the standard minimum compliance problem

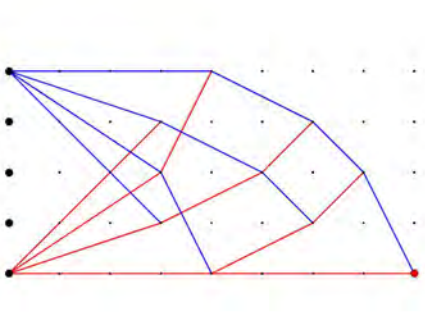

(B) Final layout for the standard minimum volume problem

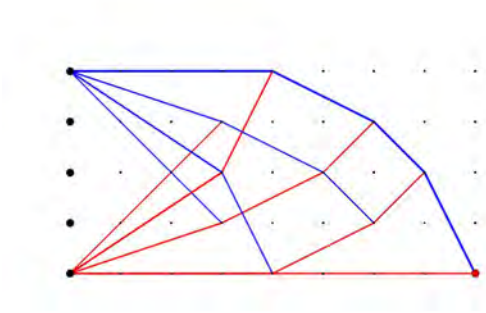

(C) Final layout for the renalysis-based minimum compliance problem

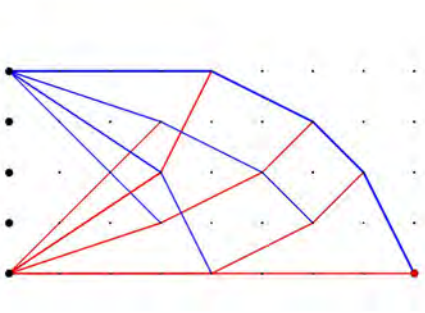

(D) Final layout for the renalysis-based minimum volume problem

FIGURE 5.6: Layouts of structures with topology changes from the optimization process

TABLE 5.3: Comparison of all four formulations for the Cantilever example

Formulation	Objective	Constraint	Matrix factorizations	PCG iter.
Min. comp., standard	7.947	7	200	-
Min. vol., standard	6.998	7.947	200	-
Min. comp., with CA	7.947	7	11	232
Min. vol., with CA	6.998	7.947	11	254

of $f_V = 7$ as in the first formulation. The optimized structure layouts of both problems are presented in Figure 5.6. After obtaining results for both problems in the standard approach, approximations by reanalysis are integrated in both problems using the PCG method for solving the set of linear equilibrium equations. Similar to before, in the first problem the volume constraint is set to $V^* = 7$, the minimum compliance reanalysis-based procedure reached an objective value of $f_C = 7.947$. During 200 design cycles only 11 Cholesky decompositions were preformed. Throughout the other 189 design cycles, a total number of 232 PCG reanalysis iterations were utilized for approximating the solution. With a compliance constraint of $C^* = 7.947$, the minimum volume reanalysis-based

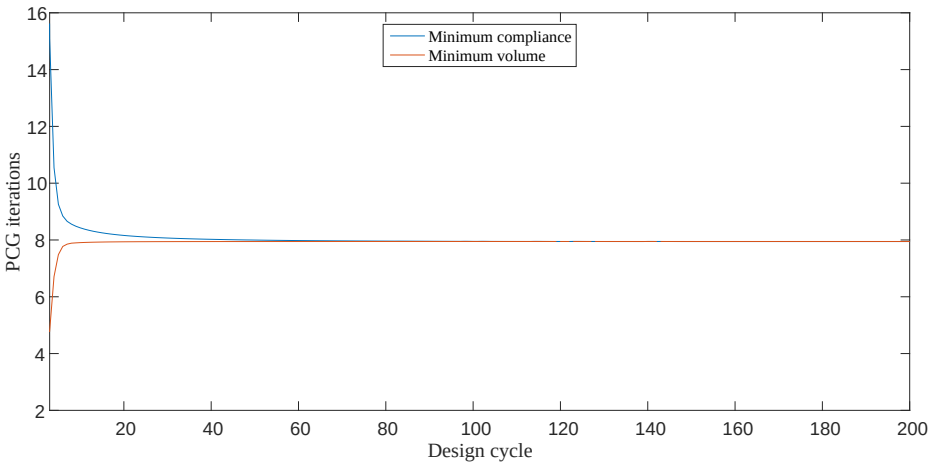

FIGURE 5.7: Value of compliance per design cycle for both formulations

procedure reached an objective value of $f_V = 7$. During 200 design cycles also only 11 Cholesky decompositions were preformed. Throughout the other 189 design cycles, a total number of 254 PCG reanalysis iterations were utilized for approximating the solution. The results above are summarized in Table 5.3 and point out for both problems that the integration of reanalysis by PCG provides the same results as the standard approach.

It is clear that computational effort is saved due to fewer factorizations of the stiffness matrix. A slight advantage of the maximum compliance formulation was noted where less PCG iteration are required overall. In Figure 5.7 the compliance is presented throughout design iterations and the idea of stiff reference matrix for the minimum volume formulation can be recognized. Another demonstration of the reanalysis procedure is shown in Figure 5.8, where 0 PCG iterations means standard analysis. As the optimization advanced, the reanalysis can open wider gaps and save more computational time, mainly because the changes in the stiffness matrix are less significant.

Michell structure

Consider the ground structure shown in Figure 5.9, modeled and analyzed in the same way as in the previous example. The width in x direction is $L_x = 3$ and the height in y direction is $L_y = 2$. The domain is divided into 18 and 12 nodes in x and y directions respectively. The ground structure is assembled with 3134 bars and 494 degrees of freedom and the connectivity number is 3. The structure is subjected to a single load

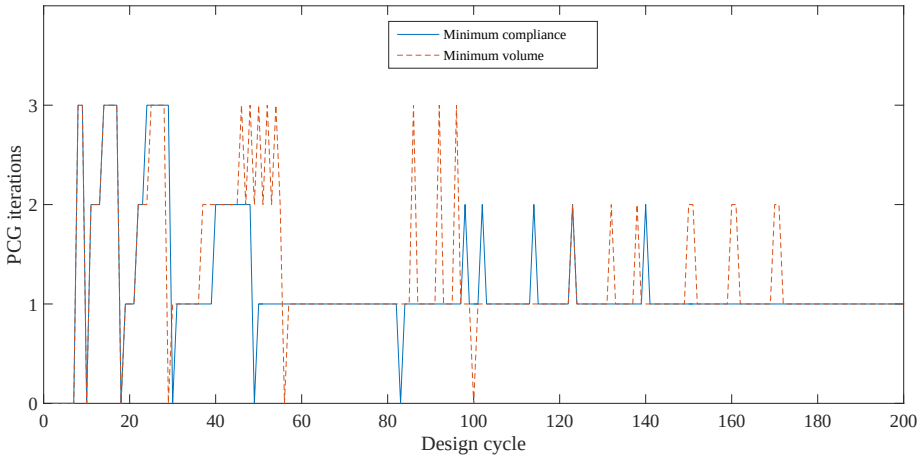

FIGURE 5.8: Number of PCG iteration per design cycle for both formulations

on one side and fixed by two nodes on the other side as presented in Figure 5.9. In this example, the optimization is implemented by two formulations exactly like the previous example. The stopping criteria on the maximum change in the bars densities was set to 10^{-6}. A maximum number of 200 optimization cycles were set for both formulations.

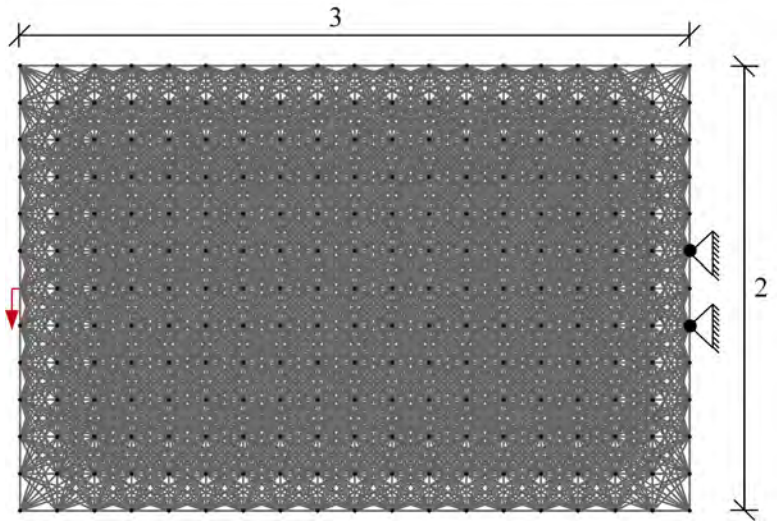

FIGURE 5.9: Initial ground structure for topology optimization

For the minimum compliance problem the structure starts with equal car densities that satisfy the volume constraint and every iteration the bars are updated using the optimality criteria (OC) procedure. The volume is set to $V^* = 2.31$ and the final value of the objective function is $f_C = 200.8$. The minimum volume formulation is solved also by the OC method where the compliance is set to $C^* = 200$ and the result is the exact same structure with volume of $f_V = 2.31$ as in the first formulation. The optimized structure

of both problems are presented in Figure 5.12. After obtaining results for both topology optimization standard problems, approximations by reanalysis are integrated in both problems using the PCG method for solving the set of linear equilibrium equations. For the first problem setting the volume constraint to $V^* = 2.31$, the minimum compliance reanalysis-based procedure reached an objective value of $f_C = 200.8$. During 200 design cycles, 15 Cholesky decompositions were preformed. Throughout the other 185 design cycles, a total number of 299 PCG reanalysis iterations were utilized for approximating the solution. With a compliance constraint of $C^* = 200$, the minimum volume reanalysis-based procedure reached an objective value of $f_V = 2.3$. During 200 design cycles only 15 Cholesky decompositions were preformed. Throughout the other 185 design cycles, a total number of 298 PCG reanalysis iterations were utilized for approximating the solution. The results above are summarized in Table 5.4 and point out for both problems that the integration of reanalysis by PCG provides the same results as the standard approach.

TABLE 5.4: Comparison of all four formulations for the Michell example

Formulation	Objective	Consraint	Matrix factorizations	PCG iter.
Min. comp., standard	200.8	2.31	200	-
Min. vol., standard	2.31	200	200	-
Min. comp., with CA	200.8	2.31	15	299
Min. vol., with CA	2.3	200	15	298

Additionally, computer effort in saved due to less factorizations of the stiffness matrix every design cycle. No advantage was found for any particular formulation in this example. In Figure 5.7 the compliance is presented throughout the design iterations and the idea of stiff reference matrix for the minimum volume formulation can be recognized again.

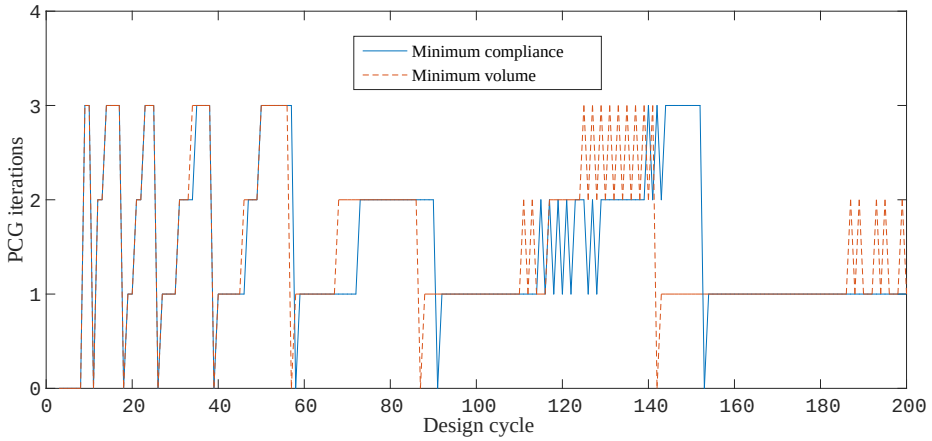

FIGURE 5.10: Number of PCG iteration per design cycle for both formulations

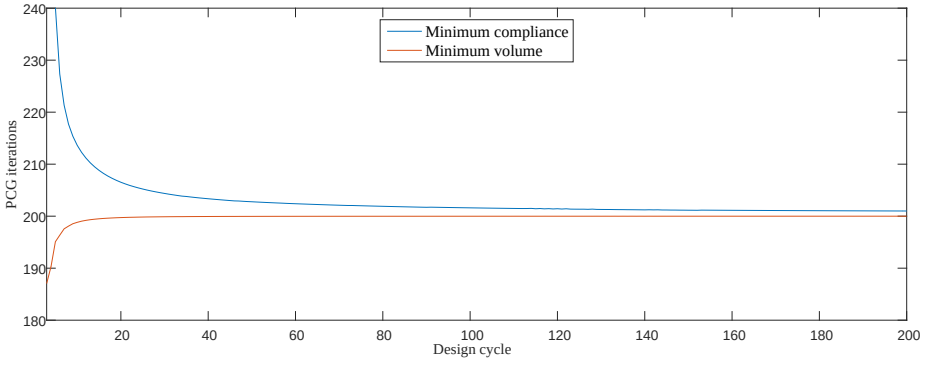

FIGURE 5.11: Value of compliance per design cycle for both formulations

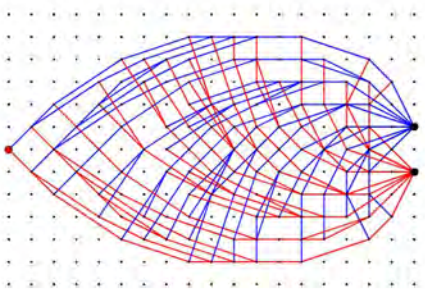

(A) Final layout for the standard minimum compliance problem

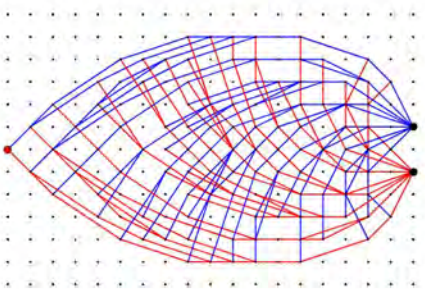

(B) Final layout for the standard minimum volume problem

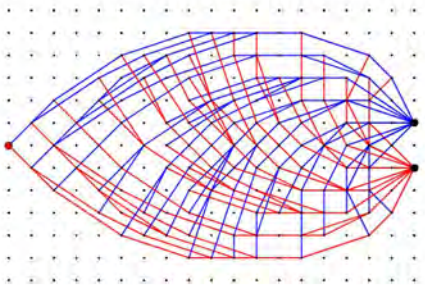

(C) Final layout for the renalysis-based minimum compliance problem

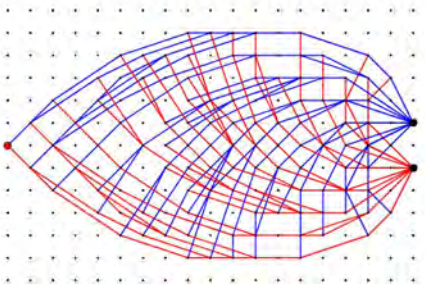

(D) Final layout for the renalysis-based minimum volume problem

FIGURE 5.12: Layouts of structures with topology changes from the optimization process

5.3 Summary

This chapter presented numerical examples in which reanalysis was implemented into the optimization process for linear truss structures. In Section 5.2.1, CA and PCG were tested for different truss structures with topology changes. The equivalence of both methods was demonstrated. The low condition number of the pre-conditioned system shows some advantage for approximations with a stiff reference matrix. However, this was not observed in the actual results of the optimization problems. Two full examples of topology optimization problems with reanalysis in Section 5.2.2 provided good results compared to the standard solution. By utilizing only 3 basis vectors, between 90%-95% of matrix factorizations were avoided in the reanalysis solution. Despite the approximations made for the response calculations, the final optimization layouts for each formulation were similar and practically the same for the standard solution and the approximated one. However, both formulations provided the same relative efficiency and the benefit of one formulation over the other was not detected. Note that while the PCG and CA method also require computer operations, using very few iterations (3 in this case) allows one to save significant computational effort, especially for large scale problems.

Chapter 6

Reanalysis in topology optimization with geometric nonlinearity

This chapter presents the assimilation of reanalysis methods in the solution of continuum topology optimization problems with geometrical nonlinearity assumptions in the structural model. In Section 6.1 the two optimization problems are formulated, followed by the sensitivity analysis derivation and a discussion on numerical considerations. In Section 6.2 three main reanalysis schemes are presented: 1) Re-using the solution (RUS); 2) Re-using the tangent stiffness matrix (RUK); 3) RUK with approximated sensitivity analysis by CA. In Section 6.3 several numerical examples demonstrate the effectiveness of the proposed schemes.

6.1 GNL topology optimization

For a given load, a structure may deform such that the initial shape configuration is different from the deformed one. These structures are said to be under geometric nonlinearity (GNL). The Newton-Raphson incremental-iterative solution procedure presented in Chapter 3 is carried out for solving the non-linear governing equations. A common method used in the context of structural nonlinearity solutions is the displacement control method. An external normalized force vector is set and a single displacement is

prescribed. The total number of unknowns remains unchanged except from the prescribed displacement u_p which is replaced with an unknown load factor θ that multiplies the normalized external load. Nonlinearity included in the model of optimized structures is an important subject that has only in the last two decades begun to receive research attention. In this section two different topology optimization problems are defined: 1) Maximizing the global end-compliance under a volume constraint; 2) Minimizing the volume under an end-compliance constraint. In order to solve the optimization problem, sensitivity analysis is performed for the problems' functionals. Numerical issues usually arise when merging topology optimization problems with structures modeled with GNL.

6.1.1 Problem formulations

The aim of the first optimization problem is to find the stiffest design while considering structural nonlinearities. Displacement-controlled analysis, presented above in Section 3.4, is performed to solve the governing equations. Defining an appropriate objective function is slightly different than in the linear case. For the simple case of maximizing the end-compliance, the objective function f_c is as follows:

$$\begin{aligned} \min_{\boldsymbol{\rho}} \quad & f_c = -\theta \mathbf{f}_{ext,p}^T \mathbf{u}_p \\ \text{s.t.}: \quad & g_v = \sum_{e=1}^{N} v_e \rho_e \leq V^* \\ & 0 < \rho_{min} \leq \rho_e, \quad e = 1...N \\ \text{with}: \quad & \mathbf{R}(\mathbf{u}) = \mathbf{f}_{int} - \theta \hat{\mathbf{f}}_{ext} = 0 \end{aligned} \tag{6.1}$$

Where u_p is the the prescribed displacement value and θ is the force load factor.

For the second problem formulation the objective function is simply the structural volume and the constraint is the term calculated above as the objective function. The constraint functional g_c is set to make the end-compliance larger or equal to the constant

compliance value of C^*,

$$\begin{aligned} \min_{\boldsymbol{\rho}} \quad & f_v = \sum_{e=1}^{N} v_e \rho_e \\ \text{s.t.}: \quad & g_c = \theta \mathbf{f}_{ext,p}^T \mathbf{u}_p \geq C^* \\ & 0 < \rho_{min} \leq \rho_e, \quad e = 1...N \\ \text{with}: \quad & \mathbf{R}(\mathbf{u}) = \mathbf{f}_{int} - \theta \hat{\mathbf{f}}_{ext} = 0 \end{aligned} \tag{6.2}$$

Since both are following the same finite element discretization it is relatively straightforward to switch between the two formulations. The optimization is solved with convex approximations by the Method of Moving Asymptotes (MMA) (Svanberg, 1987) as presented in Chapter 2.

6.1.2 Sensitivity analysis

Sensitivity analysis is derived as follows. The augmented function of the end-compliance is set by adding zero terms to the function and multiplying these terms by $\boldsymbol{\lambda}$

$$\hat{f}_c = -\theta \hat{\mathbf{f}}_{ext,p}^T \mathbf{u}_p - \boldsymbol{\lambda}^T \left(\theta \hat{\mathbf{f}}_{ext} - \mathbf{f}_{int} \left(\boldsymbol{\rho}, \mathbf{u} \left(\boldsymbol{\rho} \right), \theta \right) \right) \tag{6.3}$$

where $\boldsymbol{\lambda}$ is an arbitrary vector containing the adjoint variables. Differentiation of the augmented function with respect to a certain element density variable provides

$$\frac{\partial \hat{f}_c}{\partial \rho_e} = -\frac{\partial \theta}{\partial \rho_e} \hat{\mathbf{f}}_{ext,p}^T \mathbf{u}_p - \boldsymbol{\lambda}^T \frac{\partial \theta}{\partial \rho_e} \hat{\mathbf{f}}_{ext} + \boldsymbol{\lambda}^T \frac{\partial \mathbf{f}_{int}}{\partial \rho_e} + \boldsymbol{\lambda}^T \frac{\partial \mathbf{f}_{int}}{\partial \mathbf{u}} \frac{\partial \mathbf{u}}{\partial \rho_e}. \tag{6.4}$$

Note that in practice the derivatives are applied to the filtered and projected densities $\overline{\widetilde{\rho}}$. The sensitivities are found by the use of the chain rule, as shown above in Equation (2.11).

Rearranging the equation and using the tangent stiffness matrix corresponding to the end equilibrium point $\mathbf{K} = \frac{\partial \mathbf{f}_{int}}{\partial \mathbf{u}}$ we obtain

$$\frac{\partial \hat{f}_c}{\partial \rho_e} = -\frac{\partial \theta}{\partial \rho_e} \left(\hat{\mathbf{f}}_{ext,p}^T \mathbf{u}_p + \boldsymbol{\lambda}^T \hat{\mathbf{f}}_{ext} \right) + \boldsymbol{\lambda}^T \frac{\partial \mathbf{f}_{int}}{\partial \rho_e} + \boldsymbol{\lambda}^T \mathbf{K} \frac{\partial \mathbf{u}}{\partial \rho_e}. \tag{6.5}$$

The prescribed DOF u_p in known and does not depend on the design variables. Denoting f as a subscript for free non-prescribed DOF gives

$$\frac{\partial \hat{f}_c}{\partial \rho_e} = -\frac{\partial \theta}{\partial \rho_e}\left(\hat{\mathbf{f}}_{ext,p}^T \mathbf{u}_p + \boldsymbol{\lambda}^T \hat{f}_{ext,p}\right) + \boldsymbol{\lambda}^T \frac{\partial \mathbf{f}_{int}}{\partial \rho_e} + \boldsymbol{\lambda}^T \mathbf{K} \frac{\partial \mathbf{u}}{\partial \rho_e}. \tag{6.6}$$

From the first RHS term, in case of a single external load and single prescribed DOF, the value of the adjoint vector at the prescribed point is $\boldsymbol{\lambda}_p = -u_p$. In order to avoid computing $\frac{\partial \mathbf{u}}{\partial \rho_e}$ the other adjoint terms are computed by solving the equation system

$$\mathbf{K}_{ff}\boldsymbol{\lambda}_f + \mathbf{K}_{fp}\boldsymbol{\lambda}_p = \mathbf{0} \tag{6.7}$$

and

$$\boldsymbol{\lambda}_f = \mathbf{K}_{ff}^{-1}\left(\mathbf{K}_{fp} u_p\right). \tag{6.8}$$

Once the complete adjoint vector $\boldsymbol{\lambda}$ is obtained, the final design sensitivities are

$$\frac{\partial f_c}{\partial \rho_e} = \boldsymbol{\lambda}^T \frac{\partial \mathbf{f}_{int}}{\partial \rho_e}. \tag{6.9}$$

6.1.3 Numerical considerations

For the topological optimization method to be used as a design tool, the final layout solution must be physical and constructible. As presented in Chapter 2, the Modified SIMP interpolation function, filter and Heaviside projections help achieve this goal and are utilized in the numerical examples. For crisp topological solutions it is required to drive the design toward a 0-1 layout. In this thesis elastic material properties are assumed and the elastic modulus of the each element is set as a function of its density. Using a modified SIMP scheme that includes two material phases, the interpolated Young's modulus is defined as in Equation (2.4),

$$E_e(\rho_e) = E_{\min} + \rho_e^p (E_0 - E_{\min}). \tag{6.10}$$

Only one material is distributed in our case so E_{min} represents void and is set to a small positive value for numerical reasons. E_{max} is the value of the material Young's modulus, and p is the penalization factor. Figure 2.5 represents the SIMP interpolation function for different values of penalization.

Checker-board patterns and mesh-dependence problems are crucial to overcome in order to obtain final constructible results. More explanations about these issues are presented in Chapter 2. In this chapter, the classical density filter is implemented. The filtered element density is given by Equation (2.6) and sensitivity of the filtered density with respect to a changes in design variable was found by Equation (2.9)

Density based methods such as the modified SIMP, strive to spread the material in form of solid and void only. However, there are areas, especially in the transition between phases, that the elements are not sharp 0/1 but have some intermediate values. Heaviside projections of the filtered design were found applicable to make the interface between void and material sharper. The smooth Heaviside function used in this work is

$$\overline{\widetilde{\rho}} = \frac{\tanh(\beta\,\eta) + \tanh(\beta\,(\widetilde{\rho} - \eta))}{\tanh(\beta\,\eta) + \tanh(\beta\,(1 - \eta))}. \tag{6.11}$$

The projected densities are defined as $\overline{\widetilde{\rho}}$ with a sharpness control of β and threshold point of η. Figure 2.8 represents the Heaviside function with different values of β. Derivatives of the Heaviside function are computed explicitly by

$$\frac{\partial \overline{\widetilde{\rho}}_i}{\partial \widetilde{\rho}} = \frac{\beta\,\left(1 - (\tanh(\beta\,(\widetilde{\rho} - \eta)))^2\right)}{\tanh(\beta\,\eta) + \tanh(\beta\,(1 - \eta))}. \tag{6.12}$$

The sensitivity of a function f with respect to a change in design variable ρ_e is found by the use of the chain rule for the filtered densities.

$$\frac{\partial f}{\partial \rho_e} = \sum_{i \in N_e} \frac{\partial f}{\partial \overline{\widetilde{\rho}}_i} \frac{\partial \overline{\widetilde{\rho}}_i}{\partial \widetilde{\rho}_i} \frac{\partial \widetilde{\rho}_i}{\partial \rho_e}. \tag{6.13}$$

The so-called Robust topology optimization is applied here for enforcing length scale and to provide a robust final design for manufacturing errors (Wang et al., 2011). As mentioned in Chapter 2, the main idea is to execute three different projections each one with different threshold values

$$\eta_e \;<\; \eta_i \;<\; \eta_d \tag{6.14}$$

The intermediate threshold is $\eta_i = 0.5$ and it is denoted by the i index, the projected values are $\bar{\rho}_i$. The two additional threshold values are the eroded and dilated projections, η_e and η_d respectively. Figure 6.1 shows the Heaviside functions for different threshold values. The eroded threshold is a value higher than the intermediate one and provides a

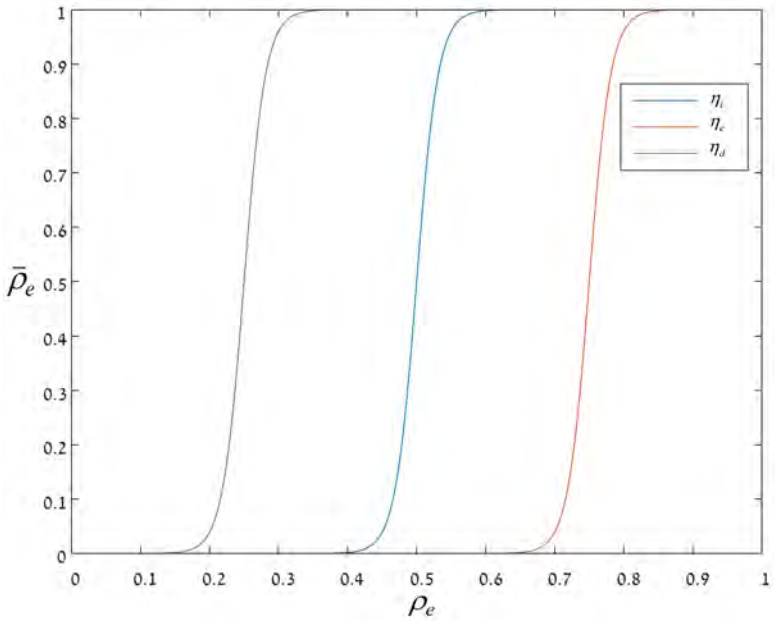

FIGURE 6.1: The 3 graphs representing three threshold values for the robust Heaviside function

thinner projected layout compared to the original. For the dilated layout, a lower value of the threshold is determined and the projected layout has thicker densities than the intermediate projected design. After applying the three projections, the eroded design is used for the calculations of stiffness and the dilated design is used for the volume calculation.

6.1.4 Convergence criteria

The convergence criteria for the Newton-Raphson method is mentioned in Chapter 3. The iterations are continued until appropriate convergence is satisfied. Throughout this thesis, the value of the iterative unbalanced forces is measured relatively to the external forces added in the current increment:

$$\frac{\left\| {}^{t+\Delta t}\mathbf{f}_{ext} - {}^{t+\Delta t}\mathbf{f}_{int}^{(i-1)} \right\|_2}{\left\| {}^{t+\Delta t}\mathbf{f}_{ext} - {}^{t}\mathbf{f}_{ext} \right\|_2} \leq \varepsilon \tag{6.15}$$

When this relative norm of the residual forces is smaller than ε, it is said that the incremental solution converged. As mentioned, numerical problems appear in the part of the design where elements obtain soft material properties. A solution for this phenomena is to ignore when computing the convergence criteria the elements that have close to zero density. A discussion on this topic was presented above in Chapter 2.

6.2 Re-using information

In this chapter, the nonlinear structural analysis is performed with procedures based on re-using information. The concept is based on the fact that analysis solutions of sequential design cycles, are similar as a result of the layouts' similarity. Hence, information from previous optimization cycles may be reused for the subsequent solution of the nonlinear structural analysis problems. The aim is to reduce computational effort by solving the nonlinear analysis equations with fewer Newton iterations or by reducing the number of factorized tangent stiffness matrices. In the following, three schemes are described based on reusing the solution and the factorized tangent stiffness matrix.

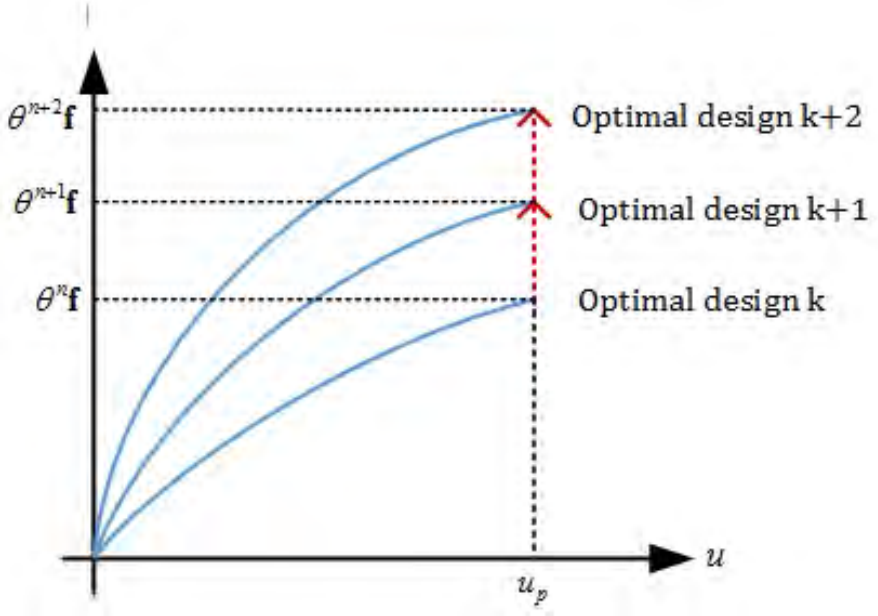

FIGURE 6.2: An illustration of the RUS scheme together with the solution by displacement control

Re-using the solution (RUS) The response computed for one structure is used for solving efficiently an updated design with fewer Newton iteration. The application of Newton-Raphson scheme requires an initial guess for the starting iteration point. Re-using a solution similar to the response of the structure as an initial guess can increase the convergence rate.

In topology optimization the design changes are modest and therefore the final displacement solutions are similar in subsequent design cycles. Intuitively, saving the solution from a previous design cycle and reusing it as an initial guess for the next design can

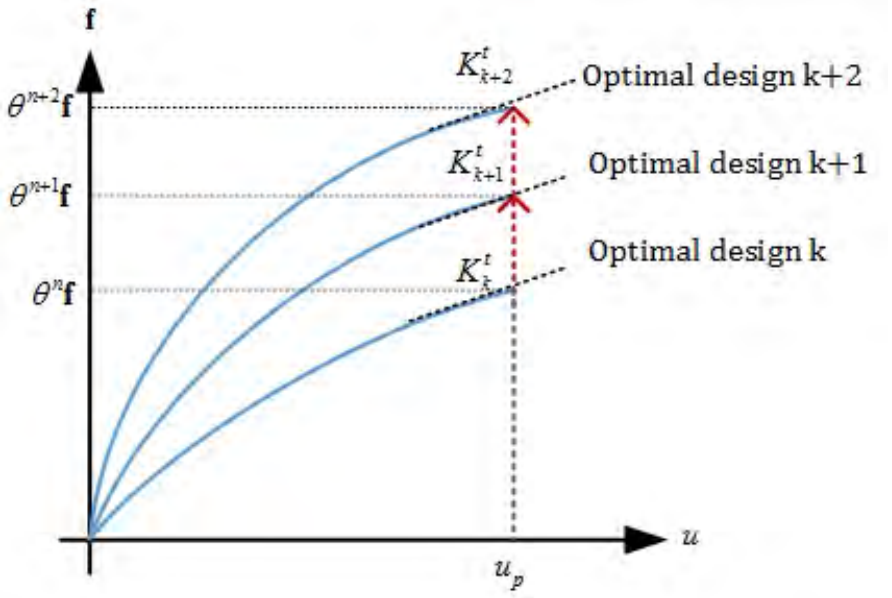

FIGURE 6.3: An illustration of the RUK method. The tangent stiffness matrix is reused for the next optimal design cycle

reduce the number of Newton iterations required. Displacement control has another advantage for solving with the RUS schema because the prescribed DOF is fixed, thus at this point the initial guess is accurate as shown in Figure 6.2. Essentially, $\mathbf{u}$ and θ are reused as an initial guess for the Newton-Raphson solution and convergence can be achieved with fewer iterations and inducing fewer matrix factorizations.

Re-using the factorized tangent stiffness (RUK) Extending the previous RUS method, this scheme is inspired by the Modified Newton-Raphson (MNR) procedure, where the tangent stiffness matrix is factorized once in the beginning of each incremental step. Obviously the convergence is expected to require more iterations compared to the standard Newton-Raphson. However, the factorized stiffens matrix is given so only forward and backward substitutions are required at each iteration. For nonlinear topology optimization with Modified Newton-Raphson, we use $\mathbf{K}$ and $\mathbf{u}$ from design cycle k as the tangent stiffness matrix and initial solution for design cycle $k+1$. The stiffness matrix of the optimized design step is decomposed once at the end of the analysis for the calculations of the sensitivity analysis. The decomposed stiffness matrix $\mathbf{K}$ is then reused for the next optimization step as shown in Figure 6.3. In case convergence is not achieved, the full solution will be obtained by RUS.

RUK with approximated sensitivity analysis This method is exactly like the RUK scheme only that the stiffness matrix, corresponding to the final solution, is saved every design cycle and reused. A certain design from cycle k is fully analyzed and the sensitivity is computed. Now for the following design cycles the stiffness matrix from cycle k is reused for the MNR analysis. After obtaining the final response the sensitivity adjoint vector $\boldsymbol{\lambda}$ is approximated by the PCG method, where $\mathbf{K}$ from cycle k is reused as the matrix pre-conditioner. Throughout the optimization processes, if convergence was not obtained by the above, full Newton-Raphson (FNR) scheme was applied.

6.3 Numerical examples

This section presents several numerical examples that demonstrate the computational approaches presented above. A clamped beam and simply supported beam will be considered with moderate and large prescribed displacement, 3 examples in total. The optimization problem in Equations (6.1) and (6.2) are solved with convex approximations by the Method of Moving Asymptotes (MMA). In the RUK scheme with reanalysis by the PCG method the following controls were set:

1. The standard Cholesky decomposition is preformed for the 1st iteration and when the residual PCG solution exceeded 10^{-3};
2. For the first 5 and every 10 design cycles, an exact solution is computed;
3. A maximum number of 5 PCG reanalysis iterations are allowed.

In cases that the analysis did not converge, a full scheme was applied for the solution. For obtaining smooth results and imposing the length scale of the final layout, the robust Heaviside projection presented in Equation (6.11) was applied. For the eroded projected densities the threshold value was set to $\eta_e = 0.6$ and the dilated was fixed to $\eta_d = 0.4$. The optimization started with a low value of $\beta = 1$, and increasing it slowly every design iteration by 0.1.

6.3.1 Example 1: Moderate deformations of a clamped beam

In this example, topology optimization of a clamped beam is performed. The clamped beam problem is a benchmark problem in the context of geometrical nonlinearity (GNL) due to the significant differences of the optimized layout compared to linear assumptions. The nonlinear Finite Element Method (FEM) developed in Chapter 3 is utilized for the discretization of the structural model. The design domain shown in Figure 6.4 is assumed to be a rectangular structure of dimensions $L_x \times L_y = 200 \times 40$, discretized by a grid containing nelx $\times$ nely $= 200 \times 40$ square finite elements. The load is evenly distributed between 6 neighboring nodes, in order to prevent local buckling of loaded finite elements. The displacement at the top node in the center is prescribed throughout all design cycles to the value of $\delta = 0.1L_y$. Further parameters are given in Table 6.1. Despite the inherent symmetry of the problem, symmetry about the y axis was forced on the sensitivity analysis and the design densities in order to ensure a smooth solution without numerical issues.

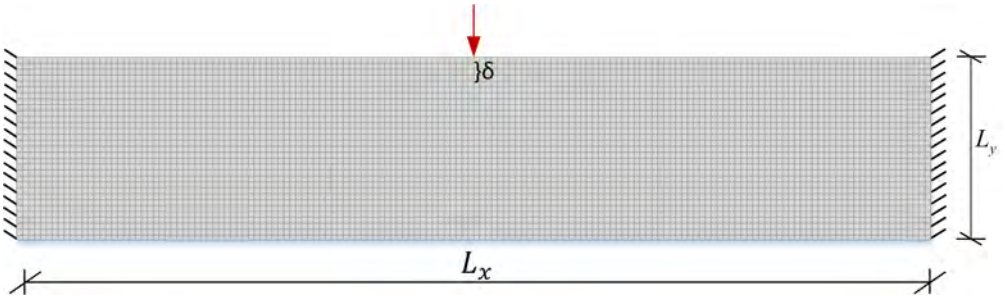

FIGURE 6.4: A Clamped beam domain with a top-central prescribed displacement node for example 1

TABLE 6.1: Parameters for Example 1

Parameter	Value
E_{min}	10^{-3}
E_{max}	10^{3}
ν	0.3
SIMP penalty	3
Filter radius	2.5

Maximum end-compliance problem was first solved under the volume constraint of $V^* = 0.3$ and with all three schemes presented above in Section 6.2. In Table 6.2, results from the first optimization problem are presented. The table shows the number of Newton iteration needed for every solution scheme and the total number of stiffness matrices factorized during the optimization process. With the standard full

Newton-Raphson scheme, 395 solutions of the residual equations where preformed for 100 design cycles. Adding the number of sensitivity analyses we obtain 495 matrix factorizations. Re-using the solution by the RUS scheme, only 211 Newton iterations were performed with 311 matrix factorizations, reducing 37% of matrix decompositions. Furthermore, with RUK 444 Newton iterations were required with 137 matrix factorizations that were preformed allover, only 27% compared to the standard scheme. Adding reanalysis of the adjoint equation by PCG provides a much lower number of 56 matrix factorizations, 11.3% compared to the starting point. After 100 design cycles the objective compliance function reached the value of 328.5. Although for the last scheme the value is slightly different, the final structures are practically the same as shown in Figure 6.5. For the linear case considering only small deformations, the layout of the optimized structure would be two long compressed bars. For the GNL problem this structure is not stable and may buckle. Hence the final layout is assembled by long bars under tension and relatively shorter compressed bars.

In Figures 6.6a and 6.6b the values of the end-compliance and volume constraint are presented per design cycle respectively, as observed all schemes converged in the same manner.

Figure 6.7a shows the number of Newton iterations per design cycles. Here the effectiveness of RUS is clearly demonstrated. The number of matrix factorizations per design iteration are shown in Figure 6.7b.

Solution scheme	Newton iterations	Matrix factorization	Compliance
Full Newton	395	495	328.5
RUS	211	311	328.5
RUK	444	137	328.5
RUK with PCG	413	56	329.3

TABLE 6.2: Results from solving the maximum end-compliance problem formulation

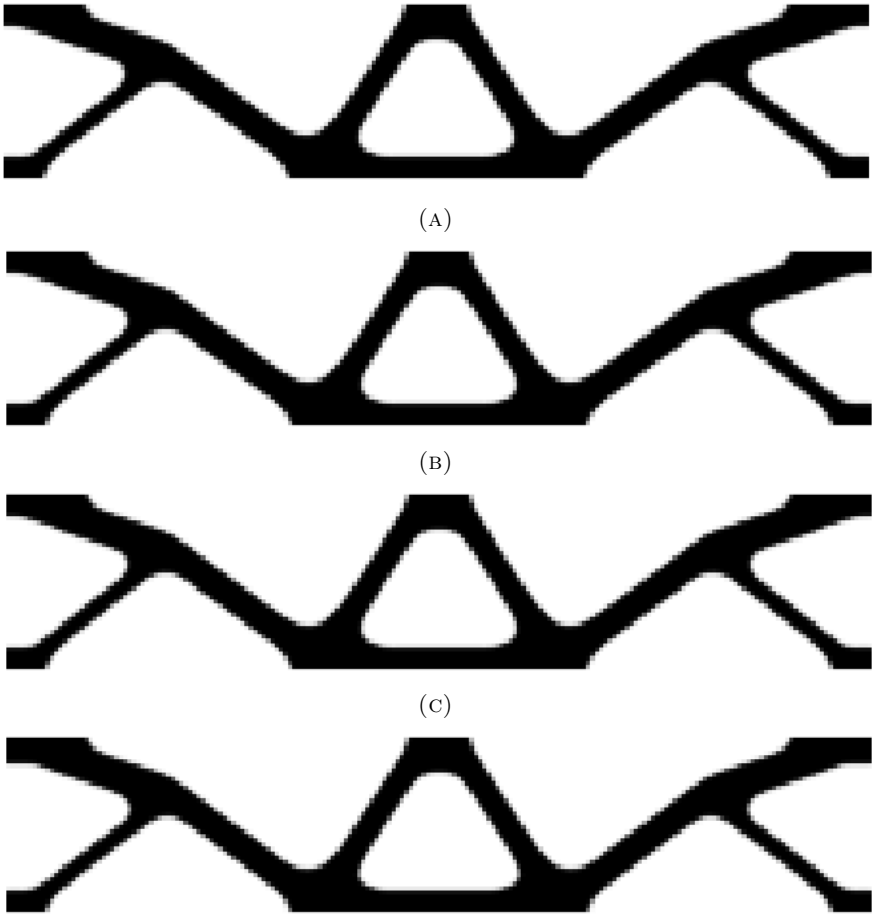

(A)

(B)

(C)

(D)

FIGURE 6.5: Final layout solutions of the maximum end-compliance problem for all 4 schemes after 100 design cycle: (A) Full Newton-Raphson; (B) RUS; (C) RUK; (D) RUK with PCG

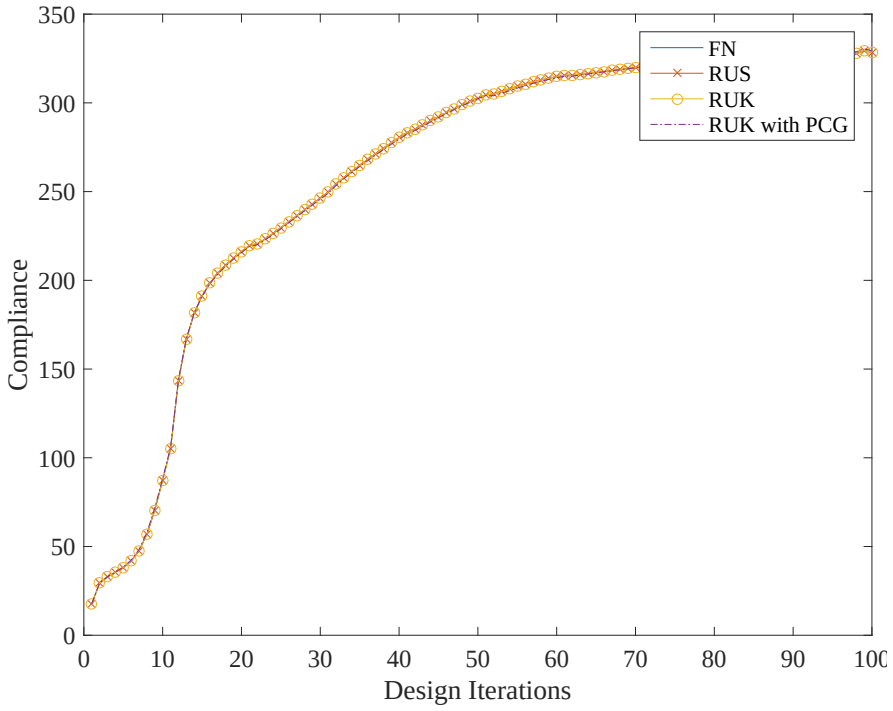

(A) Compliance value at each design cycle

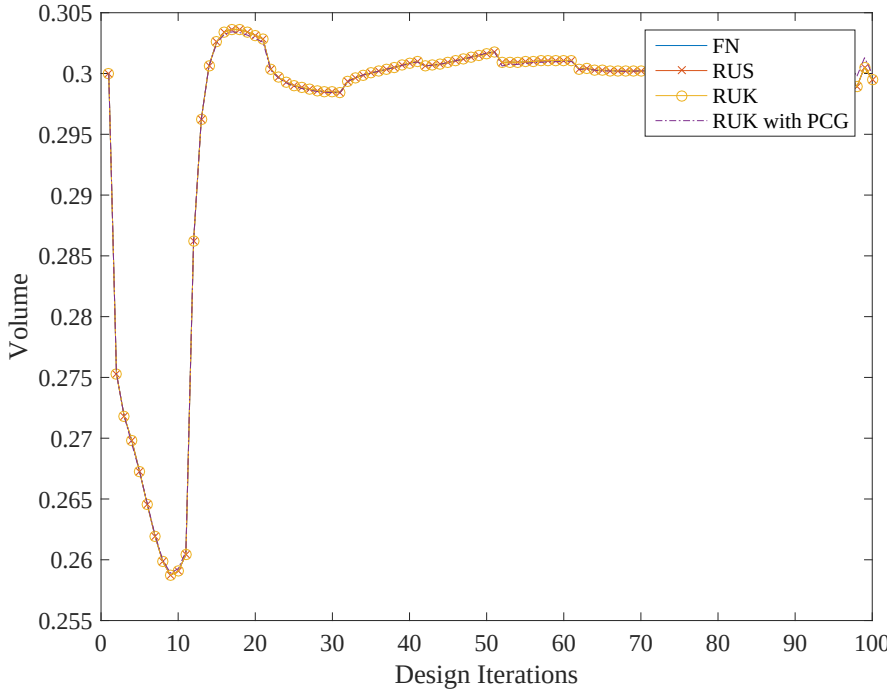

(B) Volume fraction at each design cycle

FIGURE 6.6: Numerical performance of the topology optimization process of maximum end-compliance formulation, for all 4 schemes

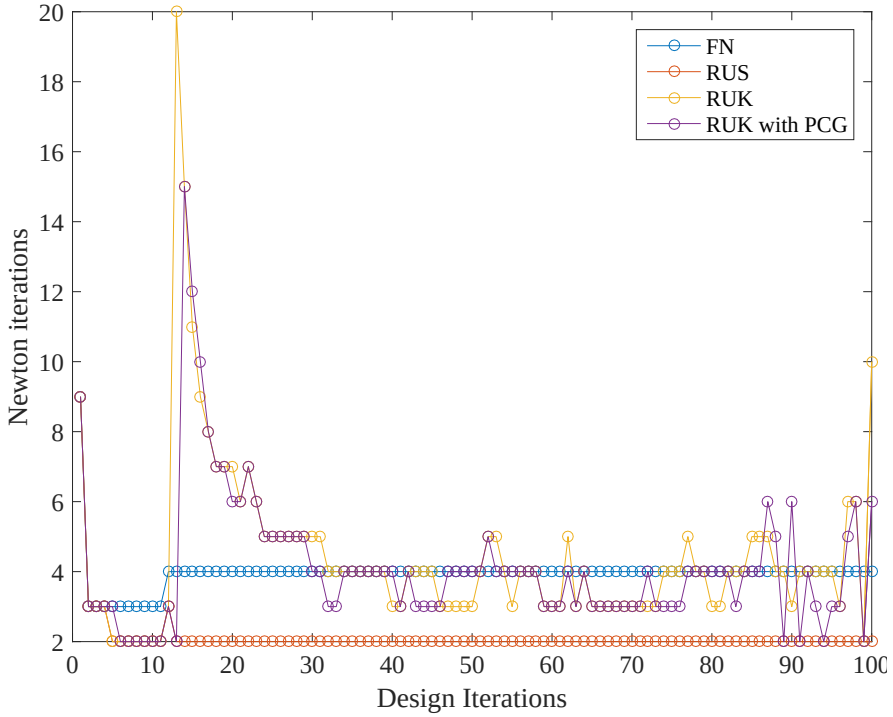

(A) Newton-Raphson iterations per design cycle

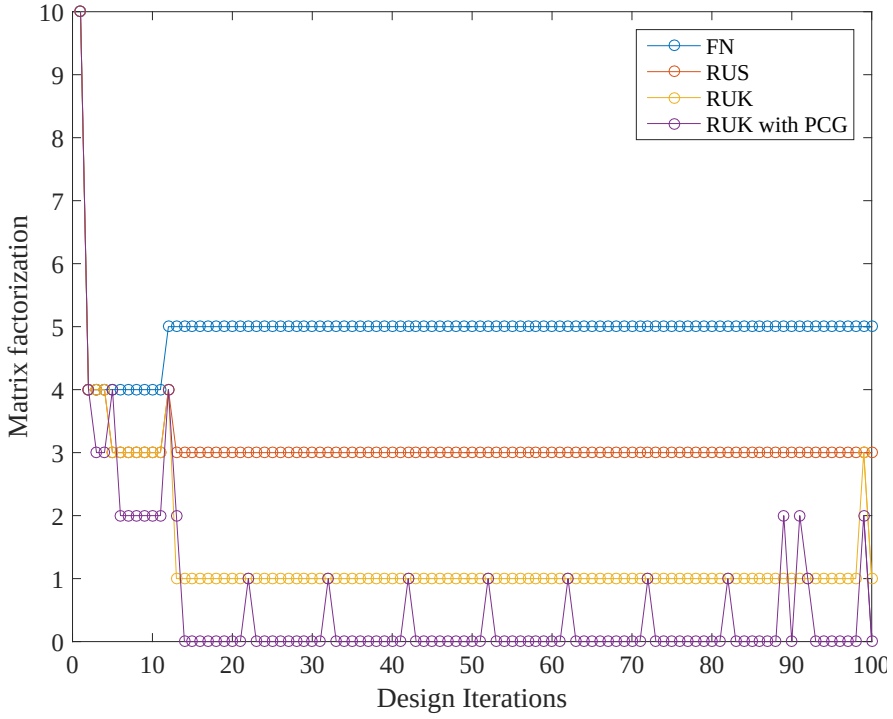

(B) Number of matrix factorizations preformed for every design cycle

FIGURE 6.7: Computational performance of the analysis for the maximum end-compliance formulation, for all 4 schemes

Minimum volume problem was solved under the end-compliance constraint of $C^* = 328.5$ obtained from solving the first formulation. In Table 6.3, results from the optimization problem are presented. The table shows the number of Newton iteration needed for every solution scheme and the total number of stiffness matrices factorized during the optimization process. With the standard full Newton-Raphson scheme, 406 solutions of the residual equations where preformed for 100 design cycles. Adding the number of sensitivity analyses we obtain 506 matrix factorizations. Re-using the solution by the RUS scheme, only 214 Newton iterations were performed, reducing 47.3% of the Newton iterations. Furthermore, with RUK 452 Newton iterations were required with 124 matrix factorizations that were preformed allover, only 24% matrix factorizations compared to the standard scheme. Adding reanalysis of the adjoint equation by PCG provides a number of 36 matrix factorizations, 7% less than the starting point. After 100 design cycles the objective volume function reached the value of 0.3. Final layouts of the schemes are all the same and are shown in Figure 6.8.
In Figures 6.9a and 6.9b the values of the end-compliance constraint and the volume objective are presented per design cycle respectively, as observed all schemes converged in the same manner.
Figure 6.10a shows the number of Newton iterations per design cycles. Here the effectiveness of RUS is clearly demonstrated. The number of matrix factorizations per design iteration are shown in Figure 6.10b.

A comparison between the solution by RUK with PCG of both formulations points out a computational advantage of the second formulation. The minimum volume formulation was able to converge using only 36 matrix factorizations, while for the end-complince problem formulation 56 matrix factorizations where performed.

Solution scheme	N-R iterations	Matrix factorization	Volume frac.
Full Newton	406	506	0.3
RUS	214	314	0.3
RUK	452	124	0.3
RUK with PCG	462	36	0.3

TABLE 6.3: Results from solving the minimum volume problem formulation

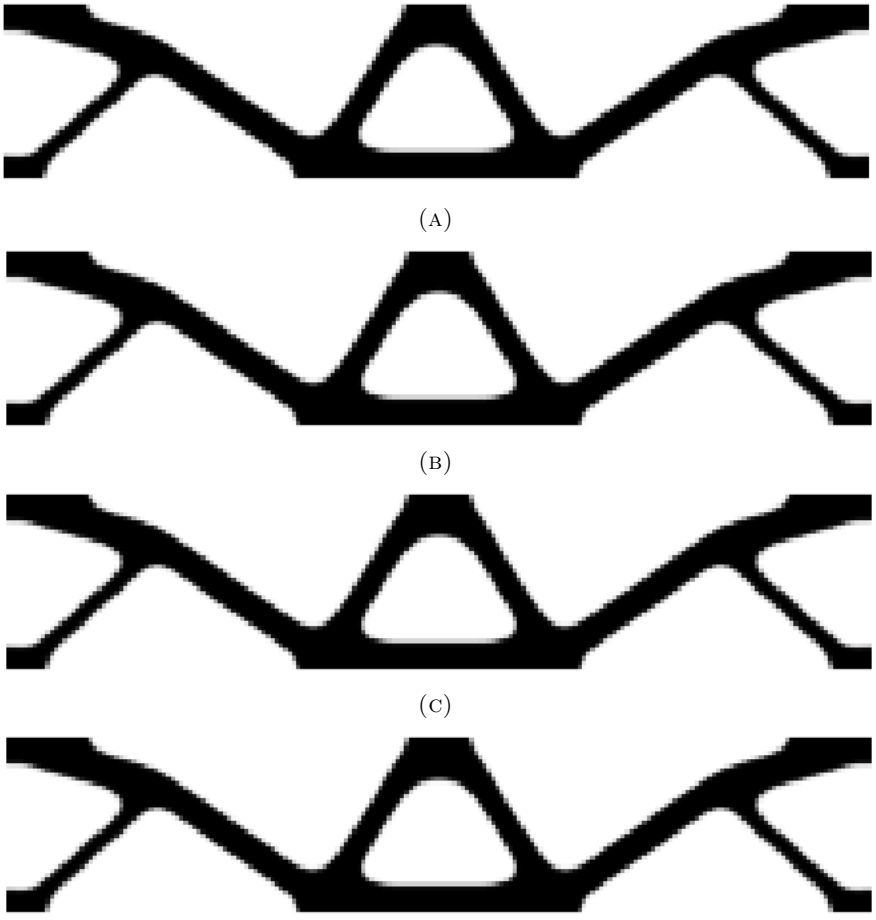

(A)

(B)

(C)

(D)

FIGURE 6.8: Final layout solutions of the minimum volume problem for all 4 schemes after 100 design cycles: (A) Full Newton-Raphson; (B) RUS; (C) RUK; (D) RUK with PCG

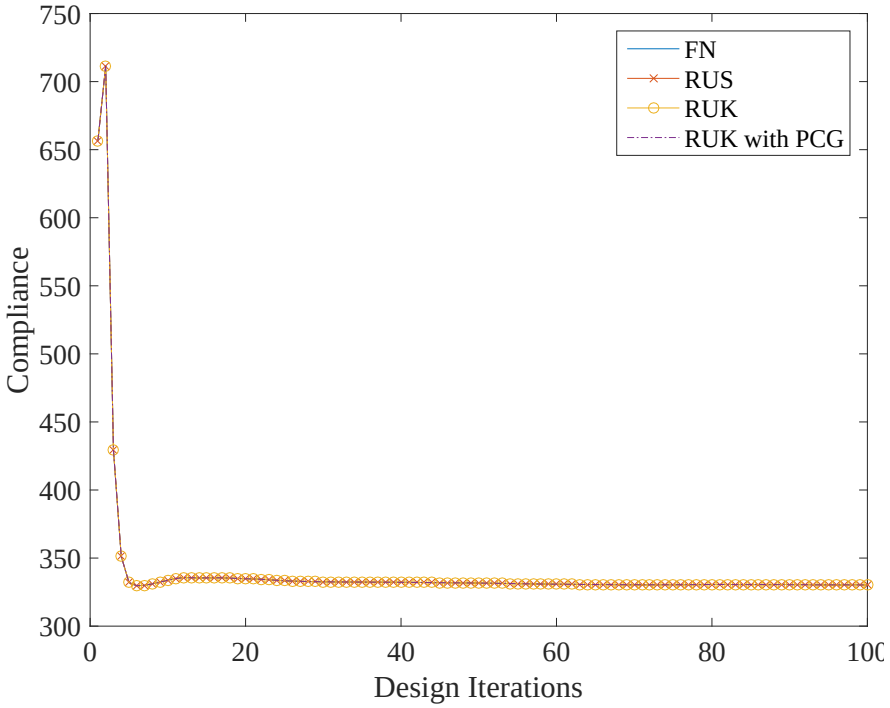

(A) Compliance value at each design cycle

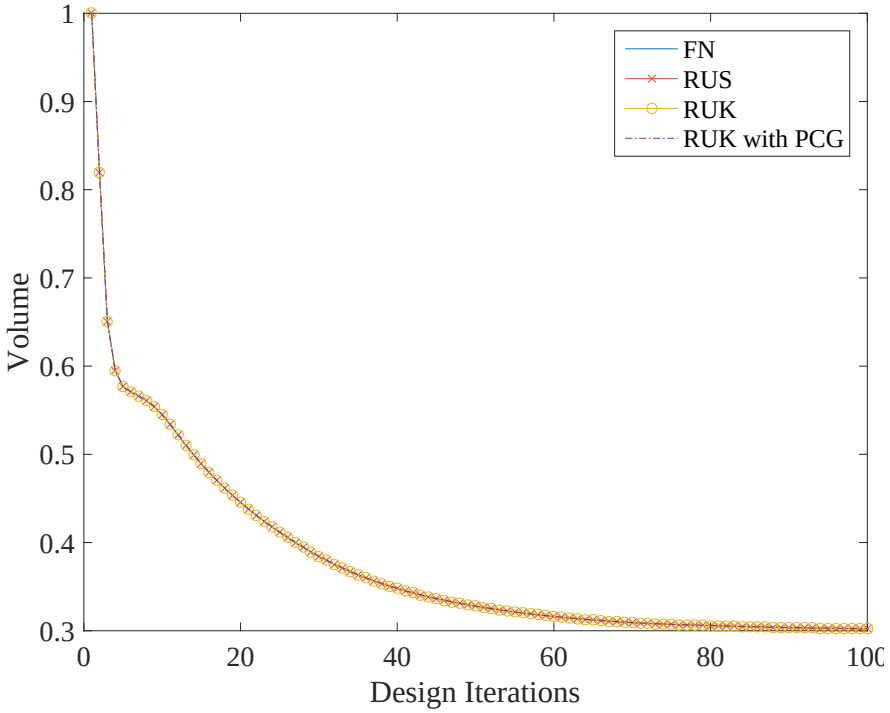

(B) Volume fraction at each design cycle

FIGURE 6.9: Numerical performance of the topology optimization process of minimum volume formulation, for all 4 schemes

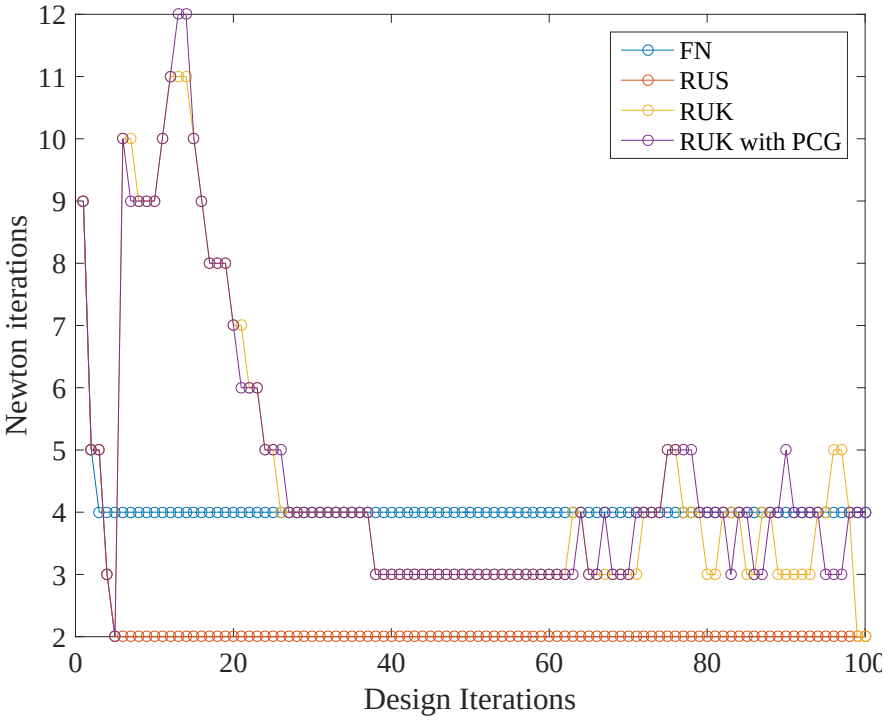

(A) Newton-Raphson iterations per design cycle

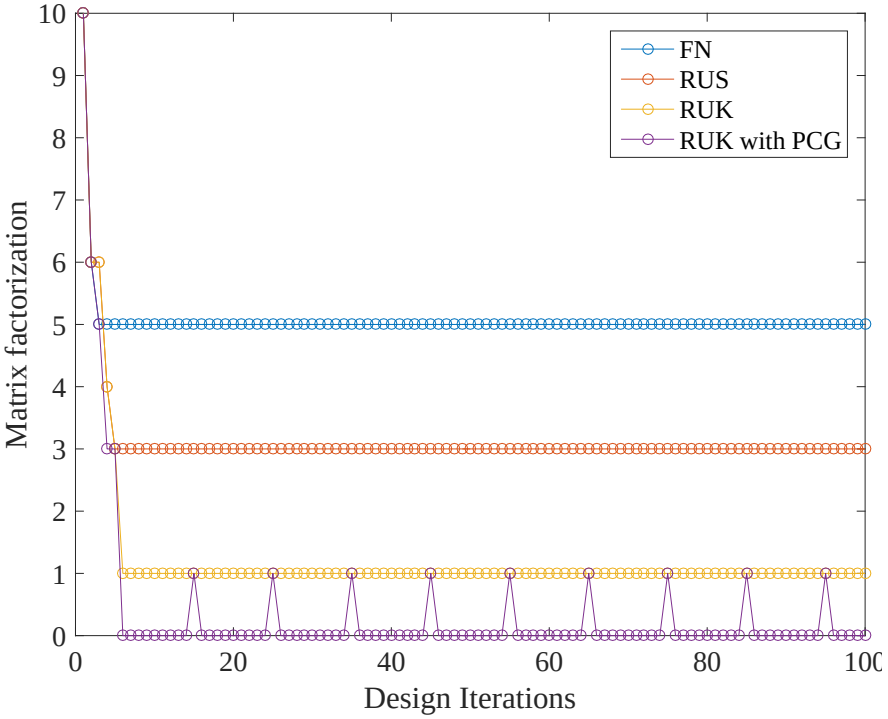

(B) Number of matrix factorizations preformed for every design cycle

FIGURE 6.10: Computational performance of the analysis for the minimum volume formulation, for all 4 schemes

6.3.2 Example 2: Large deformations of a clamped beam

In this example the clamped beam is considered again as the domain of the topology optimization problem. The design domain shown in Figure 6.11 is assumed to be a rectangular structure of dimensions $L_x \times L_y = 200 \times 40$, discretized by a grid containing nelx $\times$ nely $= 200 \times 40$ square finite elements. The load is evenly distributed between 6 neighboring nodes, in order to prevent local buckling of loaded finite elements. The displacement at the top node in the center is prescribed throughout all design cycles. The value of the prescribed displacement in this example is 3 times larger than the previous and is set to the value of $\delta = 0.3L_y$. Further parameters are given in Table 6.4. Similar to the previous example symmetry was enforced about the y axis on the densities and sensitivity analysis.

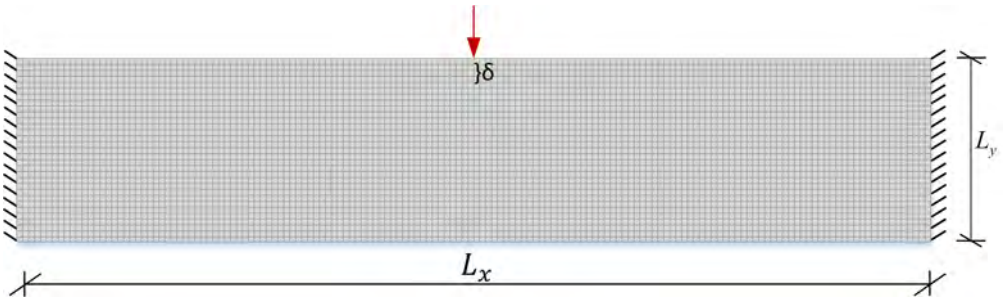

FIGURE 6.11: A Clamped beam domain with a top-central prescribed displacement node for example 2

TABLE 6.4: Parameters for Example 2

Parameter	Value
E_{min}	10^{-3}
E_{max}	10^{3}
ν	0.3
SIMP penalty	3
Filter radius	2.5

Maximum end-compliance problem was solved under the volume constraint of $V^* = 0.3$ with all three schemes presented above. In Table 6.5, results from the optimization problem solution are presented. The table shows the number of Newton iteration needed for every solution scheme and the total number of stiffness matrices factorized during the optimization process. With the standard full Newton-Raphson scheme, 791 solutions of the residual equations where preformed for 100 design cycles.

Adding the number of sensitivity analyses we obtain 891 matrix factorizations. Re-using the solution by the RUS scheme, only 253 Newton iterations were performed, 32% of the Newton iterations compares to the full scheme. Furthermore, with RUK 495 Newton iterations were required with 192 matrix factorizations that were preformed allover, only 24% compared to the standard scheme. Adding reanalysis of the adjoint equation by PCG provides a much lower number of 89 matrix factorizations, 10% compared to the starting point. After 100 design cycles the objective compliance function reached the value of about 2930.

In Figures 6.13a and 6.13b the values of the end-compliance and volume constraint are presented per design cycle respectively. During the optimization process local buckling occurred. As a result, the convergence of the structural analysis was difficult and sometimes the analysis did not converge. Therefore, it can be seen that in the standard schema the analysis was not always able to converge for the entire load and the optimizations convergence was not smooth. For the other schemes, the analysis converged easily due to the smart guess of the initial displacement vector. However, despite the differences in the optimization convergence, all final layouts are practically the same as shown in Figure 6.12. The Final layout is similar to the optimized structure in the previous example. Here the small compressed bars are omitted. Due to the larger force applied on the bars the compressed bars buckle.

Figure 6.14a shows the number of Newton iterations per design cycles. Here the effectiveness of RUS is clearly demonstrated. The number of matrix factorizations per design iteration are shown in Figure 6.14b.

Solution scheme	N-R iterations	Matrix factorization	Compliance
Full Newton	791	891	2935
Reuse U	253	353	2927
Reuse K	495	192	2906
PCG	480	89	2928

TABLE 6.5: Results from solving the maximum end-compliance problem formulation

Minimum volume problem was solved under the end-compliance constraint of $C^* = 2935$ obtained from solving the first formulationwith the standard scheme. In Table 6.6, results from the optimization problem in Equation (6.2) are presented. The table shows the number of Newton iteration needed for every solution scheme and the

total number of stiffness matrices factorized during the optimization process. With the standard full Newton-Raphson scheme, 809 solutions of the residual equations where preformed for 100 design cycles. Adding the number of sensitivity analyses we obtain 909 matrix factorizations. Re-using the solution by the RUS scheme, only 215 Newton iterations were performed, reducing almost 73% of the Newton iterations. Furthermore, with RUK 461 Newton iterations were required with 125 matrix factorizations that were preformed allover, only 13.7% matrix factorizations compared to the standard scheme. Adding reanalysis of the adjoint equation by PCG provides a number of 36 matrix factorizations, 4% compared to the starting point. After 100 design cycles the objective volume function reached the value of 0.3. Final layouts of the schemes are all the same and are shown in Figure 6.15.
In Figures 6.16a and 6.16b the values of the end-compliance constraint and the volume objective are presented per design cycle respectively, as observed all schemes converged in the same manner.
Figure 6.17a shows the number of Newton iterations per design cycles. Here the effectiveness of RUS is clearly demonstrated. The number of matrix factorizations per design iteration are shown in Figure 6.17b.

A comparison between the solution by RUK with PCG of both formulations indicates again an even higher computational advantage of the second formulation. The minimum volume formulation was able to converge using only 36 matrix factorizations, while for the first problem 89 matrix factorizations where performed.

Solution scheme	N-R iterations	Matrix factorization	Volume
Full Newton	809	909	0.3
Reuse U	215	315	0.3
Reuse K	461	125	0.3
PCG	468	36	0.3

TABLE 6.6: Results from solving the minimum volume problem formulation

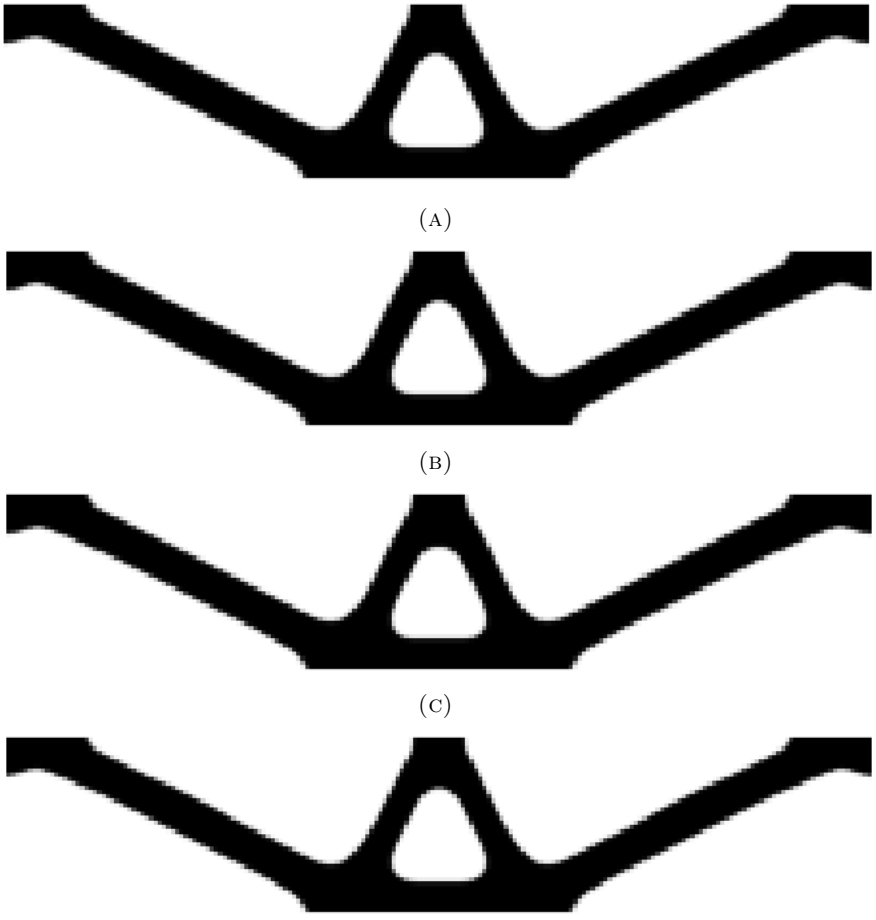

(A)

(B)

(C)

(D)

FIGURE 6.12: Final layout solutions of the maximum end-compliance problem for all 4 schemes after 100 design cycle: (A) Full Newton-Raphson; (B) RUS; (C) RUK; (D) RUK with PCG

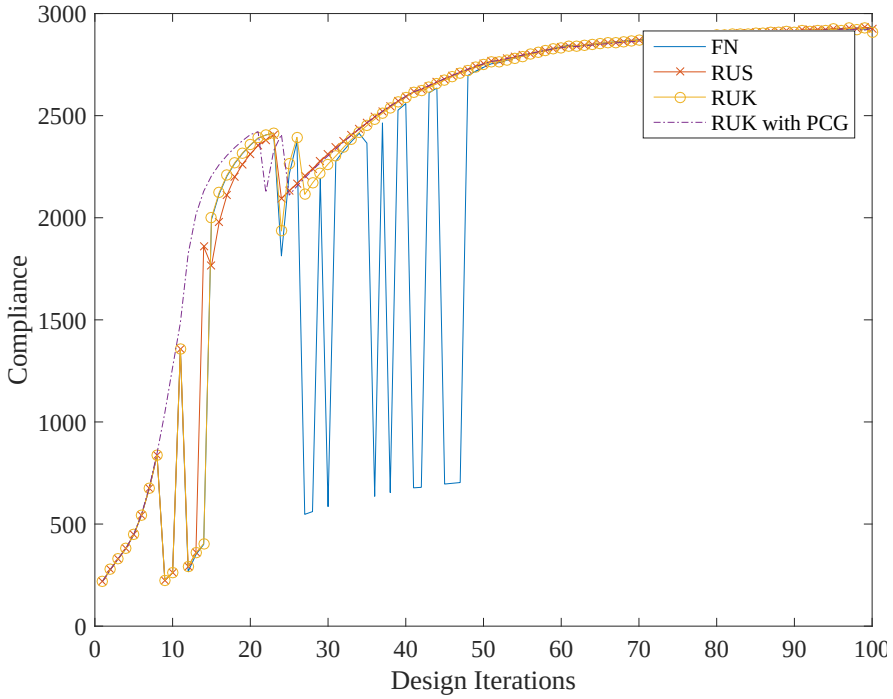

(A) Compliance value obtained from every design cycle

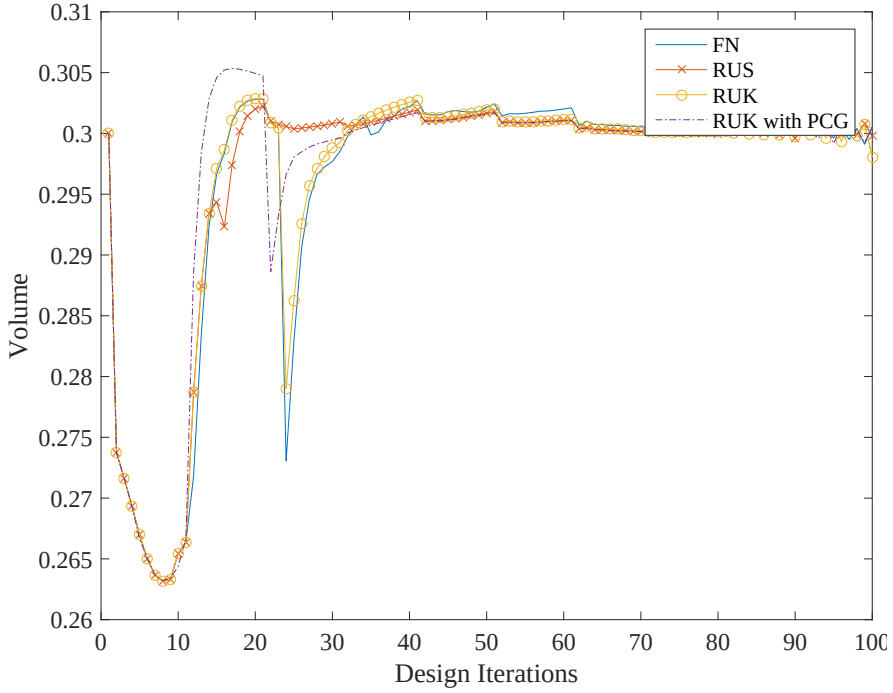

(B) Volume fraction obtained from every design cycle

FIGURE 6.13: Numerical performance of the topology optimization process of maximum end-compliance formulation, for all 4 schemes

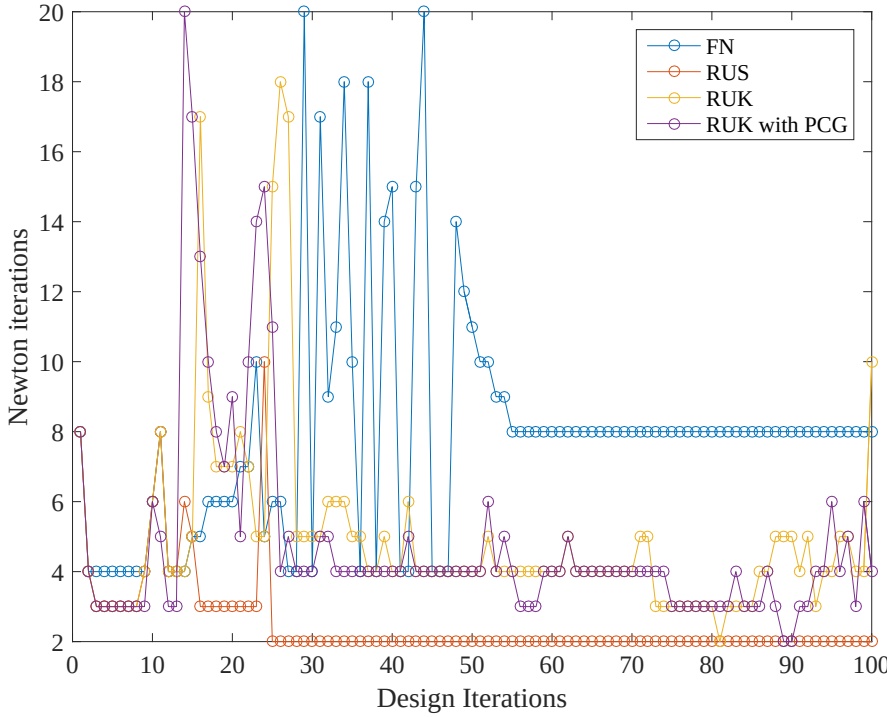

(A) Newton-Raphson iterations per design cycle

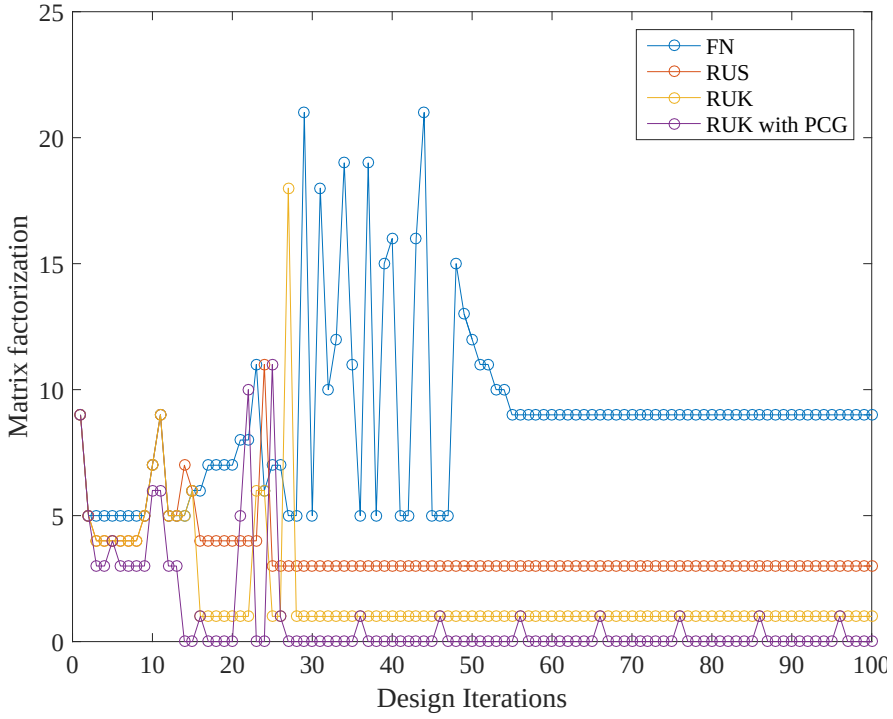

(B) Number of matrix factorizations preformed for every design cycle

FIGURE 6.14: Computational performance of the analysis for the maximum end-compliance formulation, for all 4 schemes

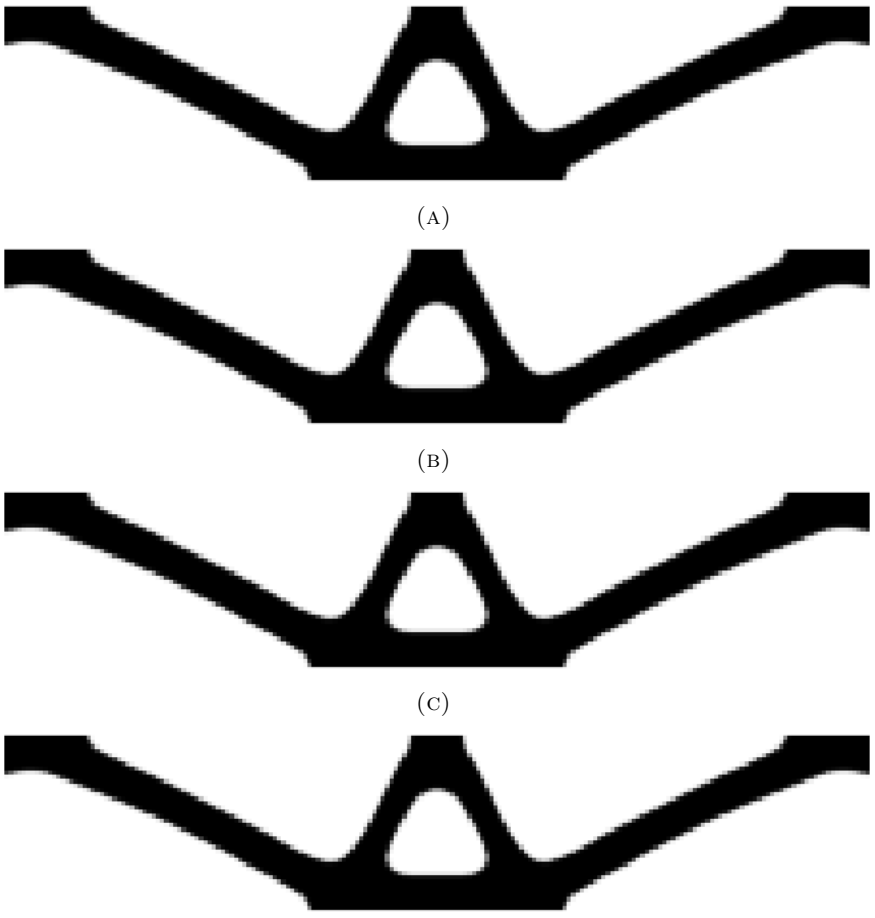

(A)

(B)

(C)

(D)

FIGURE 6.15: Final layout solutions of the minimum volume problem for all 4 schemes after 100 design cycle: (A) Full Newton-Raphson; (B) RUS; (C) RUK; (D) RUK with PCG

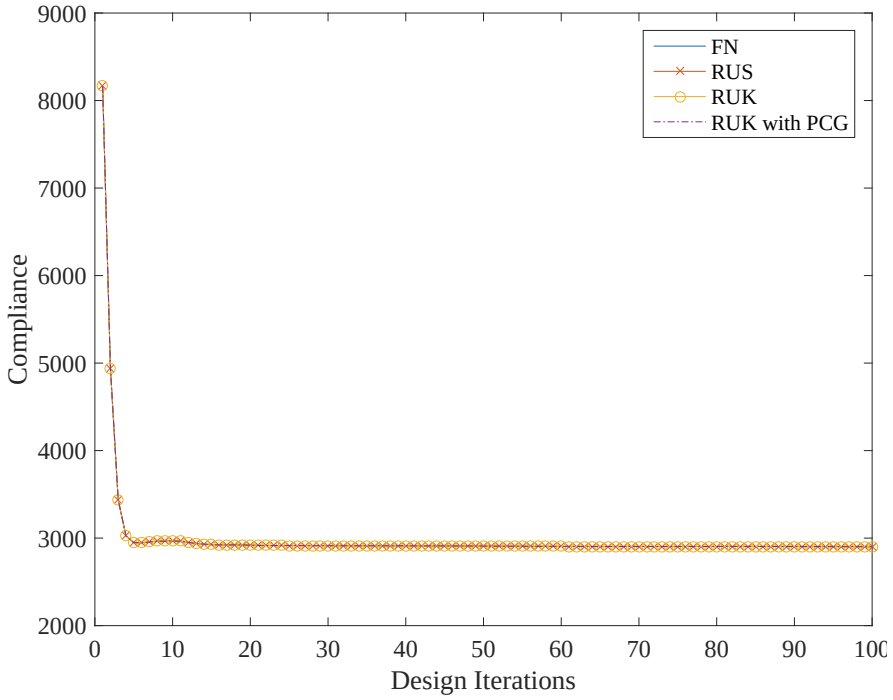

(A) Compliance value at each design cycle

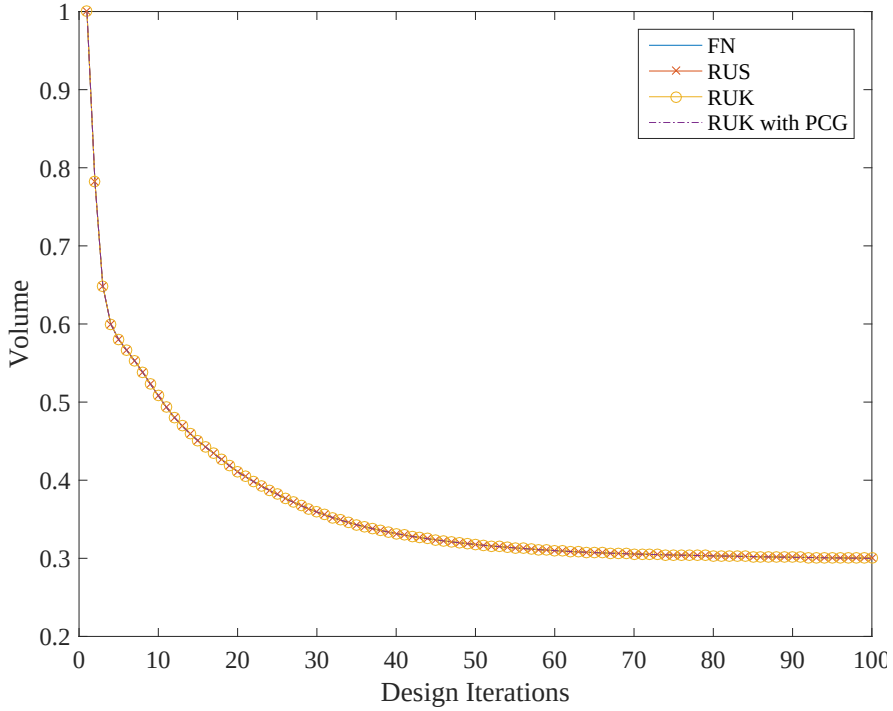

(B) Volume fraction at each design cycle

FIGURE 6.16: Numerical performance of the topology optimization process of minimum volume formulation, for all 4 schemes

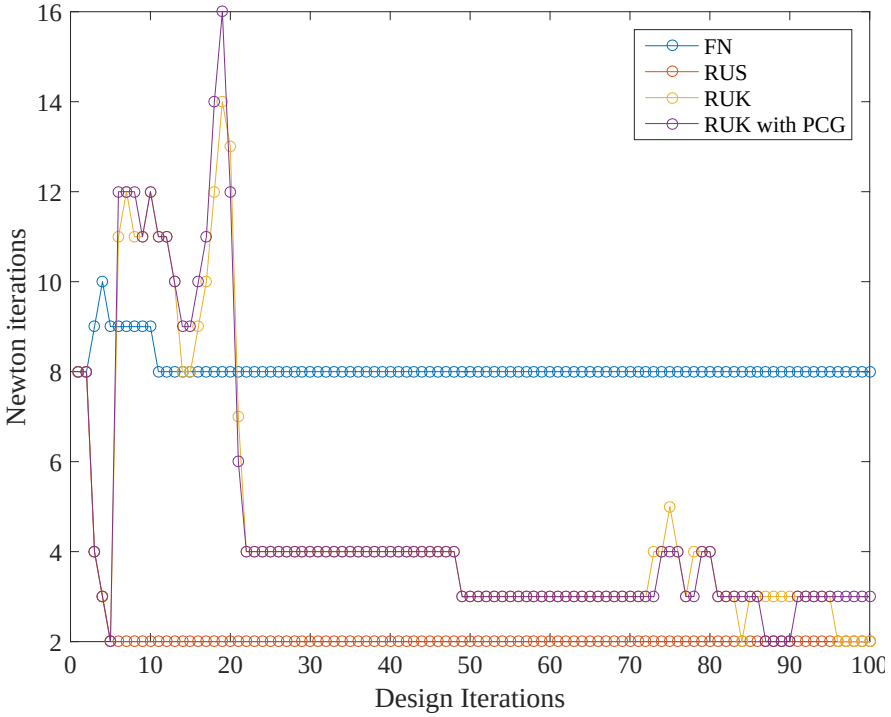

(A) Newton-Raphson iterations per design cycle

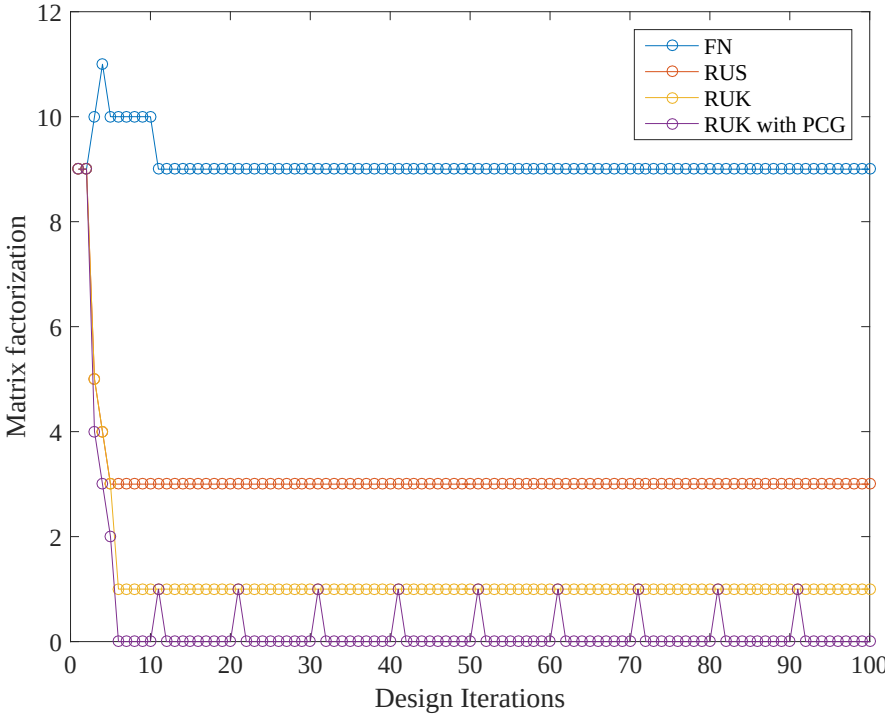

(B) Number of matrix factorizations preformed for every design cycle

FIGURE 6.17: Computational performance of the analysis for the minimum volume formulation, for all 4 schemes

6.3.3 Example 3: Axial deformations of a beam

In this example, topology optimization of a simply supported beam is performed. The main purpose of this example is to obtain an Euler's column that is buckling safe. In the next Chapter 7, a similar problem will be examined but with solving the eigenvalue problem. The design domain shown in Figure 6.18 is assumed to be a rectangular structure of dimensions $L_x \times L_y = 200 \times 40$, discretized by a grid containing nelx $\times$ nely $= 200 \times 40$ square finite elements. Due to the high geometric nonlinearity of the problem the value of E_{min} was set to a value of 1 in order to avoid local buckling of void areas. Additionally, as opposed to the two previous examples the value of the Heaviside sharpness control β is increased only every 25 iterations by 1.0. Further parameters are given in Table 6.7. In the center-middle of each edge a thickness of $0.3L_y$ elements are pinned (12 elements). These boundary conditions do not provide a pure Eulerian column but are modeled in order to avoid local buckling. The load is evenly distributed between 14 neighboring nodes, in order to prevent local buckling of local finite elements. The elements related to the loaded nodes are set to be constant solid elements. A node on the right side is prescribed throughout all design cycles to the value of $\delta = 0.125L_y$. For the large deformation effect an imperfection was set by shifting the prescribed node from the center by one element. For achieving an optimized solution for buckling in both directions and avoiding numerical imperfection symmetry was enforced about both x and y axis on the sensitivity analysis and the design densities.

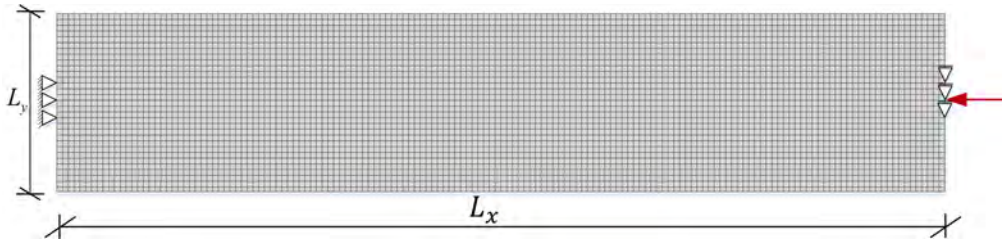

FIGURE 6.18: A simply supported beam domain with a top-central prescribed displacement node for example 3

TABLE 6.7: Parameters for Example 3

Parameter	Value
E_{min}	1
E_{max}	10^3
ν	0.3
SIMP penalty	3
Filter radius	2.5

Maximum end-compliance problem was first solved under the volume constraint of $V^* = 0.5$ and with all three schemes presented above in Section 6.2. In Table 6.8 results from the optimization problem are presented. The table shows the number of Newton iteration needed for every solution scheme and the total number of stiffness matrices factorized during the optimization process. With the standard full Newton-Raphson scheme, 1297 Newton iterations where preformed for 200 design cycles. Adding the number of sensitivity analyses we obtain 1497 matrix factorizations. Re-using the solution by the RUS scheme, 432 Newton iterations were performed, 33.3% compared to the full Newton-Raphson scheme. Furthermore, with RUK 994 Newton iterations were required with 242 matrix factorizations that were preformed allover, only 16.1% compared to the standard scheme. Adding reanalysis of the adjoint equation by PCG provides a lower number of 62 matrix factorizations, 4.1% compared to the starting point. After 200 design cycles the objective compliance function reached the value of 1938.8. Although for the last scheme the value is slightly different, the final structures are practically the same as shown in Figure 6.19. The optimized layout for the linear case would be a simple long bar. This is not stable when large deformations are considered. Therefore the final layout provides stabilty using two large arches with internal reinforcement bars.
In Figures 6.20a and 6.20b the values of the end-compliance and volume constraint are presented per design cycle respectively, as observed all schemes converged in the same manner. The non-smoothness of the convergence is related to the change of the Heaviside sharpness control β.
Figure 6.21a shows the number of Newton iterations per design cycles. The number of matrix factorizations per design iteration are shown in Figure 6.21b.

Solution scheme	N-R iterations	Matrix factorization	Compliance
Full Newton	1297	1497	1938.8
Reuse U	432	632	1938.8
Reuse K	994	242	1938.8
PCG	1008	62	1945.4

TABLE 6.8: Results from solving the maximum end-compliance problem formulation

Minimum volume problem was solved under the end-compliance constraint of $C^* = 1939$ obtained from solving the first formulationwith the standard scheme. In Table 6.9, results from the optimization problem in Equation (6.2) are presented. The

table shows the number of Newton iteration needed for every solution scheme and the total number of stiffness matrices factorized during the optimization process. With the standard full Newton-Raphson scheme, 1401 solutions of the residual equations where preformed for 200 design cycles. Adding the number of sensitivity analyses we obtain 1601 matrix factorizations. Re-using the solution by the RUS scheme, only 428 Newton iterations were performed, 30.5% less than the Full-Newton scheme. Furthermore, with RUK 1067 Newton iterations were required with 237 matrix factorizations that were preformed allover, only 14.8% matrix factorizations compared to the standard scheme. Adding reanalysis of the adjoint equation by PCG provides a number of 59 matrix factorizations, 3.7% compared to the starting point. After 200 design cycles the objective volume function reached the value of 0.52, slightly higher than the volume constraint for previous problem. Final layouts of the schemes are all similar and are shown in Figure 6.22.

In Figures 6.23a and 6.23b the values of the end-compliance constraint and the volume objective are presented per design cycle respectively, all schemes converged in the same manner.

Figure 6.24a shows the number of Newton iterations per design cycles. The number of matrix factorizations per design iteration are shown in Figure 6.24b.

A comparison between the solution by RUK with PCG provides a slight computational advantage of the second formulation. The minimum volume formulation was able to converge using only 59 matrix factorizations, while for the end-complince problem formulation 62 matrix factorizations where performed.

Solution scheme	N-R iterations	Matrix factorization	Volume
Full Newton	1401	1601	0.52
Reuse U	428	628	0.52
Reuse K	1067	237	0.52
PCG	1065	59	0.519

TABLE 6.9: Results from solving the minimum volume problem formulation

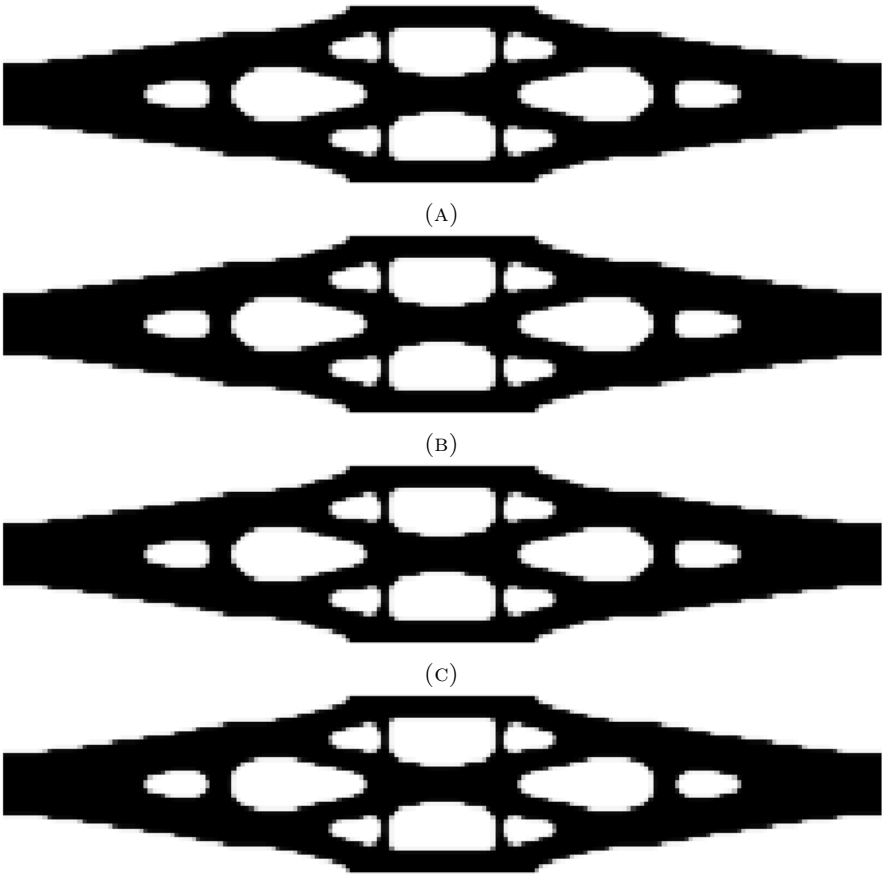

(A)

(B)

(C)

(D)

FIGURE 6.19: Final layout solutions of the maximum end-compliance problem for all 4 schemes after 200 design cycle: (A) Full Newton-Raphson; (B) RUS; (C) RUK; (D) RUK with PCG

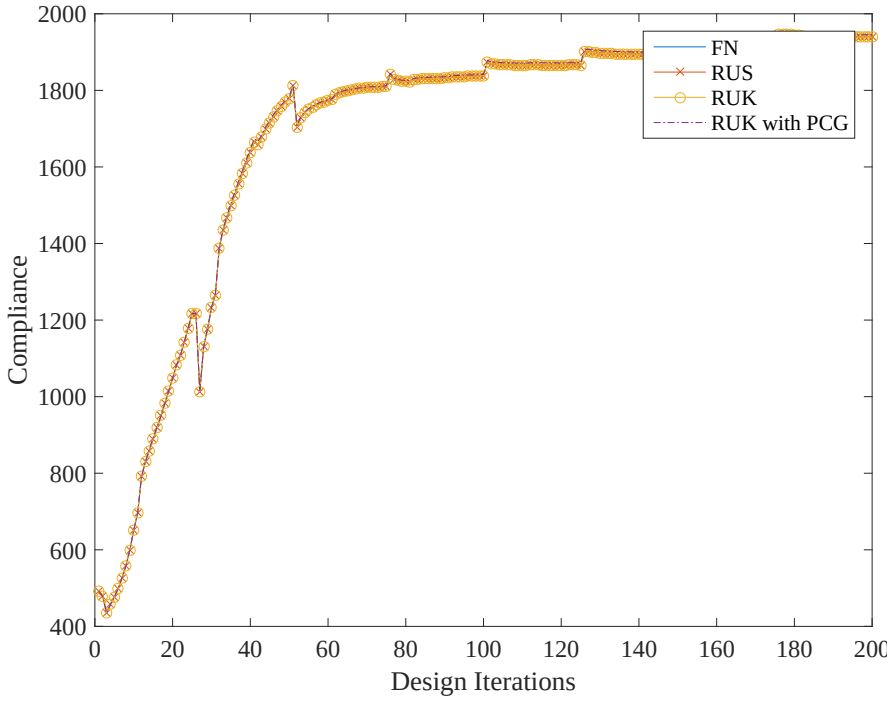

(A) Compliance value at each design cycle

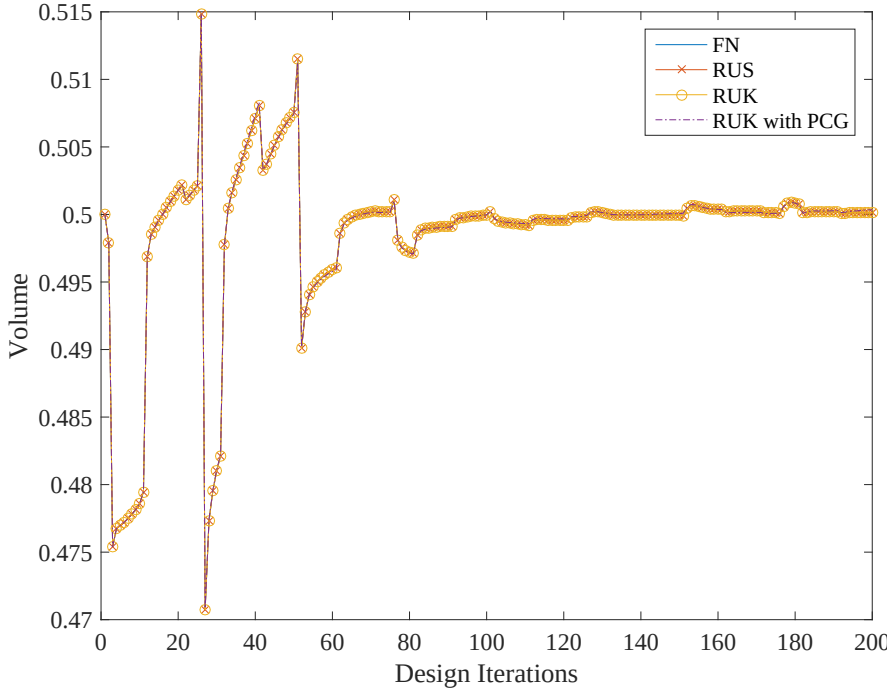

(B) Volume fraction at each design cycle

FIGURE 6.20: Numerical performance of the topology optimization process of maximum end-compliance formulation, for all 4 schemes

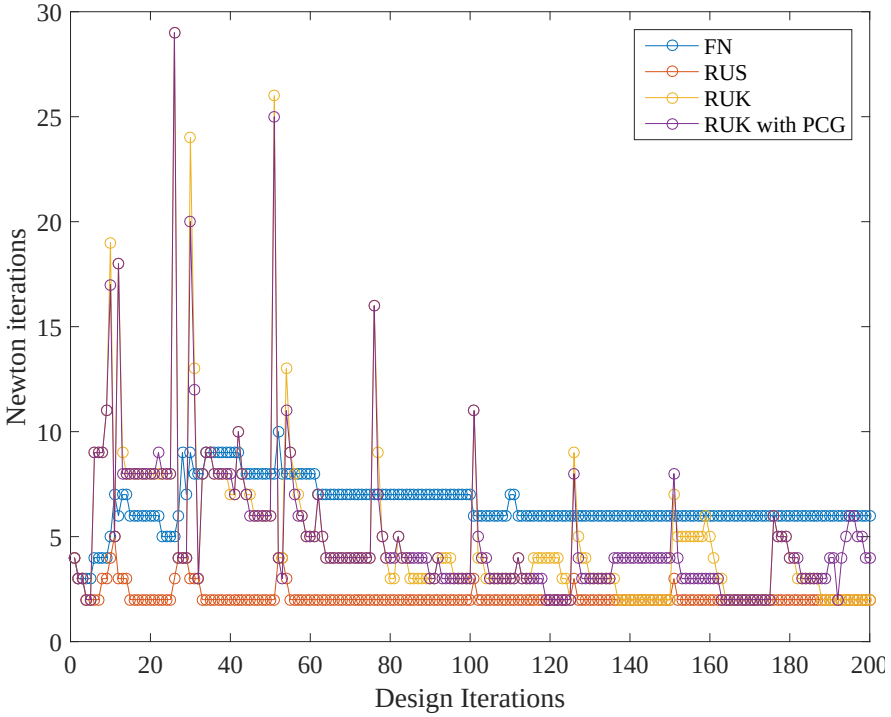

(A) Newton-Raphson iterations per design cycle

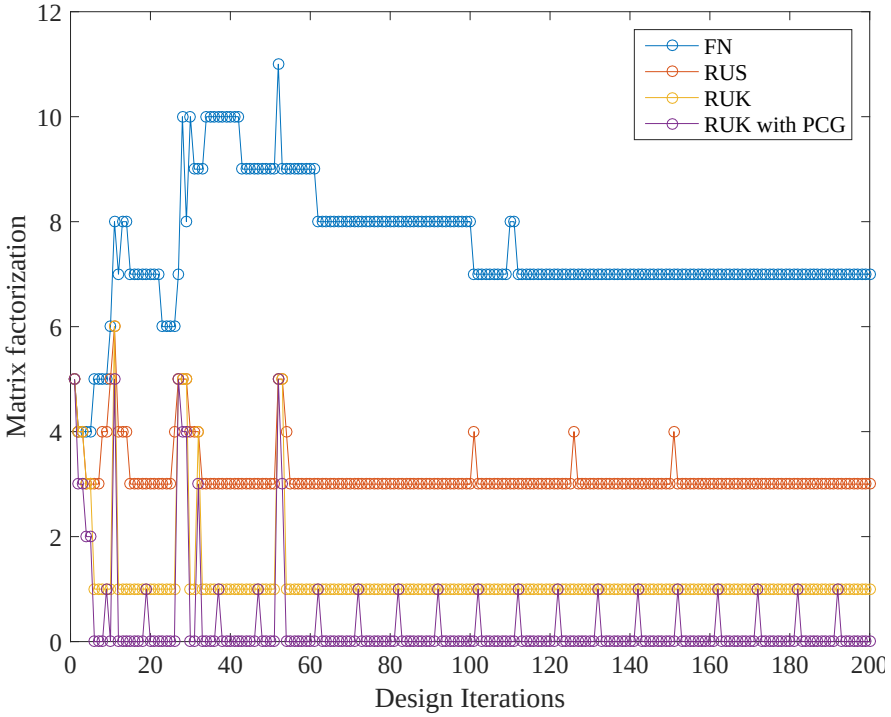

(B) Number of matrix factorizations preformed for every design cycle

FIGURE 6.21: Computational performance of the analysis for the maximum end-compliance formulation, for all 4 schemes

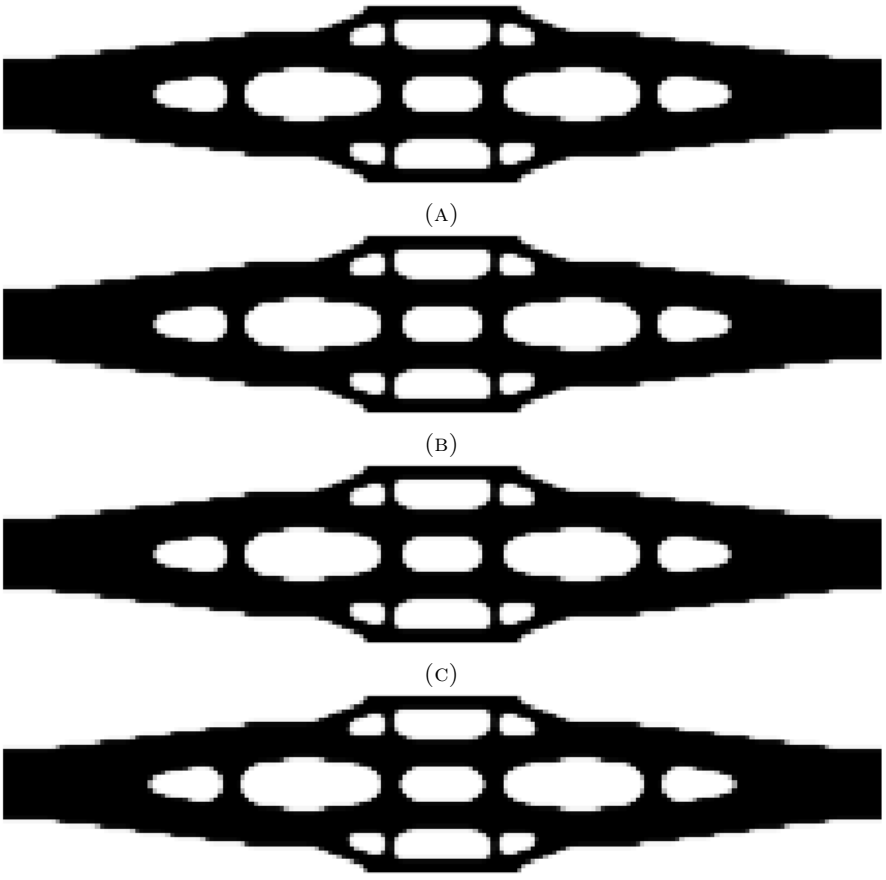

(A)

(B)

(C)

(D)

FIGURE 6.22: Final layout solutions of the minimum volume problem for all 4 schemes after 200 design cycle: (A) Full Newton-Raphson; (B) RUS; (C) RUK; (D) RUK with PCG

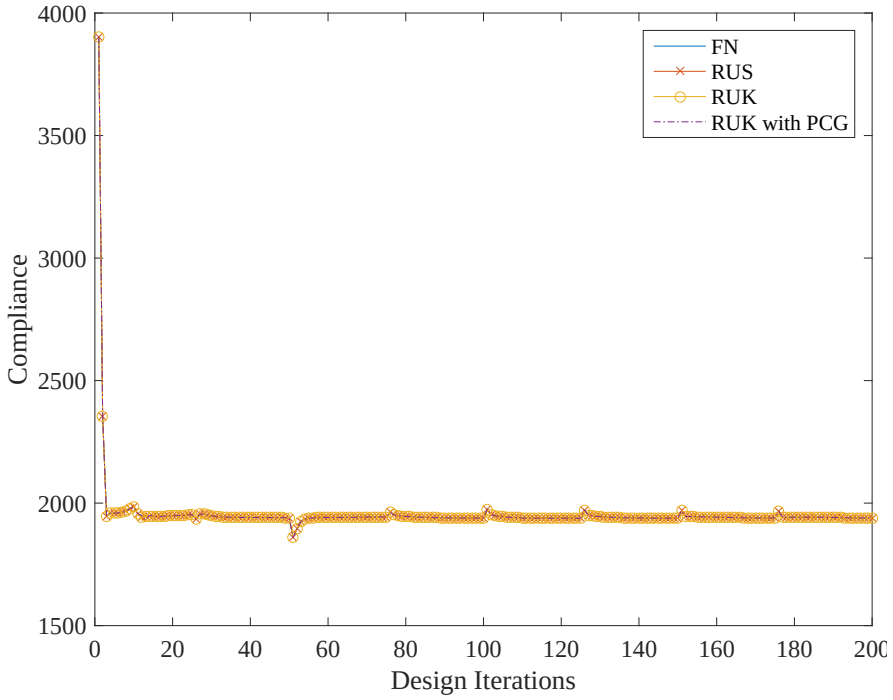

(A) Compliance value at each design cycle

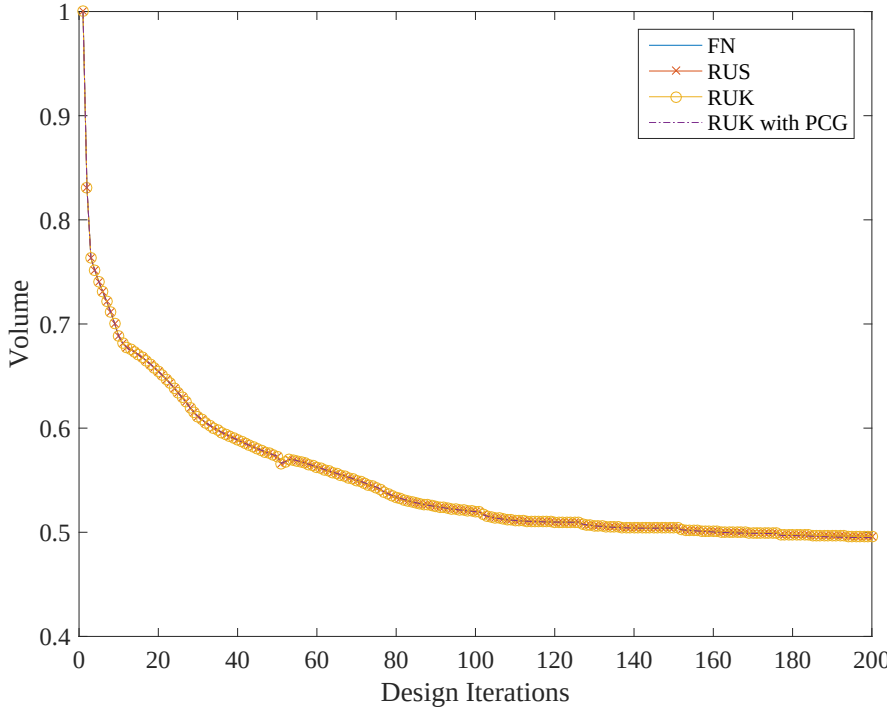

(B) Volume fraction at each design cycle

FIGURE 6.23: Numerical performance of the topology optimization process of minimum volume formulation, for all 4 schemes

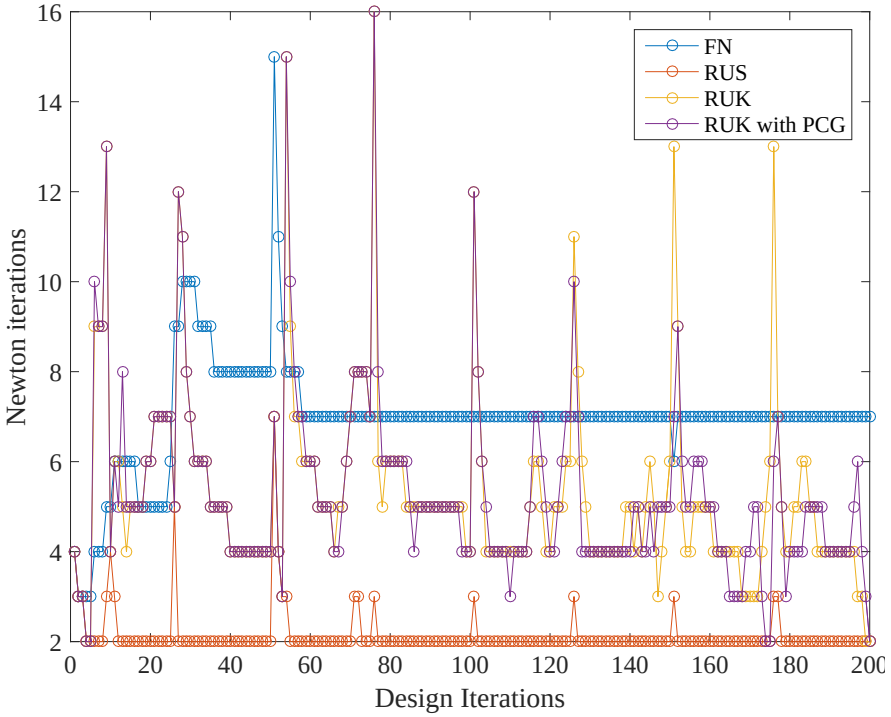

(A) Newton-Raphson iterations per design cycle

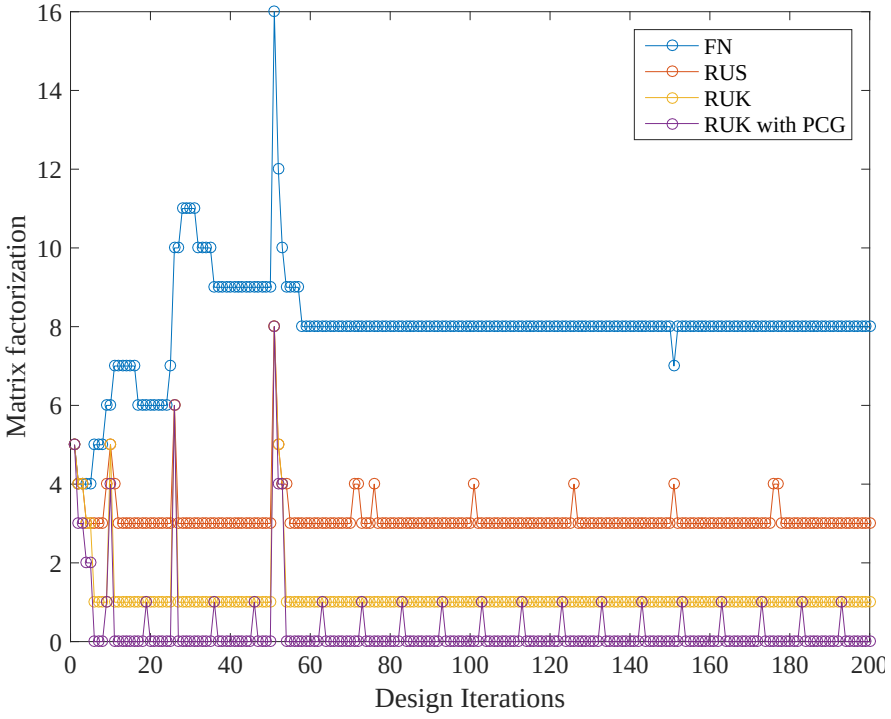

(B) Number of matrix factorizations preformed for every design cycle

FIGURE 6.24: Computational performance of the analysis for the minimum volume formulation, for all 4 schemes

6.4 Summary

This chapter presented numerical experiments that demonstrate reanalysis methods in topology optimization of GNL structures. Two different problem formulations were considered, the maximization of the end-compliance and minimization the of the volume. Computational effort was significantly reduced by three reanalysis sachems: RUS, RUK and the former with approximate sensitivity analysis. Approximation of the sensitivity adjoint vector with PCG method was suggested in this research work, allowing additional savings in computational cost. Note that the optimized result in some cases was slightly different, however the layouts obtained are practically the same. In RUS, the number of iterations was roughly cut to half. Although problems with large displacements yielded higher results, still between 40%-50% of Newton iterations were reduced. As can be expected in the RUK scheme, the number of Newton iterations increased significantly. Nevertheless, it was possible to see a reduction in the number of matrix factorizations across all the optimization process. It is possible to identify for both methods above that there is a certain advantage of computational operation saving but it is difficult to predict in advance which method will be more effective. The last scheme saves a specific tangent stiffness matrix and reuses it sequentially in a number of design cycles. This information can be used in addition to approximate the adjoint vector of the sensitivity analysis using a only 5 PCG iteration or less. This last scheme was able to save a large number of matrix factorizations. Between 4% to 11% factorizations were preformed compared to the full solution. A certain advantage was found for the minimum volume formulation where the reference matrix is stiffer. For a given reanalysis of a structural optimization problem the minimum volume formulation was able to converge with about half the number of matrix factorizations compared to the maximum end-compliance formulation.

Chapter 7

Reanalysis in buckling optimization

In this chapter linear buckling analysis is implemented in topology optimization and reanalysis techniques are established for computational efficiency. Examples with geometrical nonlinearity were tested in Chapter 6 where the response was calculated by an incremental analysis, providing a complete structural behavior. For estimating the critical stability load this procedure may result in high computational effort and even non-convergence. An alternative option is to analyze the structure using linearized buckling analysis that was introduced in Section 3.4.2. Solving repeatedly the eigenvalue problem for the analysis still requires long computational time. A potentially more efficient alternative is to use reanalysis by CA to reduce the linearized buckling eigenvalue problem as presented in Chapter 4. The approximated buckling load is set as an objective and constraint in two topology optimization problem formulations that will be presented in Section 7.1.1. Sensitivity analysis is developed accordingly in Section 7.1.2 and two numerical examples are carried out. First a compressed cantilever beam in Section 7.2.1 and second a simply supported beam in Section 7.2.2

7.1 Buckling topology optimization

Once the linearized eigenvalue problem of Equation (3.39) is posed, the design problem is formulated in two ways: (1) Maximizing the lowest buckling load factor under a volume

constraint; (2) minimizing the structure's volume under a constraint on the buckling load. Our goal is to solve the optimization problem for both design formulations and compare efficiency using reanalysis by the CA method.

7.1.1 Problem formulation

For the first optimization problem the objective is to maximize critical buckling factor $\tilde{\beta}$. As $\mathbf{K}_L$ is positive definite and as $\mathbf{K}_G$ may not be so, it is convenient to work with $1/\tilde{\beta}$ as the eigenvalue (Bendsøe and Sigmund, 2003). The optimization problem is thus stated to minimize the reciprocal of the first critical buckling load as follows:

$$\begin{aligned}
\min_{\boldsymbol{\rho}} \quad & \left\{ \tilde{\lambda} = \max_{i=1..Ndof} \frac{1}{\tilde{\beta}_i} \right\} \\
\text{s.t.:} \quad & \sum_{e=1}^{N_{elm}} v_e \rho_e \leq V^* \\
& 0 < \rho_{\min} \leq \rho_e \leq 1 \qquad e = 1, ..., N_{elm} \\
\text{with:} \quad & \left[\mathbf{K}_G + \tilde{\lambda}_i \mathbf{K}_L \right] \boldsymbol{\Phi}_i = 0 \qquad i = 1, .., N_{dof}
\end{aligned} \tag{7.1}$$

Where V^* is the a constant value of the volume. Both formulation are modeled, analyzed and solved in the same way so switching between the formulations is quite straightforward,

$$\begin{aligned}
\min_{\boldsymbol{\rho}} \quad & \sum_{e=1}^{N_{elm}} v_e \rho_e \\
\text{s.t.:} \quad & \tilde{\lambda} \leq \lambda^* \\
& 0 < \rho_{\min} \leq \rho_e \leq 1 \qquad e = 1, ..., N_{elm} \\
\text{with:} \quad & \left[\mathbf{K}_G + \tilde{\lambda}_i \mathbf{K}_L \right] \boldsymbol{\Phi}_i = 0 \qquad i = 1, .., N_{dof}
\end{aligned} \tag{7.2}$$

where in this case the constraint is a critical load λ^* that stays constant during the design process.

Problem formulation for additional buckling modes

Throughout the research work on the critical buckling load optimization, it was found that in some design cycles the first buckling mode changes, thus there is a switching of

modes and buckling load factor. Therefore, the optimization is not smooth and additional buckling modes should be taken into account in the objective function. One way to reformulate the problem in Equation (7.1) is the bound formulation:

$$\begin{aligned} \min_{\boldsymbol{\rho}} \quad & \alpha \\ \text{s.t.:} \quad & \tilde{\lambda}_j \leq \alpha \qquad j = 1, ..., m \\ & \sum_{e=1}^{N_{elm}} v_e \rho_e \leq V^* \\ & 0 \leq \rho_e \leq 1 \qquad e = 1, ..., N_{elm} \end{aligned} \tag{7.3}$$

$$\text{with:} \quad \left[\mathbf{K}_G + \tilde{\lambda}_i \mathbf{K}_L\right] \boldsymbol{\Phi}_i = 0 \qquad i = 1, .., m \tag{7.4}$$

where a number of m eigenvalues are considered and set as constraints to be smaller or equal to α.

All the mathematical optimization problems in this Chapter are solved using convex approximation by the Method of Moving Asymptotes (MMA) proposed by Svanberg (Svanberg, 1987) as presented in chapter 2. As this method is gradient based, sensitivity information of the objective and the constraints with respect to the design variables are needed.

7.1.2 Sensitivity analysis

Calculating the sensitivities of the buckling load is similar to the well known eigenfrequency optimization. However, in contrast to the mass matrix, the geometric stiffness sensitivity depends on the deformation sensitivities and is not easily computed. Starting with the linearized buckling problem from Equation (3.39), the buckling load of a structure is the smallest positive value of $\tilde{\lambda}$ which solves the eigenvalue problem

$$(\mathbf{K}_G + \tilde{\lambda}_i \mathbf{K}_L)\bar{\boldsymbol{\Phi}}_i = 0 \quad i = 1, 2... \tag{7.5}$$

where $\mathbf{K}_L$ is the linear stiffness matrix of the structure, $\mathbf{K}_G$ is the geometric stiffness matrix; $\tilde{\lambda}_i$ is the i'th load factor; $\bar{\boldsymbol{\Phi}}_i$ is the corresponding buckling mode vector normalized to satisfy $\bar{\boldsymbol{\Phi}}_i^T \mathbf{K}_L \bar{\boldsymbol{\Phi}}_i = 1$. Note that for our finite element discretization, both stiffness matrices are functions of the design variable $\boldsymbol{\rho}$ and the geometric stiffness matrix depends also on $\mathbf{u}$, the displacement vector solution of the linear equilibrium equations.

Direct differentiation of the eigenvalue problem in Equation (7.5) for a single eigenvalue provides:

$$\frac{\partial \mathbf{K}_G}{\partial \bar{\rho}_e}\bar{\mathbf{\Phi}}_i + \mathbf{K}_G\frac{\partial \bar{\mathbf{\Phi}}_i}{\partial \bar{\rho}_e} + \frac{\partial \tilde{\lambda}_i}{\partial \bar{\rho}_e}\mathbf{K}_L\bar{\mathbf{\Phi}}_i + \tilde{\lambda}_i\frac{\partial \mathbf{K}_L}{\partial \bar{\rho}_e}\bar{\mathbf{\Phi}}_i + \tilde{\lambda}_i\mathbf{K}_L\frac{\partial \bar{\mathbf{\Phi}}_i}{\partial \bar{\rho}_e} = 0 \tag{7.6}$$

Pre-multiplying Equation (7.6) by $\bar{\mathbf{\Phi}}_i^{\mathbf{T}}$

$$\bar{\mathbf{\Phi}}_i^T\frac{\partial \mathbf{K}_G}{\partial \bar{\rho}_e}\bar{\mathbf{\Phi}}_i + \bar{\mathbf{\Phi}}_i^T\mathbf{K}_G\frac{\partial \bar{\mathbf{\Phi}}_i^T}{\partial \bar{\rho}_e} + \bar{\mathbf{\Phi}}_i^T\frac{\partial \tilde{\lambda}_i}{\partial \bar{\rho}_e}\mathbf{K}_L\bar{\mathbf{\Phi}}_i + \tilde{\lambda}_i\bar{\mathbf{\Phi}}_i^T\frac{\partial \mathbf{K}_L}{\partial \bar{\rho}_e}\bar{\mathbf{\Phi}}_i + \tilde{\lambda}_i\bar{\mathbf{\Phi}}_i^T\mathbf{K}_L\frac{\partial \bar{\mathbf{\Phi}}_i}{\partial \bar{\rho}_e} = 0 \tag{7.7}$$

Rearranging the equation

$$\frac{\partial \tilde{\lambda}_i}{\partial \bar{\rho}_e}\bar{\mathbf{\Phi}}_i^T\mathbf{K}_L\bar{\mathbf{\Phi}}_i + \bar{\mathbf{\Phi}}_i^T\left(\frac{\partial \mathbf{K}_G}{\partial \bar{\rho}_e} + \tilde{\lambda}_i\frac{\partial \mathbf{K}_L}{\partial \bar{\rho}_e}\right)\bar{\mathbf{\Phi}}_i + \bar{\mathbf{\Phi}}_i^T\left(\mathbf{K}_G + \tilde{\lambda}_i\mathbf{K}_L\right)\frac{\partial \bar{\mathbf{\Phi}}i}{\partial \bar{\rho}_e} = 0 \tag{7.8}$$

Where the eigenvectors are normalized to $\bar{\mathbf{\Phi}}_i^T\mathbf{K}_L\bar{\mathbf{\Phi}}_i = 1$. Further, since the stiffness matrices are symmetric and with Equation (7.5) we obtain:

$$\frac{\partial \tilde{\lambda}_i}{\partial \bar{\rho}_e} = -\bar{\mathbf{\Phi}}_i^T\left(\frac{\partial \mathbf{K}_G}{\partial \bar{\rho}_e} + \tilde{\lambda}_i\frac{\partial \mathbf{K}_L}{\partial \bar{\rho}_e}\right)\bar{\mathbf{\Phi}}_i. \tag{7.9}$$

Expanding Equation (7.9) by adding the zero content with the adjoint vector $\mathbf{v}^T$

$$\bar{\mathbf{\Phi}}_i^T\hat{\mathbf{K}}_G\bar{\mathbf{\Phi}}_i = \bar{\mathbf{\Phi}}_i^T\mathbf{K}_G\bar{\mathbf{\Phi}}_i + \mathbf{v}^T\left(\mathbf{K}_L\mathbf{u} - \mathbf{f}\right). \tag{7.10}$$

Now we differentiate directly the equation with respect to the density design variables

$$\bar{\mathbf{\Phi}}_i^T\frac{\partial \hat{\mathbf{K}}_G}{\partial \bar{\rho}_e}\bar{\mathbf{\Phi}}_i = \bar{\mathbf{\Phi}}_i\frac{\partial \mathbf{K}_G}{\partial \mathbf{u}}\frac{\partial \mathbf{u}}{\partial \bar{\rho}_e}\bar{\mathbf{\Phi}}_i + \mathbf{v}^T\left(\frac{\mathbf{K}_L}{\partial \bar{\rho}_e}\mathbf{u} + \mathbf{K}_L\frac{\partial \mathbf{u}}{\partial \bar{\rho}_e}\right) \tag{7.11}$$

and

$$\bar{\mathbf{\Phi}}_i^T\frac{\partial \hat{\mathbf{K}}_G}{\partial \bar{\rho}_e}\bar{\mathbf{\Phi}}_i = \left(\bar{\mathbf{\Phi}}_i^T\frac{\partial \mathbf{K}_G}{\partial \mathbf{u}}\bar{\mathbf{\Phi}}_i + \mathbf{v}^T\mathbf{K}_L\right)\frac{\partial \mathbf{u}}{\partial \bar{\rho}_e} + \mathbf{v}^T\frac{\partial \mathbf{K}_L}{\partial \bar{\rho}_e}\mathbf{u} \tag{7.12}$$

In order to avoid calculating $\dfrac{\partial \mathbf{u}}{\partial \bar{\rho}_e}$ we impose that

$$\bar{\mathbf{\Phi}}_i^T\frac{\partial \mathbf{K}_G}{\partial \mathbf{u}}\bar{\mathbf{\Phi}}_i + \mathbf{v}^T\mathbf{K}_L = 0. \tag{7.13}$$

This set of equations are solved for finding $\mathbf{v}^T$, the unknown adjoint vector. Finally the full term of the sensitivity analysis for a single eigenvalue is obtained,

$$\frac{\partial \tilde{\lambda}_i}{\partial \bar{\rho}_e} = \bar{\mathbf{\Phi}}_i^T \left(\frac{\partial \mathbf{K}_G}{\partial \bar{\rho}_e} - \tilde{\lambda}_i \frac{\partial \mathbf{K}_L}{\partial \bar{\rho}_e} \right) \bar{\mathbf{\Phi}}_i + \mathbf{v}^T \frac{\mathbf{K}_L}{\partial \bar{\rho}_e} \mathbf{u}. \tag{7.14}$$

7.1.3 Numerical considerations

For ensuring robustness and constructibility of the final design layout, the same numerical methods mentioned in the previous examples are also implemented here. Several changes and updates were made for this example. First avoiding the phenomena of artificial local modes of void elements that was discussed in Chapter 2.5.1 and in the previous example in Chapter 6.1.4, we test a slightly different SIMP interpolation function, presented in Equation (2.14). The Heaviside and filter functions are the same as in previous numerical examples. Parameters for these functions will be presented below.

7.2 Numerical examples

Two examples are tested in this section that solve the optimization problem presented above with reanalysis methods. First, a clamped beam compressed with a distributed load is presented in Section 7.2.1 and second a simple supported beam is presented in Section 7.2.2. An extension to the last example is presented in Section 7.3 considering multiple buckling loads. Both formulations presented in Section 7.1.1 are solved. Later, application of the reanalysis is implemented by reducing the eigenvalue problem with the CA method as shown in Chapter 5 and the following controls where set:

1. A full eigenvalue solution is performed for the 1st iteration and when the solution's error calculated by Equation (4.56) exceeded 10^{-1};
2. A maximum number of 4 basis vectors is allowed.

For obtaining smooth results and guaranteeing the length scale of the final layout, the robust Heaviside projection presented in Equation (6.11) was applied. For the eroded projected densities the threshold value is set to $\eta_e = 0.6$ and the dilated is fixed to $\eta_d = 0.4$. The continuation scheme starts with a low value of $\beta = 1$ and increasing every

25 design iteration by 1 with a top boundary of $\beta = 8$. A move limit of 0.5 on the density update was imposed to insure convergence.

7.2.1 Example 1: Cantilever beam

Consider the structure in Figure 7.1. One side is fixed throughout the whole side and on the other a distributed axial load is subjected together with a small load in the perpendicular direction for initiating the linear buckling effect as explained in Chapter 3. The domain is discretized by the finite element method. The dimensions of the rectangular beam are $L_x \times L_y = 50 \times 10$, each element is a 0.25×0.25 square size. The structure is loaded with a relatively small distributed load of $\frac{0.01}{L_y}$ for obtaining small pre-buckling displacements. Further parameters are given in Table 7.1. Symmetry was enforced about x axis on the sensitivity analysis and the design densities in order to achieve an optimized solution for buckling in both directions .

TABLE 7.1: Parameters for Examples 1

Parameter	Value
E_{min}	1
E_{max}	10^3
ν	0.3
SIMP penalty	3
Radius filter	2.5

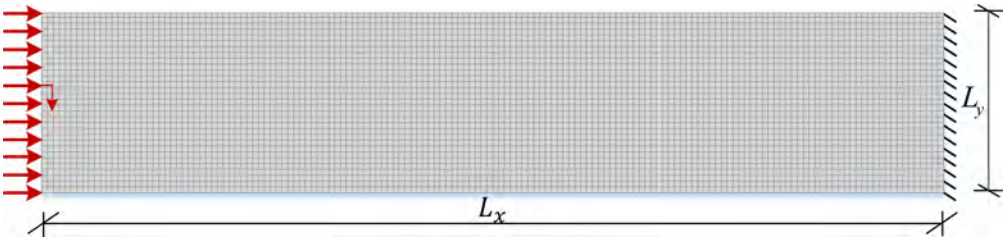

FIGURE 7.1: Cantilever beam structural domain

Maximum buckling load was first set as the objective function with a volume fraction constraint of 0.55 from the original design domain. The initial buckling load factor for the full volume of the domain is 1347. After 200 topology optimization cycles the buckling load factor increases to 5326.3 for the standard scheme and 5335.6 for the approximated scheme. Integrating the CA method provides similar optimized layouts with only 76 full eigenvalue problem solutions and 124 reduced problems by CA with only 4 basis vectors.

For the minimum volume optimization problem, the buckling load constraint was set to 5326. Both standard and approximate solutions provide similar layouts. The standard schem was able to converge to a volume fraction of 0.56 and the approximated scheme only managed to 0.57. Implementing CA in the process managed to solve a reduced problem in 97 design cycles out of 200. In Table 7.2 the results from all schemes and formulations are summarized.

In Figure 7.2 the buckling load factor is presented per design cycle for both schemes. In Figure 7.3 the volume fraction is presented. Both figures show the equivalence of both standard and approximated schemes. However, it is clear that the convergence is non smooth. This phenomenon is associated to the switching of the buckling mode during the optimization cycles. The increasing of the Heaviside sharpness control β is another reason for non-smoothness. As shown in Figure 7.4, the CA approximation does not effect the optimized result. Between the two formulations there is only a slight difference, however the concept of the optimized structure is similar. The final structure layout has two large coulmns that provide bending forces for the building and inner bars that strengthen the structure from collapsing.

TABLE 7.2: Summary of the results from the cantilever example

Cantilever example summary			
Formulation	Eigenvalue solutions with CA4	Volume	Load factor
Max Pcr - standard	-	0.55	5326.3
Max Pcr - CA	124	0.55	5335.6
Min Volume - standard	-	0.56	5326
Min Volume - CA	97	0.57	5326

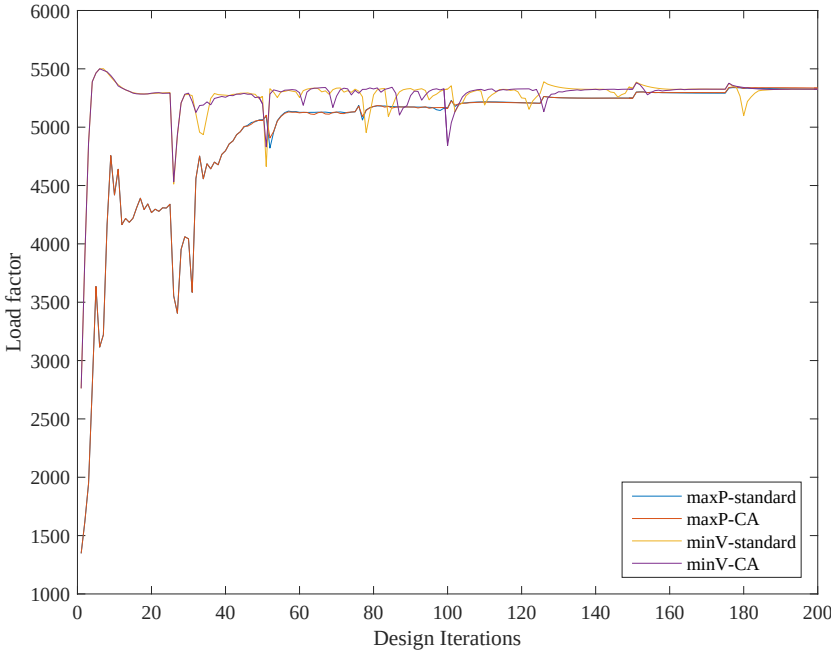

FIGURE 7.2: Buckling load factor per cycle iteration for both standard and approximated scheme for each formulation

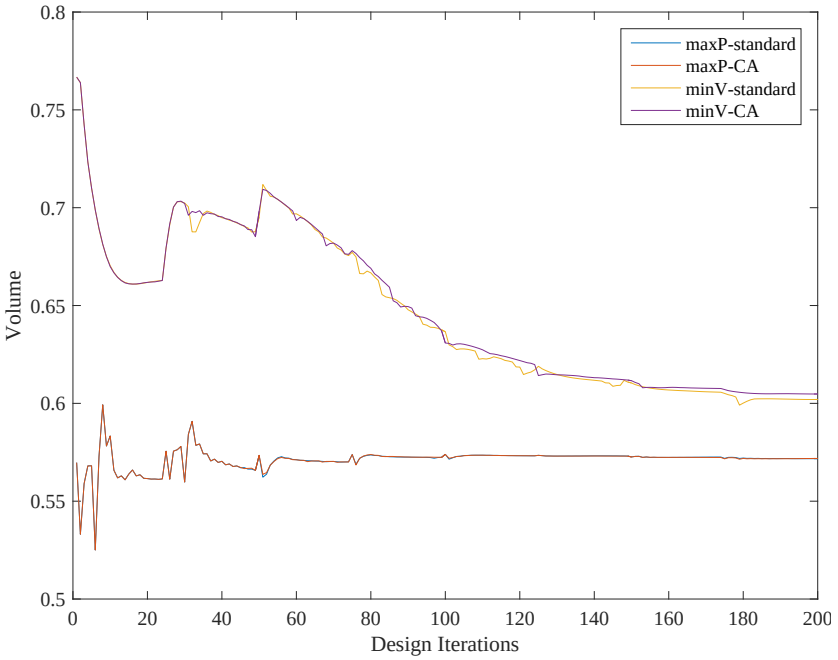

FIGURE 7.3: The dilated volume fraction per design cycle for both standard and approximated scheme for each formulation

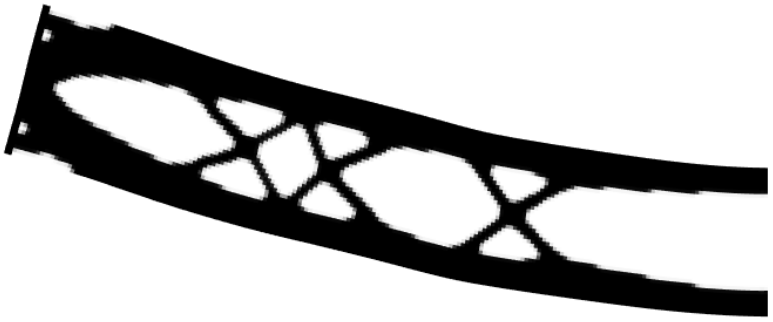

(A) Optimized layout for the maximum buckling load problem with a standard solution

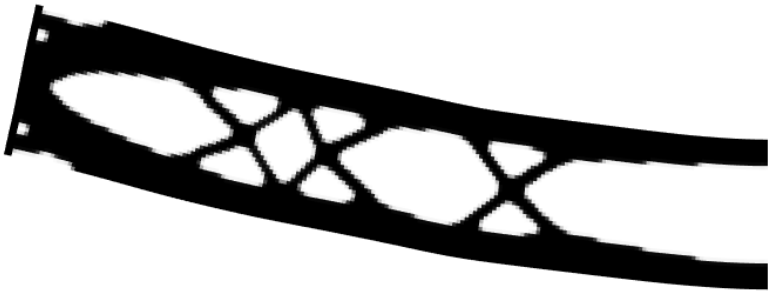

(B) Optimized layout for the maximum buckling load problem with a solution with the CA method

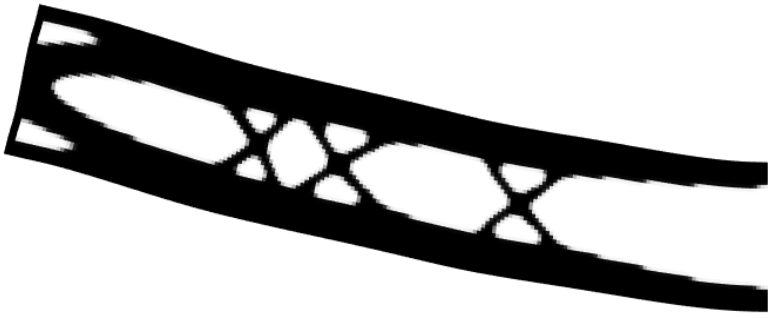

(C) Optimized layout for the minimum volume problem with a standard solution

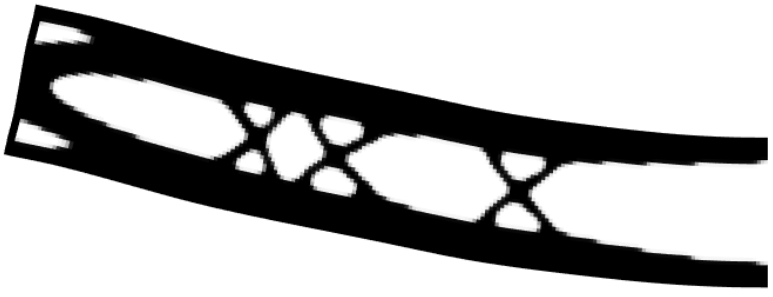

(D) Optimized layout for the minimum volume problem with a solution with the CA method

FIGURE 7.4: Final layouts after 200 design cycles for the clamped structure

7.2.2 Example 2: Simply-supported beam

Consider the structure in Figure 7.5. In the center-middle of each edge a length of a third of the height is pinned in order to avoid local buckling of local finite elements as in Example 6.3.3. The elements related to the loaded nodes are set to be constant solid elements. The load is evenly distributed between 5 neighboring nodes. A relatively small load $(1e-4P)$ in the perpendicular direction is applied for the initiating linear buckling effect. The domain is discretized by the finite element method. The dimensions of the rectangular beam are $L_x \times L_y = 50 \times 10$. Where each element is a 0.25×0.25 square size. The structure is loaded with a relatively small distributed load of $\frac{0.01}{L_y}$ for obtaining small pre-buckling displacements. Further parameters are given in Table 7.3. For achieving an optimized solution for buckling in both directions symmetry was enforced about x axis on the sensitivity analysis and the design densities.

TABLE 7.3: Parameters for Examples 2

Parameter	Value
E_{min}	1
E_{max}	10^3
ν	0.3
SIMP penalty	3
Radius filter	2.5

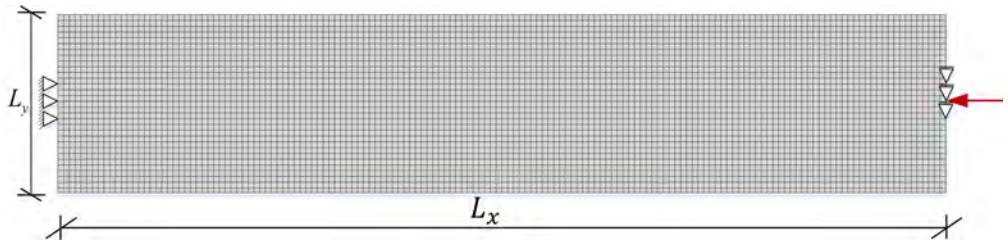

FIGURE 7.5: Simply-supported beam structural domain

Maximum buckling load was first set as the objective function with a volume fraction constraint of 0.55 from the original design domain. For the starting full volume domain the buckling load factor is 5543. With the standard scheme a load factor of 19,391 was obtain and for the approximated scheme 19,376 after 200 topology optimization cycles. Integrating the CA method provides similar optimized results with only 92 full eigenvalue problem solutions and 124 reduced problems by CA with 4 basis vectors.

For the minimum volume optimization problem, the buckling load constraint was set to $19,376$. Both standard and approximate solutions provide similar layouts. A volume

fraction of 0.565 was achieved by the standard scheme and 0.553 with approximations by CA. Integrating CA in the process managed to solve a reduced problem in 122 design cycles out of 200.In Table 7.4 the results from all schemes and formulations are summarized.

The buckling load factor per design cycle for both schemes is presented in Figure 7.6. In Figure 7.7 the volume fraction is presented. Both figures show the equivalence of both standard and approximated schemes. For the same reasons as explained above, the non-smoothness phenomena is clearly observed. As shown in Figure 7.8, the CA approximation does not effect the optimized result. Between the two formulations there is hardly any differences and the layouts are similar. The final structure layout has two large arches that provide strength for the bending of the structure. The inner bars strengthen the structure furthermore from collapsing.

TABLE 7.4: Summary of the results from the Beam example

Beam Example summary			
Formulation	Eigenvalue solution with CA4	Volume	Load factor
Max Pcr - standard	0	0.550	19,391
Max Pcr - CA	108	0.550	19,376
Min Volume - standard	0	0.565	19,376
Min Volume - CA	122	0.553	19,396

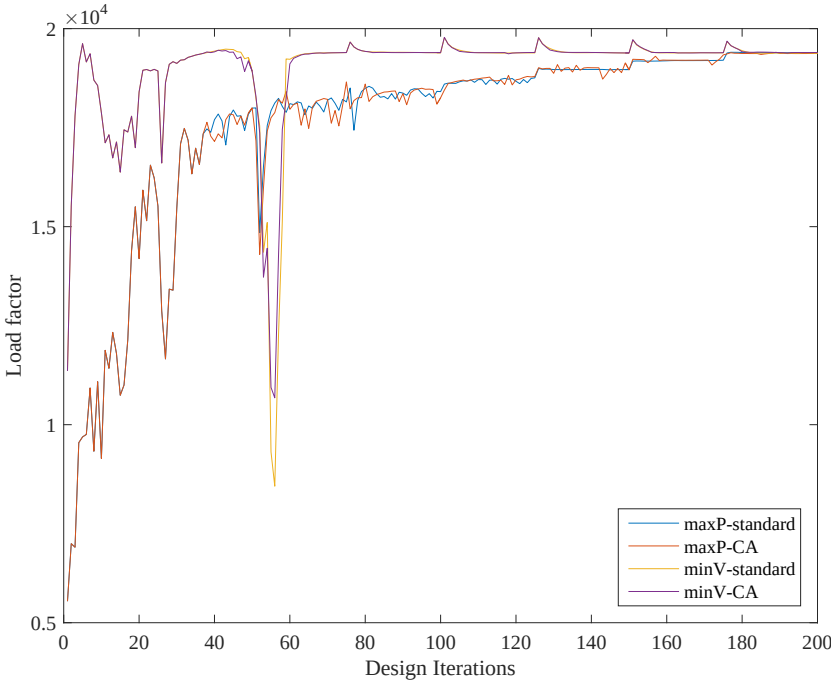

FIGURE 7.6: Buckling load factor per cycle iteration for both standard and approximated scheme for each formulation

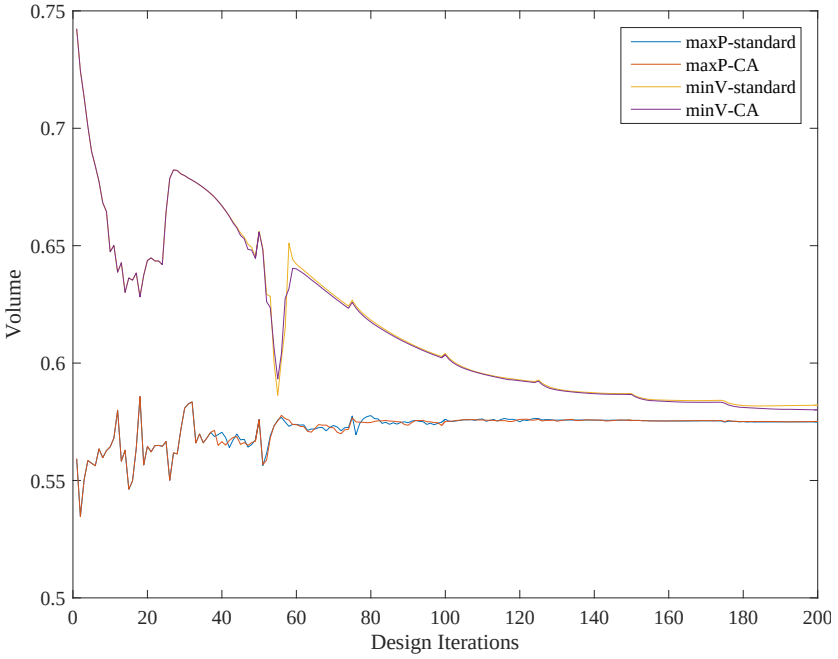

FIGURE 7.7: The dilated volume fraction per design cycle for both standard and approximated scheme for each formulation

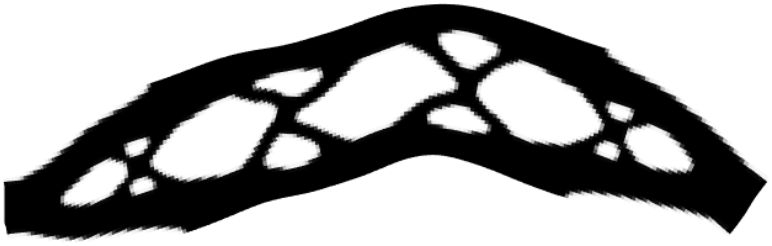

(A) Optimized layout for the maximum buckling load problem with a standard solution

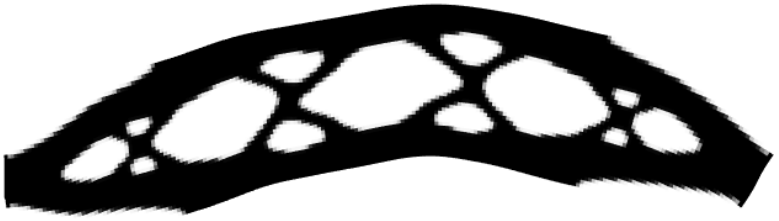

(B) Optimized layout for the maximum buckling load problem with a solution with the CA method

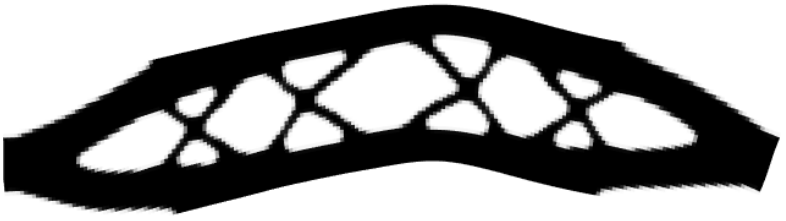

(C) Optimized layout for the minimum volume problem with a standard solution

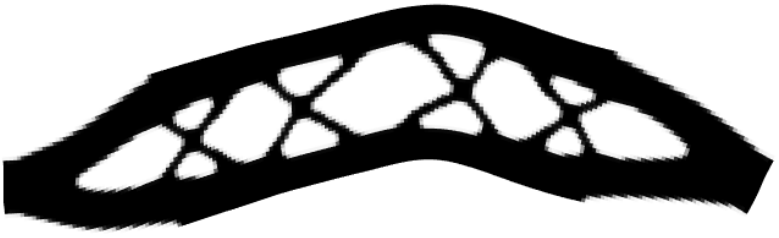

(D) Optimized layout for the minimum volume problem with a solution with the CA method

FIGURE 7.8: Final layouts after 200 design cycles for the simply supported structure

7.3 Multiple buckling modes

As mentioned in Section 7.1.1 above, the optimization suffers from a non smooth functional due to the switching of buckling modes and load factors. Now we present a small example considering additional buckling modes. The set up of the design domain is the same as the previous simply supported examples. The optimization problem that was solved is the bound formulation presented in Equation (7.3) with a volume fraction constraint of 0.55 from the original design domain. The value of the boundary factor $\alpha = 11,334$ was obtained after 500 design cycles. The load factor here is much smaller than the load factor obtained in the previous example. Hence, A less stable structure was obtained. This formulation yielded a worse solution and was more difficult to converge. Further work is needed for understanding the results and integrating the reanalysis methods in this formulation. The final layout of the optimized solution is presented in Figure 7.9

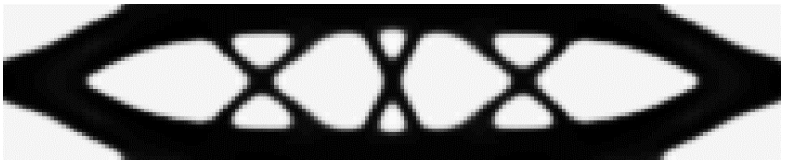

FIGURE 7.9: Final layout of the multiple buckling modes formulation

7.4 Summary

This chapter presented several cases that demonstrate the integration of reanalysis methods in topology optimization with linearized buckling. The CA method was implemented in the eigenvalue problem for reducing the problem size and solving the repeated analysis problem with lower computational cost. Two formulations were examined and solved both with a standard full solution and in an approximated manner by the CA method.

Two structures where considered, a cantilever beam and a simply supported beam. For the first example, the maximum buckling load formulation was solved under a volume fraction constraint. For 200 design cycles the reanalysis solution was able to reduce 124 full eigenproblems to a much smaller 4 by 4 problem. For the minimum volume formulation, 97 reduced eigenvalue solutions where done out of 200 design cycles. The same formulations where examined for the simply supported beam. Here in the maximum buckling load formulation 108 eigenproblems where reduced. For the second formulation,

122 problems where reduced. Roughly in both examples, between 50% to 60% of the eigenvalue problems were solved approximately by CA with only 4 basis vectors.

No advantage was found for a specific formulation and both provided similar results in terms of computational operations. The optimization solutions were found to be non smooth due to buckling mode switching. Despite this phenomena, optimized results were obtained. However, this might not be the case for all problems, especially when 3D problems are considered. Therefore, an extension to the problem considering a number of buckling modes was suggested and initial results were obtained.

Chapter 8

Conclusions and future work

Topology optimization often requires numerous repeated solutions of the analysis and sensitivity analysis equations. Accordingly, the computational cost of the solution might be very expensive ,especially when it comes to nonlinear models and large scale structures. The purpose of this work was to develop and implement numerical tools efficiently, in order to reduce the high computational effort involved in the solution. Reanalysis methods, based on the CA approach, were integrated in various numerical examples.

Conclusions

The main conclusions of this work can be roughly divided into two. First is the attempt to decrease the computational effort involved in solving the problem of topological optimization by integrating reanalysis methods. Second, choosing the most suitable formulation in the sense of computational efficiency. The literature review presented in Chapter 2 presented previous work on using reanalysis in topology optimization. Most of the publications focus on continuum structures with a linear model. In this work, the integration of reanalysis has been demonstrated for various models successfully. In Chapter 5, reanalysis using the Combined Approximations was blended well into the solution of the equilibrium equations for optimization of truss structures with linear assumptions. In all the numerical examples, reanalysis by CA managed to reduce 200 matrix decompositions to only 11-15 with practically identical optimized layouts.

In Chapter 6 continuum topology optimization with geometrical nonlinearity was considered. The assumptions of large deformations were taken into account and therefore the optimization solution is significantly more expensive. A number of comparison schemes and approximations of the sensitivities analysis were performed using CA. The intuitive RUS scheme reduced roughly 50% of of operations directly by reusing the solution as a wise initial guess. Further inspired by the modified Newton-Raphson method, RUK managed to reduce even more the number of matrix factorizations, between 20-40 percent compared to the full scheme. However there is a computational trade-off between number of matrix factorizations and additional Newton iterations required for the solution. More effort was reduced by adding to RUK approximations of the sensitivity analysis by the PCG method, less than 20% matrix were decomposed during the optimization process. In Figure 8.1, for each scheme, the reduce percentage of matrix factorizations compared to the full-Newton scheme is illustrated.

In Chapter 7 a model of linear buckling was considered. The main effort here is in the repeated solution of the eigenvalue problem. An efficient procedure for eigenproblem reanalysis based on CA was presented in Chapter 4. In all three numerical experiments, the approximate solution decreased the number of full eigenproblem solutions by 50 to 60 percent, by using only 4 basis vectors. The solution managed to converge to similar optimized structures compared to the full solution.

Further on, the question arises as to which formulation will yield a more effective solution. For the first numerical problem in Chapter 5 no advantages were found for a particular formulation and the results of the two formulations yielded similar efficiency. In the numerical examples in Chapter 6, increased efficiency was detected for the formulation of a minimum volume subject to a compliance constraint compared to the vice versa formulation. As presented in Figure 8.1, for all the examples the minimum volume formulation required less matrix factorizations. In the last numerical examples in Chapter 7, there was no significant advantage for a particular formulation and no efficiency benefit was detected using the stiff reference matrix.

This work provides additional knowledge for efficient ways to integrate reanalysis methods in topology optimization. Significant contributions of this work are in examples that are presented for the first time, including: (a) Integrating CA into truss topology optimization; (b) In topology optimization problems with GNL, approximating the

solution of the adjoint vector for the sensitivity analysis; (c) Assimilating CA in the solution of topology optimization problems concidering linearized buckling analysis. To the best of our knowledge the integration of CA in truss structures and in buckling eigenvalue problems has not been accomplished before. The contribution of this study is its ability to improve topological optimization by providing tools for efficient analysis. Thus, it will be possible to reduce the computational effort and enable a more sufficient implementation of topological optimization in computer programs.

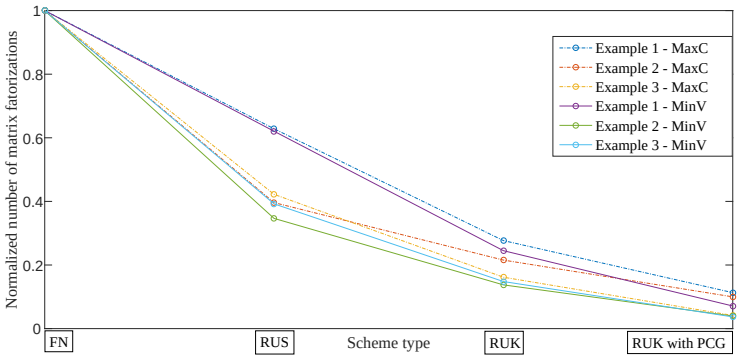

FIGURE 8.1: For the examples in Chapter 6:
The number of matrix factorizations completed in every scheme,
normalized to the standard Full-Newton scheme.

Future work

For utilizing reanalysis methods in various topology optimization problems the integration must be inclusive. A robust integration is still a difficult task and more investigations are needed. For this purpose, an investigation of a reanalysis criteria is needed, in order to make a sensible decision on when to calculate the response approximately.

Further investigation of the geometrical nonlinear problems with different formulations including hyper-elastic materials and integrating reanalysis by CA in these approaches. This can provide a better and more effective method for reducing the computational effort involved in solving optimization problems with nonlinear assumptions.

Topology optimization with the linearized buckling problems including reanalysis was first proposed in this work. Further investigation of different parameters is needed for ensuring convergence and efficiency.

Considering multiple modes of the buckling problems was mentioned at the end of Chapter 7. Integrating reanalysis method has not been preformed yet in this formulation of the problem.

As the approach was formulated based on 2D problems, a challenge is to implement the proposed formulation in 3D problems. Here direct solvers increase significantly the requirement of memory and CPU processing power. Thus iterative equation solvers are likely to be profitable. Therefore, utilizing the PCG iterative solution and reanalysis methods in general can help reduce the computational effort invested in the sequential structural analysis.

Bibliography

Aage, N., Amir, O., Clausen, A., Hadar, L., Maier, D., and Søndergaard, A. (2015). Advanced topology optimization methods for conceptual architectural design. In *Advances in Architectural Geometry 2014*, pages 159–179. Springer.

Allaire, G., Jouve, F., and Toader, A.-M. (2004). Structural optimization using sensitivity analysis and a level-set method. *Journal of computational physics*, 194(1):363–393.

Amir, O. (2015). Revisiting approximate reanalysis in topology optimization: on the advantages of recycled preconditioning in a minimum weight procedure. *Structural and Multidisciplinary Optimization*, 51(1):41–57.

Amir, O., Bendsøe, M. P., and Sigmund, O. (2009). Approximate reanalysis in topology optimization. *International Journal for Numerical Methods in Engineering*, 78(12):1474–1491.

Amir, O., Kirsch, U., and Sheinman, I. (2008). Efficient non-linear reanalysis of skeletal structures using combined approximations. *International journal for numerical methods in engineering*, 73(9):1328–1346.

Amir, O. and Sigmund, O. (2011). On reducing computational effort in topology optimization: how far can we go? *Structural and Multidisciplinary Optimization*, 44(1):25–29.

Amir, O., Sigmund, O., Lazarov, B. S., and Schevenels, M. (2012). Efficient reanalysis techniques for robust topology optimization. *Computer Methods in Applied Mechanics and Engineering*, 245:217–231.

Bathe, K.-J. (2006). *Finite element procedures*. Klaus-Jurgen Bathe.

Ben-Tal, A. and Bendsøe, M. P. (1993). A new method for optimal truss topology design. *SIAM Journal on Optimization*, 3(2):322–358.

Bendsøe, M. P. (1989). Optimal shape design as a material distribution problem. *Structural and multidisciplinary optimization*, 1(4):193–202.

Bendsøe, M. P., Ben-Tal, A., and Zowe, J. (1994). Optimization methods for truss geometry and topology design. *Structural optimization*, 7(3):141–159.

Bendsøe, M. P. and Kikuchi, N. (1988). Generating optimal topologies in structural design using a homogenization method. *Computer methods in applied mechanics and engineering*, 71(2):197–224.

Bendsøe, M. P. and Sigmund, O. (1999). Material interpolation schemes in topology optimization. *Archive of applied mechanics*, 69(9-10):635–654.

Bendsøe, M. P. and Sigmund, O. (2003). *Topology optimization: theory, methods and applications*. Springer.

Bendsoe, M. P. and Sigmund, O. (2013). *Topology optimization: theory, methods, and applications*. Springer Science & Business Media.

Bogomolni, M., Kirsch, U., and Sheinman, I. (2006). Efficient design sensitivities of structures subjected to dynamic loading. *International Journal of Solids and Structures*, 43(18-19):5485–5500.

Bogomolny, M. (2010). Topology optimization for free vibrations using combined approximations. *International Journal for Numerical Methods in Engineering*, 82(5):617–636.

Bruns, T. and Sigmund, O. (2004). Toward the topology design of mechanisms that exhibit snap-through behavior. *Computer methods in applied mechanics and engineering*, 193(36-38):3973–4000.

Bruns, T., Sigmund, O., and Tortorelli, D. A. (2002). Numerical methods for the topology optimization of structures that exhibit snap-through. *International Journal for Numerical Methods in Engineering*, 55(10):1215–1237.

Bruns, T. E. and Tortorelli, D. A. (2001). Topology optimization of non-linear elastic structures and compliant mechanisms. *Computer methods in applied mechanics and engineering*, 190(26-27):3443–3459.

Buhl, T., Pedersen, C. B., and Sigmund, O. (2000). Stiffness design of geometrically nonlinear structures using topology optimization. *Structural and Multidisciplinary Optimization*, 19(2):93–104.

Burger, M. and Stainko, R. (2006). Phase-field relaxation of topology optimization with local stress constraints. *SIAM Journal on Control and Optimization*, 45(4):1447–1466.

Chen, S. H. and Yang, X. W. (2000). Extended kirsch combined method for eigenvalue reanalysis. *AIAA journal*, 38(5):927–930.

Christensen, P. W. and Klarbring, A. (2009). Introduction. In *An Introduction to Structural Optimization*, pages 1–7. Springer.

Diaz, A. and Sigmund, O. (1995). Checkerboard patterns in layout optimization. *Structural optimization*, 10(1):40–45.

Dorn, W., Gomory, R., and Greenberg, H. (1964). Automatic design of optimal structures, j. de méchanique 3, 25–52.

Fleury, C. (1989). Efficient approximation concepts using second order information. *International Journal for Numerical Methods in Engineering*, 28(9):2041–2058.

Fuchs, M. B. (1980). Linearized homogeneous constraints in structural design. *International Journal of Mechanical Sciences*, 22(1):33–40.

Gogu, C. (2015). Improving the efficiency of large scale topology optimization through on-the-fly reduced order model construction. *International Journal for Numerical Methods in Engineering*, 101(4):281–304.

Guest, J. K., Prévost, J. H., and Belytschko, T. (2004). Achieving minimum length scale in topology optimization using nodal design variables and projection functions. *International journal for numerical methods in engineering*, 61(2):238–254.

Jog, C. S. and Haber, R. B. (1996). Stability of finite element models for distributed-parameter optimization and topology design. *Computer methods in applied mechanics and engineering*, 130(3-4):203–226.

Karush, W. (1939). Minima of functions of several variables with inequalities as side constraints. *M. Sc. Dissertation. Dept. of Mathematics, Univ. of Chicago*.

Kemmler, R., Lipka, A., and Ramm, E. (2005). Large deformations and stability in topology optimization. *Structural and Multidisciplinary Optimization*, 30(6):459–476.

Kirsch, U. (1989). Optimal topologies of truss structures. *Computer Methods in Applied Mechanics and Engineering*, 72(1):15–28.

Kirsch, U. (1991). Reduced basis approximations of structural displacements for optimal design. *AIAA J*, 29(10):1751–1758.

Kirsch, U. (1993). Efficient reanalysis for topological optimization. *Structural and Multidisciplinary Optimization*, 6(3):143–150.

Kirsch, U. (1999). Efficient, accurate reanalysis for structural optimization. *AIAA journal*, 37(12):1663–1669.

Kirsch, U. (2008). *Reanalysis of structures*. Springer.

Kirsch, U. and Bogomolni, M. (2004). Procedures for approximate eigenproblem reanalysis of structures. *International Journal for Numerical Methods in Engineering*, 60(12):1969–1986.

Kirsch, U. and Bogomolni, M. (2007). Nonlinear and dynamic structural analysis using combined approximations. *Computers & structures*, 85(10):566–578.

Kirsch, U., Bogomolni, M., and Sheinman, I. (2006). Nonlinear dynamic reanalysis of structures by combined approximations. *Computer methods in applied mechanics and engineering*, 195(33):4420–4432.

Kirsch, U., Bogomolni, M., and Sheinman, I. (2007). Efficient dynamic reanalysis of structures. *Journal of structural engineering*, 133(3):440–448.

Kirsch, U., Kocvara, M., and Zowe, J. (2002). Accurate reanalysis of structures by a preconditioned conjugate gradient method. *International Journal for Numerical Methods in Engineering*, 55(2):233–251.

Kirsch, U. and Liu, S. (1995). Exact structural reanalysis by a first-order reduced basis approach. *Structural and Multidisciplinary Optimization*, 10(3):153–158.

Kirsch, U. and Moses, F. (1999). Effective reanalysis for damaged structures. *Case Studies in Optimal Design and Maintenance Planning of Civil Infrastructure Systems*, pages 164–178.

Kirsch, U. and Papalambros, P. Y. (2001). Structural reanalysis for topological modifications–a unified approach. *Structural and Multidisciplinary Optimization*, 21(5):333–344.

Kuhn, H. and Tucker, A. (1951). Proceedings of 2nd berkeley symposium.

Ma, Z.-D., Kikuchi, N., and Cheng, H.-C. (1995). Topological design for vibrating structures. *Computer methods in applied mechanics and engineering*, 121(1-4):259–280.

Materna, D. and Kalpakides, V. K. (2016). Nonlinear reanalysis for structural modifications based on residual increment approximations. *Computational Mechanics*, 57(1):1–18.

Michell, A. G. M. (1904). Lviii. the limits of economy of material in frame-structures. *The London, Edinburgh, and Dublin Philosophical Magazine and Journal of Science*, 8(47):589–597.

Neves, M., Rodrigues, H., and Guedes, J. (1995). Generalized topology design of structures with a buckling load criterion. *Structural optimization*, 10(2):71–78.

Neves, M. M., Sigmund, O., and Bendsøe, M. P. (2002). Topology optimization of periodic microstructures with a penalization of highly localized buckling modes. *International Journal for Numerical Methods in Engineering*, 54(6):809–834.

Pedersen, C. B., Buhl, T., and Sigmund, O. (2001). Topology synthesis of large-displacement compliant mechanisms. *International Journal for numerical methods in engineering*, 50(12):2683–2705.

Pedersen, N. L. (2000). Maximization of eigenvalues using topology optimization. *Structural and multidisciplinary optimization*, 20(1):2–11.

Pedersen, P. (1970). *On the minimum mass layout of trusses*. Department of Applied Mechanics, Technical University of Denmark.

Querin, O., Steven, G., and Xie, Y. (2000). Evolutionary structural optimisation using an additive algorithm. *Finite Elements in Analysis and Design*, 34(3-4):291–308.

Rahmatalla, S. and Swan, C. C. (2003). Continuum topology optimization of buckling-sensitive structures. *AIAA journal*, 41(6):1180–1189.

Rossow, M. and Taylor, J. (1973). A finite element method for the optimal design of variable thickness sheets. *Aiaa Journal*, 11(11):1566–1569.

Rozvany, G. (1972). Grillages of maximum strength and maximum stiffness. *International Journal of Mechanical Sciences*, 14(10):651–666.

Rozvany, G. (2001). On design-dependent constraints and singular topologies. *Structural and Multidisciplinary Optimization*, 21(2):164–172.

Schmit, L. A. (1960). Structural design by systematic synthesis. In *Proc. of Second Conference on Electronic Computation ASCE, New York*, pages 105–122.

Schmit, L. A. (1981). Structural synthesis-its genesis and development. *AIAA Journal*, 19(10):1249–1263.

Schmit, L. A. and Farshi, B. (1974). Some approximation concepts for structural synthesis. *AIAA j*, 12(5):692–699.

Sherman, J. and Morrison, W. J. (1950). Adjustment of an inverse matrix corresponding to a change in one element of a given matrix. *The Annals of Mathematical Statistics*, 21(1):124–127.

Sigmund, O. (1994). *Design of material structures using topology optimization*. PhD thesis, Technical University of Denmark Denmark.

Sigmund, O. (2007). Morphology-based black and white filters for topology optimization. *Structural and Multidisciplinary Optimization*, 33(4-5):401–424.

Sigmund, O. and Maute, K. (2013). Topology optimization approaches. *Structural and Multidisciplinary Optimization*, 48(6):1031–1055.

Sigmund, O. and Petersson, J. (1998). Numerical instabilities in topology optimization: a survey on procedures dealing with checkerboards, mesh-dependencies and local minima. *Structural optimization*, 16(1):68–75.

Sigmund, O. and Torquato, S. (1997). Design of materials with extreme thermal expansion using a three-phase topology optimization method. *Journal of the Mechanics and Physics of Solids*, 45(6):1037–1067.

Starnes Jr, J. H. and Haftka, R. T. (1979). Preliminary design of composite wings for buckling, strength, and displacement constraints. *Journal of Aircraft*, 16(8):564–570.

Stolpe, M. and Svanberg, K. (2001). An alternative interpolation scheme for minimum compliance topology optimization. *Structural and Multidisciplinary Optimization*, 22(2):116–124.

Svanberg, K. (1987). The method of moving asymptotes—a new method for structural optimization. *International journal for numerical methods in engineering*, 24(2):359–373.

Venkataraman, S. and Haftka, R. T. (2004). Structural optimization complexity: what has moore's law done for us? *Structural and Multidisciplinary Optimization*, 28(6):375–387.

Wallin, M., Ristinmaa, M., and Askfelt, H. (2012). Optimal topologies derived from a phase-field method. *Structural and Multidisciplinary Optimization*, 45(2):171–183.

Wang, F., Lazarov, B. S., and Sigmund, O. (2011). On projection methods, convergence and robust formulations in topology optimization. *Structural and Multidisciplinary Optimization*, 43(6):767–784.

Wang, M. Y., Wang, X., and Guo, D. (2003). A level set method for structural topology optimization. *Computer methods in applied mechanics and engineering*, 192(1-2):227–246.

Wang, S., Sturler, E. d., and Paulino, G. H. (2007). Large-scale topology optimization using preconditioned krylov subspace methods with recycling. *International journal for numerical methods in engineering*, 69(12):2441–2468.

Woodbury, M. A. (1950). Inverting modified matrices. *Memorandum report*, 42(106):336.

Xie, Y. M. and Steven, G. P. (1993). A simple evolutionary procedure for structural optimization. *Computers & structures*, 49(5):885–896.

Zhou, M. and Rozvany, G. (1991). The coc algorithm, part ii: topological, geometrical and generalized shape optimization. *Computer Methods in Applied Mechanics and Engineering*, 89(1-3):309–336.

הפחתת המאמץ החישובי באופטימיזציה טופולוגית של מבנים באמצעות אנליזה חוזרת עם מטריצת ייחוס קשיחה

חיבור של מחקר לשם מילוי חלקי של הדרישות לקבלת תואר מגיסטר

למדעים בהנדסה אזרחית (הנדסת מבנים)

מתי ספייסר

הוגש לסנט הטכניון – מכון טכנולוגי לישראל

אדר ב׳ ה׳תשע״ט מרץ 2019

<u>הבעות תודה</u>

המחקר נעשה בהנחיית פרופ״מ עודד אמיר בפקולטה להנדסה אזרחית וסביבתית.

ברצוני להביע את תודתי והערכתי לפרופ״מ עודד אמיר על ההנחיה, הייעוץ והעזרה לאורך כל תקופת העבודה על המחקר.

אני מודה לטכניון – מכון טכנולוגי לישראל על התמיכה הכספית הנדיבה בהשתלמותי.

לבסוף אני מודה להורי ולאשתי מירב על הסבלנות, העידוד והתמיכה לאורך כל הדרך.

תקציר

אחד היעדים המשמעותיים בתחום תכנון המבנים הוא לייצר את המבנה "הטוב ביותר". בהתייחסות ל"טוב ביותר" מעורבים שיקולים כלכליים, תפקודיים, סביבתיים ועוד. אופטימיזציה מגשרת על המתח הקיים בין הרצון לתכנן מבנה קל וזול לבין האילוצים של חוזק המבנה ועמידה בתנאי השירות. דוגמא לניסוח של בעיית אופטימיזציה של מבנים היא – למצוא את העלות המינימלית לייצור המבנה בהינתן אילוצים שונים כגון גיאומטריה, עומסים, תנאי השענה וכיו"ב.

באופן מסורתי, מהנדסים מבצעים אופטימיזציה למבנים על ידי ניסוי וטעייה וניסיון מקצועי רב שנים בתכן של מבנים. שיטת עבודה זו דורשת משאבי זמן ועלות והיא אינה מניבה באופן ודאי את המבנה הטוב ביותר. כמו כן, הדרישה ההולכת וגוברת לקבלת מבנים מורכבים ויעילים יותר מקשה על היכולת של מהנדסים לספק מבנים אופטימליים על ידי כלים פשוטים שהיו בשימוש עד היום. בנוסף, בעשורים האחרונים ישנה האצה בתחום של ביצועי המחשב וקיים שימוש כמעט מוחלט בתוכנות מחשב לביצוע של אנליזות של מבנים. מסיבות אלו, קיימת מוטיבציה לשימוש בשיטות אופטימיזציה בעזרת כלים חישוביים בתעשיית תכן המבנים. אופטימיזציה טופולוגית הינה הגישה המובילה כיום בתחום זה.

כיום, קיימות בשוק תוכנות מסחריות רבות העוסקות בתחום הנזכר לעיל אשר משלבות אופטימיזציה כחלק מתהליך האנליזה שלהן. למרות כל זאת, במבנים אשר המודל החישובי שלהם מורכב וכאשר נדרש לספק תוצאות אנליזה מדויקות יותר, הכלים הקיימים מוגבלים ביכולתם לספק פתרון מדויק בזמן קצר. מגבלה זו מספקת תמריץ למציאת שיטה שתפחית את אותה עלות חישובית בתהליך האנליזה והאופטימיזציה. המחקר המתואר בחיבור זה מתמקד בשיפור תהליך האופטימיזציה הטופולוגית על ידי מתן כלי לייעול האנליזה. כך שניתן לצמצם את המאמץ החישובי ולאפשר הטמעה יעילה יותר של האופטימיזציה הטופולוגית ככלי בתוכנות מחשב.

שיטת הקירובים המשולבים (CA) באנליזה חוזרת במבנים הוצעה לראשונה על ידי קירש בהקשר של אנליזה סטטית ליניארית. המטרה בשימוש ב-CA היא להפחית את המאמץ החישובי הכרוך בפתרון חוזר של משוואות שווי המשקל. כאמור, עבור בעיות עם מספר רב של אלמנטים הפתרון של משוואות שווי המשקל מהווה את עיקר המאמץ החישובי. באנליזה חוזרת מקורבת בגישת CA נעשה שימוש בקירוב של ההזזות באמצעות טור, תוך שימוש במטריצת ייחוס מפורקת שהתקבלה באיטרציה קודמת של תהליך האופטימיזציה. הפתרון המדויק של משוואות שיווי המשקל באיטרציה הנוכחית מוחלף על ידי הפתרון המקורב. הפתרון המקורב מתקבל בעזרת הפחתת הסדר של מטריצת הקשיחות ע"י מספר מצומצם של וקטורי בסיס אשר נלקחים מהטור שפותח. מספר וקטורי הבסיס שנלקחים קובעים את גודל הקירוב (ועלותו החישובית) ואת רמת הדיוק המתקבלת.

הטמעת CA של קירש לתוך אופטימיזציה טופולוגית הומחשה לראשונה כפרוצדורה מתאימה להפחתת המאמץ החישובי על בעיה מקוננת באופטימיזציה טופולוגית של מבנה רצף, בתנאים סטטיים לינאריים.

בהמשך גם הושג ייעול חישובי ע״י שילוב של CA באופטימיזציה טופולוגית למקסימיזציה של ערכים עצמיים לתנודה.

את הבעיה הקלאסית באופטימיזציה טופולוגית, קשיחות אל מול משקל, ניתן לנסח כמקסימום קשיחות תוך אילוץ על הנפח או מינימום נפח תוך אילוץ על הקשיחות. את הניסוח הראשון ניתן גם להגדיר כמינימיזציה של עבודה חיצונית. באופן הזה המבנה עובר תהליך שינוי ממבנה גמיש למבנה קשיח יותר. זאת אומרת, שבהטמעה של CA מטריצת הייחוס הינה גמישה ביחס למטריצה של מערכת המשוואות אותה אנו רוצים לפתור באיטרציה עוקבת. בניסוח השני, מינימום נפח, המבנה באופן כללי עובר שינוי ממבנה קשיח למבנה גמיש. מטריצת הייחוס של האנליזה החוזרת הינה קשיחה ביחס למטריצה של מערכת המשוואות אותה רוצים לפתור באיטרציה הנוכחית. בשנים האחרונות, הצטברו תובנות חדשות על אופן ההטמעה המיטבי של שיטת הקרובים המשולבים באופטימיזציה טופולוגית. במחקרים קודמים נמצא ששימוש ב-CA עם מטריצת ייחוס קשיחה יכול להפחית את זמן החישוב של האופטימיזציה ב-50% לעומת השילוב של CA בניסוח ההפוך.

מטרת המחקר הינה לחקור את אופן ההטמעה של אנליזה חוזרת עם שיטת הקירובים של קירש (CA) באופטימיזציה טופולוגית של מבנים. בפרט, המחקר מתמקד בהרחבת היישום של CA עם מטריצת הייחוס הקשיחה ובהשפעתה של גישה זו על הפחתת המאמץ החישובי. המחקר הינו באופיו תיאורטי-אנליטי. במסגרת המחקר נוסחו בעיות אופטימיזציה וגישות שונות להטמעת הקירובים המשולבים של קירש באנליזה חוזרת. נעשה שימוש נרחב בכלים נומריים לפתרון בתוכנת Matlab.

תוכן החיבור כולל את הפרקים הבאים: הפרק הראשון הינו הקדמה לנושא ומוצגת המוטיבציה לביצוע המחקר ומטרתו. הפרק השני מציג מבוא קצר על אופטימיזציה טופולוגית ואנליזה חוזרת וכן סקר ספרות אודות ההתקדמות במחקר של אנליזה חוזרת ואופטימיזציה טופולוגית לאורך השנים האחרונות עד נקודות המפגש ביניהם. הפרק השלישי מוקדש להצגת המודלים המבניים של מבני מסבך ומבני רצף הכוללים אי ליניאריות גיאומטרית. הפרק מתחיל במבני מסבך ליניאריים ופתרון מערכת שווי המשקל. הפרק ממשיך ברקע קצר אודות מידול מבנה רצף עם אי ליניאריות גיאומטרית ושיטת פתרון באמצעות השיטה הקלאסית של ניוטון-ראפסון. בהמשך הפרק מוצגת בעיית הקריסה ופתרונה על ידי פתרון בעיית הערכים העצמיים לקריסה. בפרק הרביעי מוצג הפיתוח של שיטת הקירובים המשולבים של קירש בהרחבה. תחילה מוצגת אנליזה חוזרת של בעיה סטטית ליניארית ואופן חישוב וקטורי הבסיס. לאחר מכן מוצגת השיטה עבור בעיית ערכים עצמיים לקריסה ואופן קירוב הבעיה באמצעות וקטורי הבסיס. בפרק החמישי מוצגות דוגמאות נומריות לאנליזה חוזרת באופטימיזציה טופולוגית של מבני מסבך. תחילה מוצגים הניסוחים של בעיית האופטימיזציה עבור מבנה מסבך ב-2 אופנים שונים: מקסימום קשיחות עם אילוץ על הנפח ומינימום נפח עם אילוץ על הקשיחות. בנוסף ניתוחי הרגישויות מפותחים ומוצגים לצורך פתרון בעיית האופטימיזציה.

בהמשך הפרק מוצגות דוגמאות נומריות לשילוב של אנליזה חוזרת עם CA באופטימיזציה של מבני מסבך. באמצעות הפתרון המקורב הופחת המאמץ החישובי בסדר גודל אחד בכל הדוגמאות. אמנם נמצא שלמטריצת ייחוס קשיחה יש יתרון מסוים ב-CA, אך זה אינו בא לידי ביטוי בפתרון בעיית האופטימיזציה בדוגמאות אלו. הפרק השישי מציג דוגמאות נומריות עבור אנליזה חוזרת באופטימיזציה טופולוגית עבור מבני רצף עם אי ליניאריות גיאומטרית. תחילה מוצגת בעיית האופטימיזציה עבור מבני רצף עם התחשבות באי ליניאריות גיאומטרית. ניתוחי הרגישויות מפותחים עבור פתרון הבעיה ומוצגות הבעיות הנומריות עם דרכי ההתמודדות שיישמו בעבודה זו. לאחר מכן מוצעות 3 סכמות אפשריות על מנת לייעל את הפתרון של בעיית האופטימיזציה: 1- שימוש חוזר בוקטור ההזזות כניחוש ראשוני לפתרון של איטרציית התכן הבאה; 2- בהשראת MNR שימוש חוזר במטריצת הקשיחות בפתרון האנליזה; 3- על הסכמה הקודמת, הוספת חישוב מקורב של וקטור ה-Adjoint על ידי CA. בהמשך הפרק מוצגות 3 דוגמאות נומריות עבור מודלים של מבני רצף עם אי ליניאריות גיאומטרית. שלושת הסכמות מיושמות בכל דוגמא וייעול הפתרון של בעיית האופטימיזציה נמדד בחסכון של מספר פירוקים של מטריצת הקשיחות לאורך כל תהליך האופטימיזציה. נמצא שהסכמה הראשונה מצליחה להפחית את מספר פירוקי המטריצה בחצי והסכימה השנייה אף הצליחה להגיע לשליש פירוקי מטריצה לעומת פתרון מלא. הוספת קירוב לניתוחי הרגישויות מצליחה לחסוך עוד יותר לכדי 90% פחות פירוקי מטריצה בהשוואה לפתרון מלא. בנוסף מבחינת היעילות החישובית נרשם יתרון לניסוח של מינימום נפח תחת אילוץ קשיחות לעומת הניסוח ההפוך. הפרק השביעי מציג דוגמאות לאנליזה חוזרת באופטימיזציה טופולוגית לבעיות קריסה. הפורמולציה של הבעיה מוצגת בתחילת הפרק יחד עם ניתוחי הרגישויות וההתחשבויות הנומריות. לאחר מכן האנליזה המקורבת באמצעות CA מיושמת ב-2 דוגמאות נומריות שונות עם שני ניסוחי האופטימיזציה המוצגים בתחילת הפרק. מטרת השילוב של CA הינו הפחתת המאמץ החישובי בפתרון בעיית הערכים העצמיים. על כן, המדד העיקרי ליעילות החישובית הוא מספר הפתרונות המקורבים של בעיית ערכים עצמיים לקריסה בכל תהליך האופטימיזציה. בדוגמאות אלו בין 50 ל-60 אחוז מאיטרציות התכן חושבו באופן מקורב על ידי CA וכך נחסך מאמץ חישובי ניכר.

האופטימיזציה הטופולוגית מוטמעת כיום, בעיקר בתחומי התעופה והרכב, ככלי אינטגרלי בתוך תהליך תכן המבנים. עם זאת, הדרישה של התעשייה למבנים מורכבים, אשר מביאים למספר רב של אלמנטים במודל, בנוסף לשאיפה לפתרון מדויק, מגדילות משמעותית את המאמץ החישובי של האופטימיזציה ומקשות על מתן פתרון בזמן סביר. סיבה זו נותנת תמריץ למציאת דרך להקטנת העלות החישובית של האופטימיזציה מבלי לפגוע בדיוק הפתרון. תרומתו העיקרית של מחקר זה היא ביכולתו לשפר את תהליך האופטימיזציה הטופולוגית על ידי מתן כלי לייעול האנליזה. כך ניתן לצמצם את המאמץ החישובי ולאפשר הטמעה יעילה יותר של האופטימיזציה הטופולוגית בתוכנות מחשב.